Bentonite and Latex Colloid Migration Experiments in a Granite Fracture on a Metre Scale to Evaluate Effects of Particle Size and Flow Velocity

NWMO TR-2009-26 November 2009

Peter Vilks

Neil H. Miller

Atomic Energy of Canada Limited

nwmo
NUCLEAR WASTE MANAGEMENT ORGANIZATION
SOCIÉTÉ DE GESTION DES DÉCHETS NUCLÉAIRES

Nuclear Waste Management Organization
22 St. Clair Avenue East, 6th Floor
Toronto, Ontario
M4T 2S3
Canada

Tel: 416-934-9814
Web: www.nwmo.ca

Bentonite and Latex Colloid Migration Experiments in a Granite Fracture on a Metre Scale to Evaluate Effects of Particle Size and Flow Velocity

NWMO TR-2009-26

November 2009

Peter Vilks and Neil H. Miller
Atomic Energy of Canada Limited

ABSTRACT

Title: **Bentonite and Latex Colloid Migration Experiments in a Granite Fracture on a Metre Scale to Evaluate Effects of Particle Size and Flow Velocity**
Report No.: **NWMO TR-2009-26**
Author(s): Peter Vilks and Neil H. Miller
Company: Atomic Energy of Canada Limited
Date: November 2009

Abstract

One of the objectives of SKB's Colloid Dipole Project was to evaluate the potential of bentonite colloids to facilitate radionuclide transport. The field scale experiment undertaken at the Äspö TRUE-1 site was to use latex spheres as a proxy for bentonite colloids, To support this project, laboratory scale colloid migration experiments, using both bentonite and latex colloids, were performed in the Quarried Block (QB) sample, a 1m x 1m x 0.7 m block of granite containing a single, well characterized, variable aperture fracture. The main purpose of this laboratory program was to improve on the understanding of physical retardation processes that effect colloid mobility, and to provide additional information that could not be obtained at the field-scale such as bentonite versus latex colloid transport, particularly at low flow rates and different water compositions.

The purpose of this report is to present the results of the experimental program performed in 2007 that included (1) performing experiments with latex colloids in saline water, (2) exploring the effects of particle size on bentonite and latex colloid transport, (3) providing additional colloid transport data, for longer distances and low velocities, and (4) characterizing colloid deposition on fracture surfaces by post-test analysis.

Latex spheres, which are almost perfectly spherical and available as monodisperse (single-sized) suspensions, provide a useful tool for identifying the effects of particle size, structure and surface charge density on colloid transport. Experimental results showed that the transport behaviour of latex spheres in a natural fracture was consistent with filtration theory in which particle size determined the probability of particle interceptions with fracture surfaces or stagnant zones. Unlike bentonite colloids, latex colloids were more mobile in saline water, with migration properties influenced by the size of their flocs. In dilute water and under low flow experimental conditions, the prolonged residence times resulted in a tendency for bentonite and latex colloids to become fixed within the fracture system.

The results of the laboratory scale colloid migration experiments confirm that the conditions that limit colloid transport are typical of those found at depths and in rock settings that are proposed for deep geological repositories. These include the high ionic strength of brackish or saline water in which colloid stability in suspension is reduced, low groundwater flow velocities, and transport paths exhibiting fracture aperture heterogeneity and surface roughness that promote colloid entrapment and retention. The results also show that some colloid transport may occur under high flow rates and in waters with low ionic strength and neutral pH. However, even under dilute conditions, colloid transport from a deep geological repository system would tend to be limited by the reduced number of fractures, the inherent complexity of these pathways and lower porosity.

TABLE OF CONTENTS

LIST OF TABLES

Page

LIST OF FIGURES

Page

1. INTRODUCTION

In recent years, experimental evidence has suggested that within Deep Geologic Repositories (DGR) buffer and backfill materials in contact with groundwater may release bentonite colloids containing sorbed radionuclides. This is of particular concern to sites which currently have low ionic strength groundwater, for example as found at the Swiss Grimsel Test Site (GTS). Although many sites, such as the Äspö Hard Rock Laboratory (HRL), have saline water, there is a concern that during periods of glaciation dilute melt water may be able to infiltrate to repository depth. This scenario could result in erosion and degradation of the buffer and backfill materials of a DGR.

To address observations of bentonite colloid transport in experiments at the GTS (Mori et al. 2003), and by apparent plutonium colloid migration at the Nevada Test Site (Kersting et al. 1999), SKB initiated a program of in-situ colloid migration experiments at the Äspö Hard Rock Laboratory (HRL), as part of the Colloid Dipole Project. SKB's Colloid Dipole Project was initiated in 2000 (SKB 2004). The location for the in-situ colloid migration experiment was the TRUE-1 site, which was the location of the first stage of the Tracer Retention Understanding Experiments (TRUE), described by Winberg et al. (2000). The tracer injection borehole (KXTT4) and the tracer recovery borehole (KXTT3) intersect Feature A at a separation distance of 4.68 m. Feature A, with a total thickness of 0.05 to 0.09 m, contains a main fracture which follows a reactivated mylonite. Feature A is relatively simple, with a single fracture, having an aperture estimated in the range of 1 to 3 mm. Feature A has a transmissivity of 8×10^{-9} to 4×10^{-7} m^2/s, and a specific storage of 1×10^{-6} to 2×10^{-5} m^{-1}, based on hydraulic response tests. The groundwater chemistry of Feature A is classified as saline, with Cl > 5000 mg/L. The main cation:anion components are Na-Ca-Mg-K:Cl-SO_4-HCO_3. The TDS varies from 7.0 to 10.2 g/L, giving an ionic strength of 0.15 to 0.23 mol/L.

In 2006 the in-situ colloid migration experiments were performed at the TRUE-1 site, using KXTT4 and KXTT3 as the injection and withdrawal boreholes. The colloid tracers included 50 and 100 nm latex spheres, and uranine as the solute tracer. Solute and colloid tracers were injected separately. The experimental flow conditions were based on scoping calculations that identified minimum flow rates required to produce measurable tracer recovery. The injection rate for colloids was 10 mL/min and the withdrawal rates were 300 and 800 mL/min, resulting in an average groundwater velocity of about 0.9 m/h. This is significantly higher than natural groundwater velocities, which may be closer to 0.005 m/h. The results from the TRUE-1 site were used to initiate planning for new experiments, possibly at the TRUE-Block site. Bentonite colloids were not used because laboratory experiments had shown that they were not stable in the saline Äspö groundwaters.

In 2006 a program of laboratory migration experiments, which were funded by OPG's Deep Geologic Repository Technology Program (DGRTP), was performed at AECL's Whiteshell Laboratories with the intention of complementing the field tests at Äspö (Vilks and Miller 2007). This program included migration experiments using both bentonite and latex colloids that were performed in the single fracture within a block of granite (Figure 1) to (1) contribute information that was useful in planning concurrent field tests at Äspö and (2) provide additional information that cannot be obtained on the field-scale regarding bentonite versus latex sphere colloid transport, particularly at low flow rates.

Figure 1: Quarried Block Sample Opened for Inspection of Fracture Surfaces

The goal of the lab-scale experiments was to characterize the transport of bentonite colloids together with latex spheres as a function of flow velocity and groundwater ionic strength. The latex spheres provide a link between lab-scale experiments and the field scale experiments undertaken at the Äspö TRUE-1 site. The specific focus of the laboratory experiments was to identify flow velocities and water compositions that favour bentonite colloid transport.

Migration experiments with bentonite colloids and 100 nm latex spheres were performed using deionized water as the suspending media, with progressively decreasing flow velocities of 0.4, 0.034 and 0.0047 m/h. The final tracer test for 2006 consisted of filling the Quarried Block with synthetic Äspö groundwater and injecting bentonite colloids suspended in deionized water, followed by tracer-free synthetic Äspö groundwater.

The 2006 laboratory experiments (Vilks and Miller 2007) found that in dilute water at high flow velocities around 0.4 m/h, typical of field-scale tracer tests, bentonite and 100 nm latex colloids had similar transport behaviour, displaying good mobility and recovery. This suggests that high flow conditions may not discriminate between the transport properties of colloids of various sizes, and therefore, one should not base the understanding of colloid transport solely on the basis of field tests using high flow. Intermediate flow rates, with average velocities around 0.034 m/h, provided conditions under which the differences in transport behaviour of bentonite and 100 nm latex colloids became evident. The transport of bentonite colloids was significantly reduced, while that of 100 nm latex was not. At the very low flow rates, around 0.0047 m/h, more typical of natural flow rates, bentonite colloids were transported at a significantly reduced rate. Although the transport of 100 nm latex colloids was also reduced, the latex was more mobile than bentonite.

At low flow rates bentonite colloid transport was dominated by the small particles (4 to 15 nm), while the larger bentonite colloids (100 nm to 1 micron) were not readily transported in the experimental time frame. In contrast, the 100 nm latex colloids were efficiently transported, in agreement with the results of previous studies, and as predicted by filtration theory. The reason for the observed difference in the size related behaviour of bentonite and latex colloids has not been established. Possible explanations could be the higher density of bentonite

colloids, the more complex charge distribution on bentonite surfaces, different surface geometry between bentonite and latex colloids and that the larger particles in bentonite tracer suspensions were actually flocs that dispersed into smaller particles while residing in the fracture.

In saline, Äspö type ground waters bentonite colloids were flocculated and not mobile. Approximately 10 percent of bentonite colloids deposited in the presence of saline water, were mobilized when saline water was replaced by dilute water under conditions of high flow.

Colloid suspensions appear to influence the breakthrough curves of co-injected solute tracers. Although this effect needs further investigation, it is recommended that experimental programs studying colloid transport include injections of colloid-free solute tracers to help reduce the uncertainties in interpretation of test results.

In 2007 the work scope formerly funded by OPG's DGRTP was taken over by Canada's Nuclear Waste Management Organization (NWMO). This report describes the results of an experimental program, funded by NWMO and SKB, intent on improving the understanding of mechanisms that influence bentonite colloid transport in fractured rock. The objectives of the experimental program were to address some of the remaining issues from the 2006 laboratory colloid migration experiments by performing experiments with latex colloids in saline water, to explore the effects of particle size on bentonite and latex colloid transport, and to provide additional colloid transport data, suitable for modelling, for longer transport distances and low transport velocities.

1.1 DISCUSSION OF COLLOID TRANSPORT THEORY

Historically it has been known that colloid mobility is determined by water velocity, particle size, particle density, particle geometry and colloid surface chemistry. Since the diffusion rate of colloids may be orders of magnitude lower than for dissolved molecules, advective processes would tend to control colloid transport. Particle size and geometry play a major role through their effect on sedimentation rates and on the ability of the geologic media to physically strain colloids from moving fluid. Colloid chemistry determines the nature and stability of particle surface charges, which affect the ability of colloids to stay in a stable suspension, or to be adsorbed to geologic media.

Properties of the hydrologic system (fracture) also have a major influence on colloid mobility. Since colloid transport appears to be significantly reduced at low water velocities, experimental systems should evaluate the effect of average flow rate and attempt to simulate natural flow conditions as closely as practicable. When transport in a single fracture is considered the fracture aperture distribution should have a significant effect by channelling flow and influencing the variation in local flow velocity. Variations in flow velocity might play a role in trapping colloids in certain regions of the fracture system. Colloid retention may also be influenced by fracture surface roughness and the presence of sand to silt size mineral deposits that could increase the surface area for attachment or even act as porous media filters on a local scale for larger colloid particles. Fracture mineral surface chemistry will also influence colloid retention through surface charge effects. Finally, the water chemistry (pH, ionic strength, proportions of univalent and divalent cations) will have a significant influence on colloid stability (coagulation and settlement) and the ability of colloids to stick to mineral surfaces.

The filtration of particles through porous media has been described by an empirical equation (Iwasaki 1937) that describes particle removal from solution with first-order kinetics with respect to particle concentration in the fluid (C):

$$\frac{dC}{dx} = -\lambda C \qquad (1)$$

where the distance travelled through a porous medium is x, and λ is the filtration coefficient. The filtration coefficient is determined by measuring the change in particle concentration from the initial concentration (C_0) to the concentration (C(L)) after the fluid has travelled a distance L:

$$C(L) = C_0 e^{-\lambda L} \qquad (2)$$

The filtration coefficient is a function of particle size, so that (Eq. 2) only applies to particles with a uniform size. In a porous medium, the filtration coefficient can be expressed as a function of the probability of the particle colliding with the media (η), the probability of the particle sticking to the media (α), the diameter of the grains in the porous media (d), and the porosity of the media (f).

$$\lambda = \frac{3}{2}(1-f)\frac{\alpha\eta}{d} \qquad (3)$$

To account for the effect of particle size, physical/chemical filtration has been modelled by Yao et al. (1971), who calculated a filtration coefficient based upon the probability of particles colliding with the media (η). The probability of particles sticking to the media, or sorption efficiency (α), was assumed to be constant or equal to 1. The value for η is determined by particle density, grain size of the media, water velocity, and the size of migrating particles. Particle collisions with the media will increase with particle size for particles larger than about 0.2 μm, which are affected by gravitational sedimentation. Larger particles are also likely to be stopped by straining as their size approaches that of spaces between solid surfaces. However, for very small colloids the probability of colliding with the media will actually increase with decreasing particle size. In the absence of sedimentation, particle migration towards the media will be strongly influenced by particle diffusion, which increases with decreasing particle size. Assuming the sorption efficiency (α) remains the same, there is a certain particle size that has a minimum filtration coefficient for a given filtration medium. For example, the filtration coefficient for a medium of 0.4-mm glass beads had a minimum for particles from 0.6 to 5 μm, depending upon the particle density. As shown by Yao et al. (1971), the filtration coefficient also increases with lower flow rates, because of the increase in the probability of particle collisions with the media (η). For example, a 1 μm particle may have a clean medium filtration coefficient of around 0.1 cm^{-1} with a water flow rate of 100 m/d, but with a flow of 10^{-2} m/d the filtration coefficient increases to 10^2 cm^{-1} (McDowell-Boyer et al. 1986). For reference, natural flow velocities in plutonic rocks of the Canadian Shield are usually less than 5 x 10^{-3} m/d (Vilks and Bachinski 1994).

A detailed review of colloid transport in fibrous porous media, which takes into account various forces acting on a particle, is given by Guzy et al. (1983). These forces include (1) inertial

forces, (2) Brownian motion, (3) gravitational settling and buoyancy, (4) London-van der Waals attraction, (5) the electric double layer, and (6) hydrodynamic drag. Colloid transport and capture in an ideal fracture, with flow rates from 0.5 to 2 cm/s, is discussed by Bonano and Beyeler (1984). The transport model they used included the effects of fluid drag, gravity, London-van der Waals forces, and the electric double layer, but it did not consider diffusion. The model predicted that particle capture increased with particle size and production rate. The fluid velocities considered did not affect the capture rate. Particles tended to travel in regions of the highest fluid velocities, and therefore may travel faster than the average fluid velocity. This effect is also known as hydrodynamic chromatography (de Marsily 1986), since particles of different size can be separated on the basis of their elution velocities through porous media. The ratio between particle velocity and fluid velocity is usually between 1 and 1.1, with 1.4 being an extreme case (de Marsily 1986).

In this study, since the transport media is a fracture, the porosity and grain diameter terms used in porous media models would be replaced by terms representing the geometry of the fracture, as described by Chrysikopoulos and Abdel-Salam (1997). The filtration of particles in a fractured media is determined by the following phenomena:

- Particle collision with a fracture surface (Quantified as a probability of 0 to 1.) This is influenced by the ability of particles to escape streamlines by diffusion or sedimentation, which is determined by competition between flow velocity and particle diffusion or sedimentation rates.
- Particle capture within a stagnant zone of lesser or no flow.
- Particle sticking to geologic media (Defined as the probability of sticking to a surface once a collision has been made.). The ability of a particle to stick is influenced by (1) axial fluid pressure, (2) friction between particles and surfaces, (3) Van der Waals attraction opposing the repulsive forces of like charge on particles and the rock media, (4) the interaction of opposite charges, and (5) chemical bonding.

1.2 LABORATORY EXPERIMENTS PERFORMED IN A QUARRIED BLOCK

The Quarried Block (QB) sample is a 1m x 1m x 0.7 m block of granite containing a single, well characterized, through-going variable aperture fracture. The fracture is clean in that it is free of fracture filling minerals. The unique advantages of using the QB to study colloid transport in fractures are:

- Experiments can be performed on an intermediate scale, bridging the gap between small scale laboratory experiments (several cm) and larger scale field experiments (several m).
- Since the fracture can be accessed by numerous boreholes it is possible to set up different test flow systems with different separation distances, and it is possible to survey tracer distributions within the fracture while tracer tests are in progress.
- It is possible to vary the groundwater compositions, which is not possible at the field scale.
- Unlike in field tests, one can use low flow rates more representative of natural conditions.
- After completion of tracer tests the fracture can be opened up to quantify colloid deposition on fracture surfaces.

- A digital model of the fracture aperture distribution exists, which can be used to model velocity distribution within the fracture and to simulate particle transport.

The QB sample was previously excavated from Subvertical Joint Zone 2 (JZ2), also known as the “Room 209 Fracture,” at the 240 level of AECL’s Underground Research Laboratory (URL). This Joint Zone originates from Fracture Zone 3 and terminates just below and to the south east of the 240 level. It is the only hydraulically active fracture at the 240-level.

The quarried block sample was coated with a silicone material to prevent loss of moisture from the fracture and from the interconnected pore space in the rock matrix. The block was also fitted with stainless steel frames on the top and bottom sides to help facilitate the opening and closing of the fracture. The quarried block was placed in such a way that the fracture plane was sub-horizontal to the support frame. This orientation, rather than the original sub-vertical orientation, would facilitate the instrumentation and testing of the fracture. The QB sample was opened up to expose the fracture surfaces in order to develop the fracture aperture distribution model (Figure 2) using an optical digitizing technique based on white light triangulation. Four keys located on the sides of the Quarried Block are used as reference points and guides to help reassemble the upper and lower fracture surfaces. The fracture can be accessed for sampling or tracer injection from the top of the block via 17 test boreholes, which are packed off and terminate at the fracture plane (Figure 2). Four mini-plena also provide access to the fracture plane where it intersects two sides of the block (Figure 2).

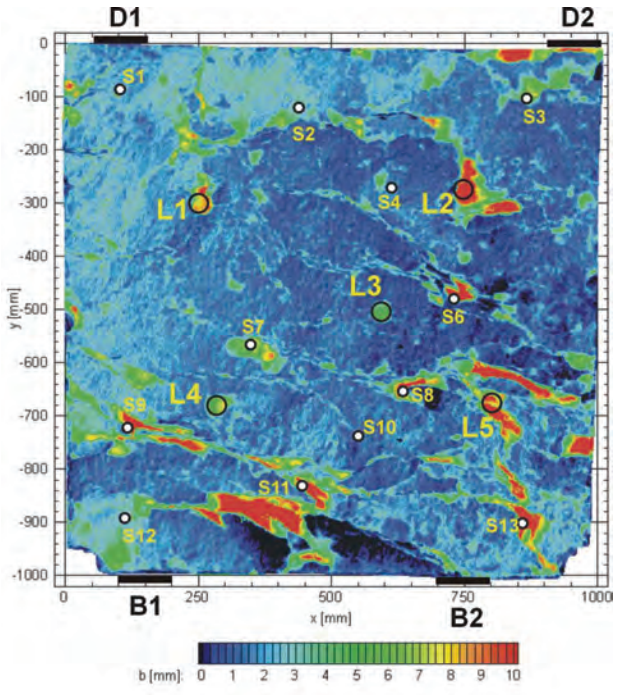

Figure 2: Borehole and Mini-plena Locations Plotted on Digitized Aperture Distribution for the QB Fracture

1.3 EXPERIMENTAL PLAN

Work scope for 2007 would focus on performing laboratory experiments to support the Colloid Dipole Project. The goal of the experiments is to improve the understanding of mechanisms responsible for bentonite colloid generation and transport in granite fractures. Phase I would be devoted to completing the study of colloid migration in saline Äspö-type groundwater, started in 2006, by performing tests with 100 nm latex spheres to provide a comparison to the transport behaviourof bentonite colloids. Phase 2 and Phase 3 would focus on performing migration experiments with bentonite and latex colloids in dilute water to improve understanding of colloid migration and to provide SKB with data that will be modelled for the purpose of estimating colloid retardation and filtration coefficients. Phase 2 would specifically focus on the effects of particle size in monodisperse and polydisperse suspensions on the transport of bentonite and latex colloids. Phase 3 would investigate latex and bentonite colloid migration using a significantly longer borehole separation distance (1100 mm), and a low flow velocity close to natural conditions. Phase 4 would consist of opening the fracture for post-test analyses that would be used to visualize and quantify the extent of colloid deposition within the fracture.

Table 1: Summary of Experiments Performed in 2007

	Activity	Tracer Test	Tracers in Order of Injection
Phase 1	Inject latex suspended in saline water (L1-L4), Flow = 50 mL/h	2007 TT1	1. Br 2. 100 nm latex + I
	Inject latex suspended in dilute water (L1-L4), Flow = 50 mL/h	2007 TT2	1. 100 nm latex + I
Phase 2	Inject latex colloids as monodisperse suspensions (L1-L4), Flow = 50 mL/h	2007 TT3	1. Br 2. 20 nm + I 3. 100 nm + I 4. 1 μm + I
	Inject polydisperse latex suspension (L1-L4), Flow = 50 mL/h	2007 TT4	1. Br 2. latex mixture + I
	Inject small (5-15 nm) bentonite colloids (L1-L4), Flow = 50 mL/h	2007 TT5	1. Br 2. 5-15 nm bent
	Inject large (100-500 nm) bentonite colloids (L1-L4), Flow = 50 mL/h	2007 TT6	1. Br 2. 100-200 nm bent
	Inject large (>500 nm) bentonite colloids (L1-L4), Flow = 50 mL/h	2007 TT7	1. Br 2. > 500 nm bent
Phase 3	Inject bentonite and latex colloids (S3-S12), Flow = 500 mL/h	2007 TT8	1. Br 2. bent 3. 100 nm latex + I
	Inject bentonite, (S3-S12), Flow = 6 mL/h	2007 TT9	1. Br 2. Bent
	Inject latex colloids (S3-S12), Flow = 6 mL/h	2007 TT10	1. 20 nm, 100 nm, 1 μm latex +I
Phase 4	Inject additional latex colloids (L1-L4), Flow = 500 mL/h Post-test Analysis	2007 TT11	1. 1 μm, 500 nm

2. COLLOID MIGRATION EXPERIMENTS

2.1 METHODS

Tracer Tests: All tracer tests were performed in the Quarried Block as dipole experiments. The separation distances varied from 380 mm (L1 to L4) to 1100 mm (S3 to S12). The tracer and tracer-free solutions were contained in separate reservoirs such that liquid levels could be maintained at the same fixed heights above the top of the block to ensure a constant head and saturation of the fracture. Water outflow was controlled by either a needle valve or peristaltic pump at the withdrawal borehole. Hydraulic heads were checked in all boreholes before the start of each tracer test to ensure that the Quarried Block is fully saturated. Water was allowed to flow between injection and withdrawal boreholes for a minimum of 24 hours before beginning tracer injections to establish a stable flow system and to monitor the flow rate. Tracer injection was initiated by using a valve to switch the source of the input to a constant head tracer reservoir. After injecting 380 to 453 mL of tracer, the source of injected water was switched back to tracer-free solution. Latex and bentonite colloid tracers were injected as separate pulses, separated by a sufficiently large volume (4 to 10 L) of tracer-free water to minimize any interference between tracers. After elution volumes ranging from 2.8 to 4.4 L since the start of a given tracer injection (one fracture volume equivalent to approximately 2.5 L), water in the fracture was sampled from the other boreholes and mini-plena attached to the sides of the block in order to determine the spatial distribution of tracers remaining in the fracture. Each sampling location was flushed with a 20 mL volume before collecting a sample, which also has a 20 mL volume. The tracer concentrations from 17 boreholes (including the injection and withdrawal holes) and the 4 mini-plena were used to produce contour plots showing tracer distributions within the fracture.

The ionic medium for tracer tests was either filtered (200 nm) deionized water or a saline synthetic Äspö-type groundwater. The saline water was made up to contain 1.70 g/L Na, 0.66 g/L Ca, 0.08 g/L Mg, 0.01 g/L K, 3.80 g/L Cl and 0.30 g/L SO_4. The solution had a pH of 7.7, a TDS of 6.55 g/L and an ionic strength of 0.14 mol/L. After being exposed to the fracture the deionized water acquired salts from the rock to give the solution an ionic strength of 0.001 mol/L and a pH of 7.5 ± 0.3. The bentonite colloids were prepared by suspending MX-80 bentonite in deionized water and allowing the suspension to settle to eliminate the larger particles. Latex colloids used in tracer tests included 20 nm, 100 nm and 1 μm sizes. Latex colloids were labeled with distinctive fluorescent dyes available in different colours [red (580/605), orange (540/560), yellow-green (505/515), blue (360/415)], with characteristic excitation and emission wavelengths (nm). Colloidal tracers were co-injected with iodide (NaI) as a conservative solute tracer. Colloid-free tracer solutions of bromide (LiBr) were injected to provide a reference breakthrough curve for solute that was not affected by the presence of colloids.

Analytical Methods: The concentration of bentonite colloids was determined by light scattering using a fluorometer with the wavelength set to 280 nm. The detection limit of this technique was 0.01 mg/L bentonite. The concentrations of latex colloids were determined by fluorescence, and the bromide concentrations were measured by ion chromatography. Iodide was determined by ion chromatography and with an ion selective electrode.

The MICROTRAC Ultrafine Particle Size Analyzer (UPA) was used to measure bentonite colloid size distribution and to provide an additional estimate of colloid concentration in the main elution

peak. The UPA is a laser based instrument that determines the size of particles between 0.0038 and 6.5 μm by dynamic light scattering. The UPA measures the Doppler shift in the frequency of light scattered by particles to determine their Brownian motion, which is related to particle size. If a sample being analyzed by the UPA has a very broad size distribution, the presence of larger particles tends to dominate the scattered light and mask the presence of smaller particles. To determine the presence of smaller particles it was necessary to remove the larger particles from a sample by filtration or centrifuging. Those samples, which contained significant amounts of particles larger than 100 nm were subjected to a two step size analyses. Samples were analyzed with the UPA before and after being centrifuged at 8000 rpm (6200 x g) for 10 minutes to remove particles larger than about 90 nm (assuming a bentonite density of 2.5). The total particle concentrations in the sample were measured with the fluorometer before and after centrifugation to determine the concentrations of large and small colloids.

Once tracer tests were complete the Quarried Block was opened up to expose the upper and lower fracture surfaces. The fracture surfaces were illuminated with UV light to induce fluorescence in deposited colloids, and to help visualize the transport paths used by latex colloids. In addition, the fracture surfaces were swabbed at specific locations in order to survey the distributions of bentonite and latex colloids.

2.2 PHASE 1: LATEX COLLOID TRANSPORT IN SALINE WATER

The objective of this experiment was to determine the transport properties of 100 nm latex spheres in saline Äspö-type groundwater to provide a comparison to the previously studied transport properties of bentonite colloids (Vilks and Miller 2007). This experiment also explored the effects of tracer density and buoyancy in transport experiments. The experimental conditions were identical to those used for studying bentonite colloid transport in saline water (Vilks and Miller 2007), using L1 as the injection hole and L4 as the withdrawal hole. Phase 1 consisted of two tracer tests. In test 2007 TT1 the injected 100 nm latex tracer was suspended in saline water so that density differences did not affect tracer transport. Latex colloid breakthrough curves were expected to be similar to the tests performed in dilute water. In test 2007 TT2 the injected 100 nm latex tracer was suspended in deionized water, to recreate the conditions in the 2006 experiment with bentonite colloids. As in the 2006 experiment, the tracer injection was followed by tracer-free Äspö-type water. Density effects were expected to direct tracer movement to the upper part (right hand) of the fracture.

Methods: Before starting Phase 1, The Quarried Block, including the main fracture and all connected pore spaces, was drained to remove the dilute water remaining from the 2006 experiments. The Quarried Block was refilled with saline Äspö-type groundwater (with TDS of 6.55 g/L and ionic strength of 0.14 mol/L), and purged to remove any entrapped air. The tracer tests were performed under conditions of intermediate flow, in which water outflow was controlled by a peristaltic pump at the withdrawal borehole, with a resulting flow rate of 50 mL/h. This flow rate corresponds roughly to an average velocity of 0.038 m/h, based on the borehole separation distance of 380 mm, and considering 500 mL as an approximate elution volume for the first major peak. Saline water was used as the tracer-free eluant in these tracer tests.

Saline water was allowed to flow between L1 and L4 for a period of 42 hours before starting tracer test 2007 TT1 with an injection of colloid-free bromide tracer, containing 75 mg/L Br as LiBr. The injected volume of the Br tracer was 484 mL. The Br tracer was followed by 1100 mL of tracer-free saline solution before injecting the second tracer, containing 17.4 g/L of 100 nm

latex colloids and 90.6 mg/L of iodide (as NaI), suspended in saline solution. The total volume of colloid tracer was 422 mL. A borehole survey was performed 2750 mL after injecting colloids. By the end of the tracer test, a total volume of 10.9 L of saline water was injected following the colloid tracer. At this point 3600 mL of saline were used for flushing the fracture through various boreholes to remove latex colloids. After this flushing, the flow field was allowed to stabilize for 62 h before starting tracer test 2007 TT2. Bromide tracer was not used in this next test because results from the previous test showed that the high salinity interfered with Br analyses. Tracer test 2007 TT2 was started by injecting 498 mL of tracer containing 75.8 mg/L of iodide and 19.4 mL of 100 nm latex colloids suspended in deionized water. After a tracer volume of 498 mL, the injection was switched to tracer-free saline water. The post-test survey was performed after 3580 mL since the start of the tracer test. The tracer test was continued for a total volume of 4647 mL.

The target concentration of latex colloids was kept in the range of 10 to 25 mg/L to reduce the risk of coagulation in saline water, while providing sufficient tracer to have a good breakthrough curve. A size analyses of the 100 nm colloid tracer, using the UPA, produced a clear peak corresponding to an average size of 100 nm. However, a size analyses of the 100 nm latex colloids suspended in the saline solution showed that the latex colloids had formed flocs with an average size of 1.6 μm.

Results: The breakthrough curves for tracer test 2007 TT1 are presented in Figure 3 and tracer recoveries are shown in Figure 4. The principal characteristics of these breakthrough curves, as well as those from all of the other tracer tests in this study, are summarized in Table 2 of the Discussion section. Although bromide was injected as the first tracer in 2007 TT1, it could not be detected in the eluted saline water due to interferences from the high concentrations of anions. The iodide, which was co-injected with the colloid, had a recovery of 86% at the reference elution volume of 3600 mL. This recovery was typical for solute tracers observed in this borehole pair for experiments with dilute water. The 100 nm latex colloid eluted slightly ahead of the iodide, although the colloid recovery was only 22%. Experiments performed with this borehole combination, using dilute water at the same flow rate, would have produced recoveries around 70% for 100 nm latex. As mentioned previously, size analysis has shown that the 100 nm latex colloids had flocculated in saline water to produce flocs with an average size of 1.6 μm. This suggests that the transport behaviour of the 100 nm colloids in saline water were determined by the size of their flocs. The results of the post test fracture survey (Figure 5) show that iodide was concentrated along the left side of the block, and had not migrated up the fracture slope to the upper right corner. This indicates that density effects were not a factor when the density of tracer solutions is matched to that of water in the fracture. Latex colloids were concentrated to the right side of the L1-L4 borehole pair.

The breakthrough curves for 2007 TT2 are shown in Figure 6, with recovery curves given in Figure 7. When the tracer was suspended in dilute water, no iodide was recovered from L4 and the recovery of latex dropped to 0.3%. The post test survey (Figure 8) shows that the iodide and latex colloids were found in the upper right hand corner. This is consistent with a buoyancy effect forcing the less dense tracer solution to migrate up the fracture slope to the upper right hand corner of the Quarried Block. Conductivity measurements were used to identify the presence of less dense, dilute water, and to show that the less dense tracer had indeed migrated up the fracture slope and would not readily flow towards the outlet borehole at L4 (Figure 9). Although the elution data from L4 indicated that latex colloids were not transported, the post test fracture survey suggests that the latex colloids had migrated to the same extent as iodide. However, it should be noted that in the fracture surveys for both tests in

saline water the measured C/Co values for latex colloids were an order of magnitude lower than for iodide.

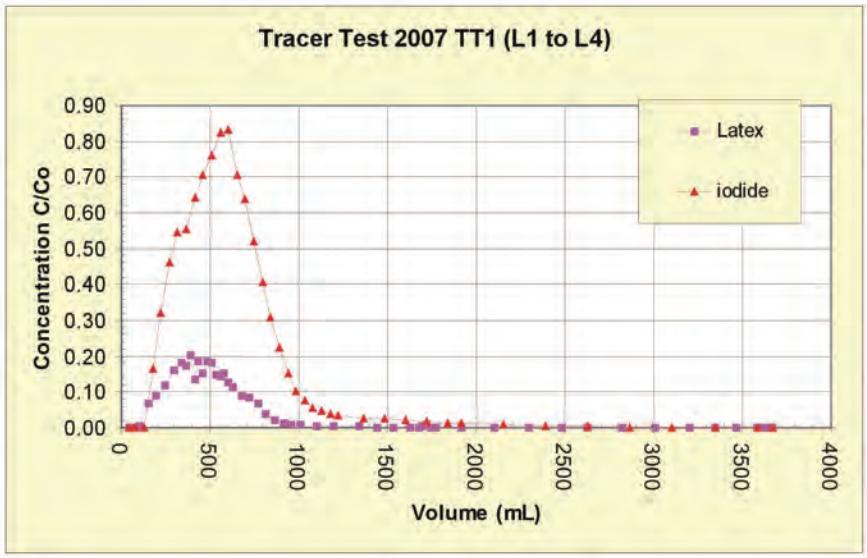

Figure 3: Breakthrough Curves for 2007 TT1

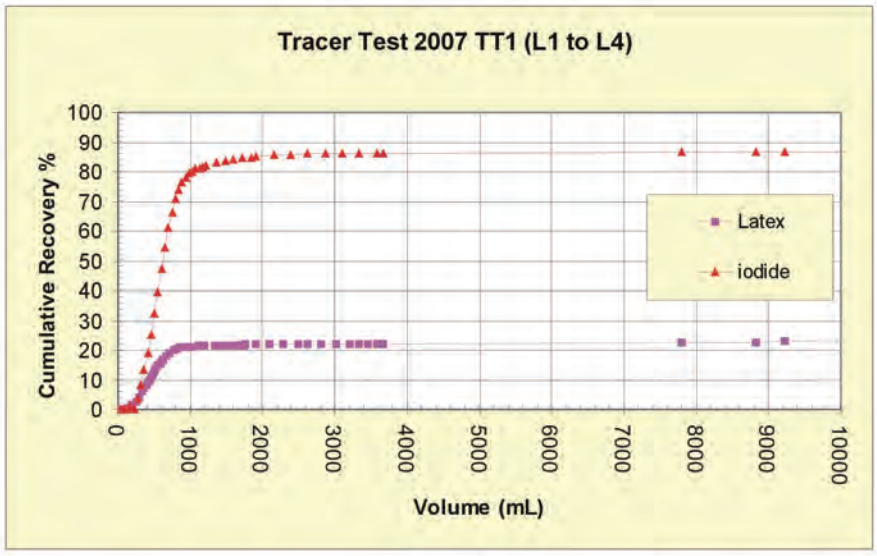

Figure 4: Recovery Curves for 2007 TT1

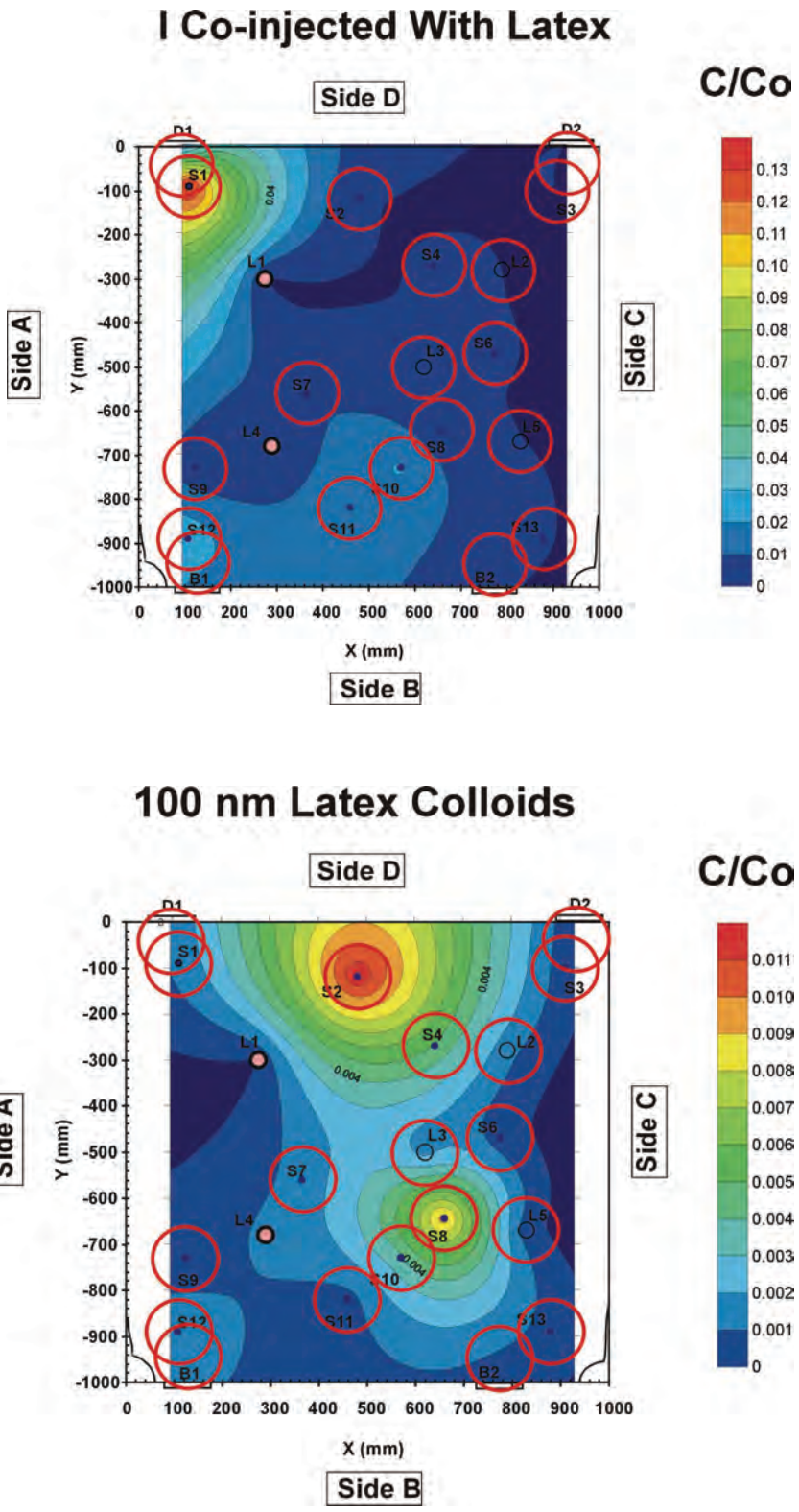

Figure 5: Post Test for 2007 TT1

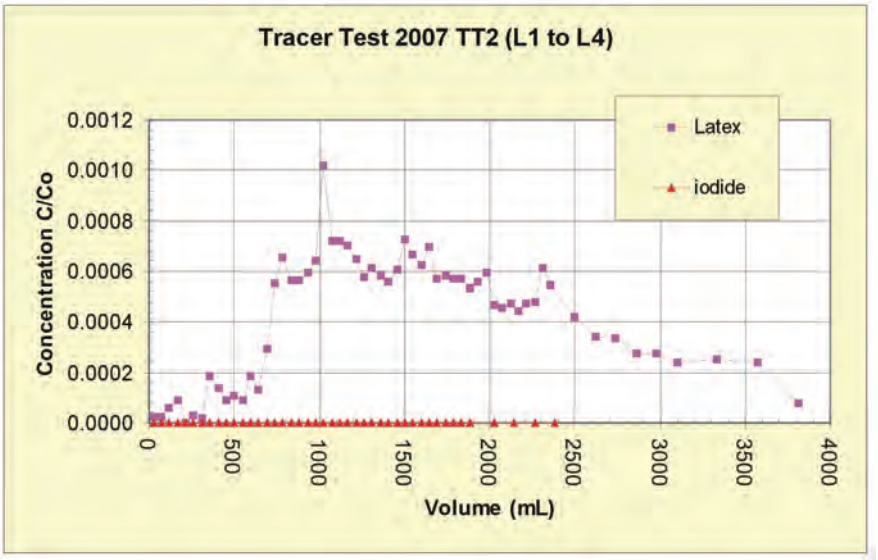

Figure 6: Breakthrough Curves for 2007 TT2

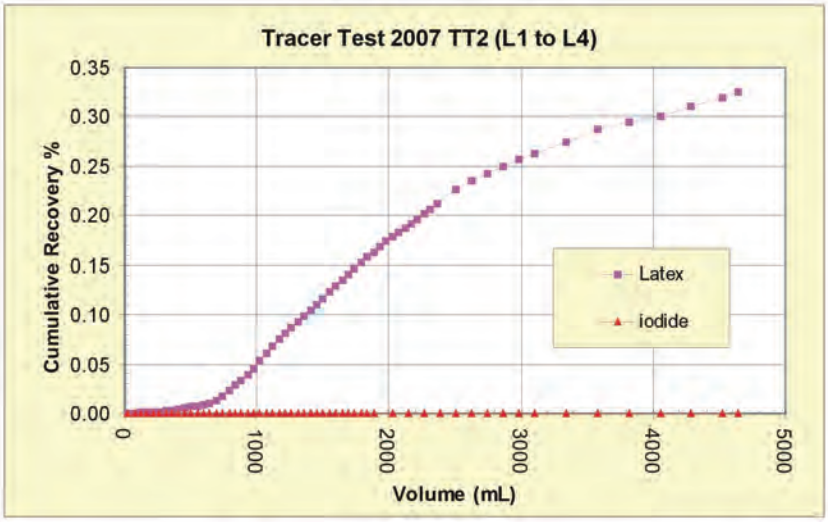

Figure 7: Recoveries for 2007 TT2

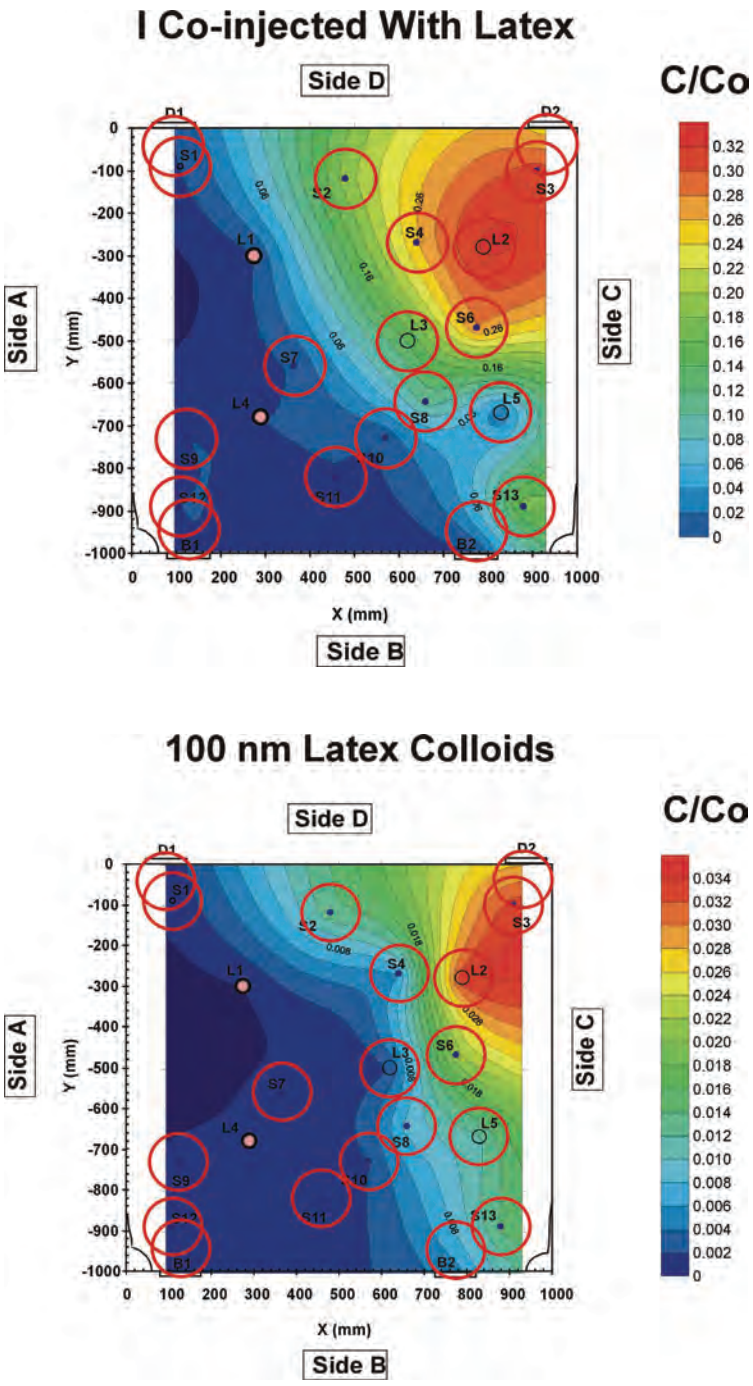

Figure 8: Post Test Survey For 2007 TT2

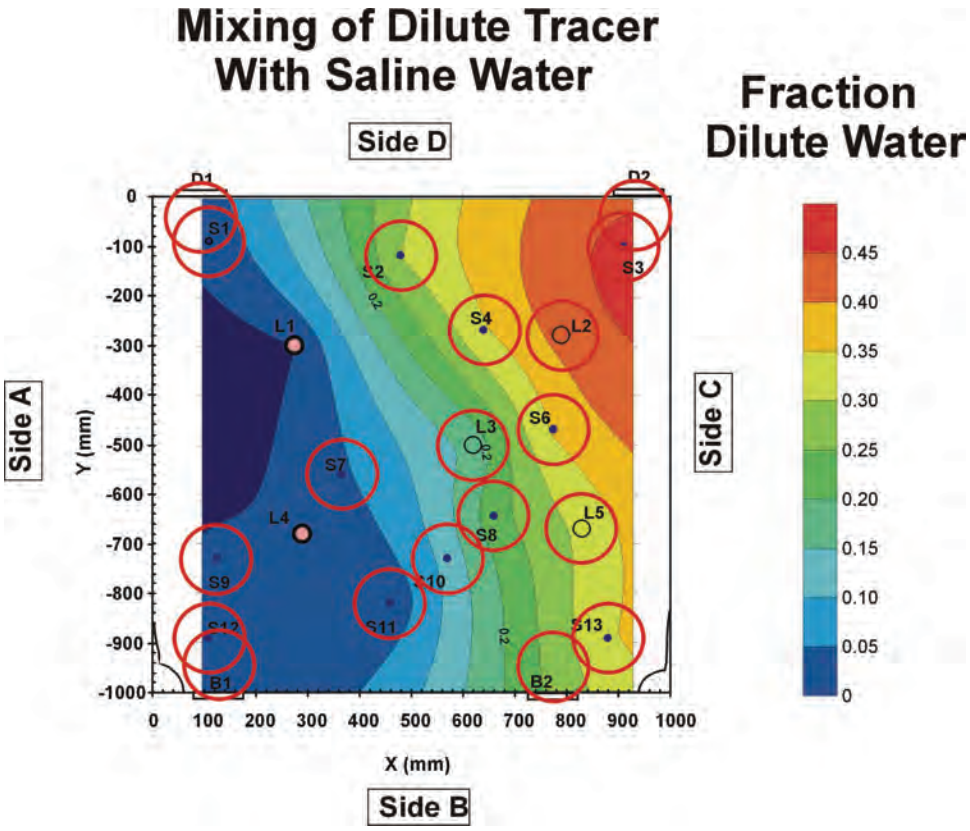

Figure 9: Distribution of Dilute Water from Tracer at the Time of the Post Test Survey (after 3580 mL Since the Beginning of Tracer Injection) Showing that the Less Dense Water from the Tracer Had Migrated Up the Slope of the Fracture Due to Buoyancy Effects

2.3 LOW IONIC STRENGTH

2.3.1 Phase 2: Effect of Particle Size on Colloid Transport

The objectives of these experiments were to improve the understanding of the effects of particle size on the transport of bentonite and latex colloids, and to determine whether these colloids are transported differently as polydisperse suspensions compared to monodisperse suspensions. The experiments were performed using the L1 and L4 borehole pair, and a flow rate of 50 mL/h, which corresponds to an average velocity of 0.038 m/h. Deionized water was used as the suspending media to ensure adequate stability for the bentonite colloids. The latex colloids included 20 nm, 100 nm and 1 μm sizes.

2.3.1.1 Effect of Size on Latex Colloid Transport

The goal of these experiments was to evaluate the transport behaviour of latex colloids with different sizes and determine whether colloid transport was affected by the interactions of colloids of different sizes. Latex colloids were used because they can be obtained with distinct narrow size ranges. First the different size latex colloids were injected as separate pulses to provide a benchmark for their transport as monodisperse suspensions. Iodide was co-injected with each pulse. Next the latex colloids were combined to make a polydisperse suspension that would be injected as a single pulse to evaluate the impact of particle-particle interactions. Iodide was again co-injected as a conservative tracer.

Methods: After the completion of tracer tests using saline water, the Quarried Block was fully drained of the higher salinity water. The fracture system was flushed with deionized water to remove traces of saline solution. The Quarried Block was then fully drained once again and then saturated with deionized water.

Deionized water was allowed to flow from L1 to L4 before initiating tracer test 2007 TT3. The first tracer to be injected was a 382 mL volume of colloid-free bromide solution, containing 88.3 mL of Br. This was followed by 658 mL of deionized water before injecting the first colloid tracer (372 mL), containing 67.1 mL of 20 nm latex colloids and 82.7 mg/L iodide. The first survey of fracture tracer concentrations was performed at 2380 mL after the start of the colloid tracer injection. The second colloid tracer was injected 2610 mL after the completion of the first colloid injection, and contained 75.4 mg/L of 100 nm colloids and 81.3 mg/L iodide. The total injected volume of the second colloid tracer was 382 mL. The second fracture survey was performed at 3610 mL after the start of the second colloid tracer injection. The final colloid injection was started 3820 mL after the finish of the previous colloid injection. The final colloid tracer (380 mL) contained 49 mg/L of 1 μm latex colloids and 82.9 mg/L of iodide. The third fracture survey was performed at 3350 mL after the injection of 1 μm colloids. Water flow between L1 and L4 was maintained until the start of the next tracer test, 2007 TT4, amounting to a total volume since the start of the 1 μm colloid injection of 19.6 L.

The first tracer to be injected during 2007 TT4 contained 88.3 mg/L bromide, and had a total volume of 355 mL. The mixed colloid tracer (374 mL) was injected 685 mL after the completion of the bromide injection. The mixed colloid tracer contained 23.1 mg/L of 20 nm colloids, 20.2 mg/L of 100 nm colloids, 14.7 1 μm colloids, and 82.7 mg/L of iodide. The fracture survey was performed 2970 mL after the start of the colloid injection. Water flow was maintained for about 6.5 L since the completion of the colloid injection.

Results: The 2007 TT3 breakthrough curves for bromide and mono-disperse latex colloids are given in Figure 10, while the breakthrough curves of bromide are compared with iodide co-injected with the different sized latex colloids in Figure 11. Tracer recovery curves are provided in Figure 12. Although the first arrivals of the colloids were not consistently ahead of the separately injected bromide, the colloidal breakthrough peaks of the colloid tracers were always slightly head of bromide (see Table 2). The colloid first arrivals and breakthrough peaks were always ahead of the co-injected iodide. The tracer recoveries at 3600 mL were 95% for bromide, 62% for 20 nm colloids (76% for co-injected iodide), 73% for 100 nm colloids (~ 90% for co-injected iodide), and 25% for 1 μm colloids (~65% for co-injected iodide). Although the recoveries of the co-injected iodide were higher than those of the colloid, there appeared to be a correlation between the iodide recovery and the type of tracer it was co-injected with. As indicated in Figure 11, the transport behaviours of colloidal tracers appear to have some

influence on the breakthrough curves of co-injected solute. The colloid recoveries indicated that the mid-sized 100 nm colloids are transported more efficiently than the other colloids. This is consistent with colloid filtration theory which predicts that the smaller colloids, with their relatively higher diffusion coefficients are more readily removed from the transport path by dispersion, while the larger colloids are more readily removed by sedimentation. The breakthrough curve of the 1 μm colloids was rapidly attenuated after 500 mL, while the other colloids had longer tails extending out to as far as 1500 mL. This suggests that the transport of the 1 μm colloids may have been dominated by a single fast transport path, while the other colloids could travel through other slower paths. The post test fracture surveys are illustrated in Figure 13. The distributions of 100 nm and 1 μm colloids were similar those of their co-injected iodide, showing deposition mainly to the left of L1-L4, along with some accumulation to the right of L4. The recovered concentrations of the 1 μm colloids were significantly lower than those of iodide and the other colloids. The distribution of 20 nm colloids appeared significantly different from iodide and the other colloid tracers due to a very high concentration in a pocket around S8 and S10.

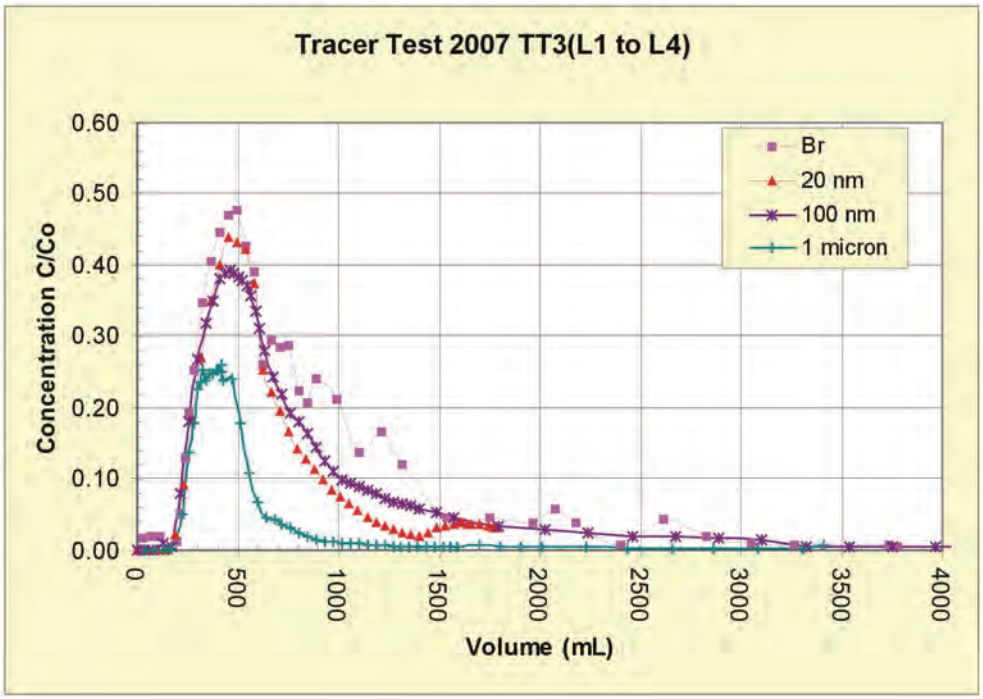

Figure 10: Breakthrough Curves Of Latex Colloids and Separately Injected Br

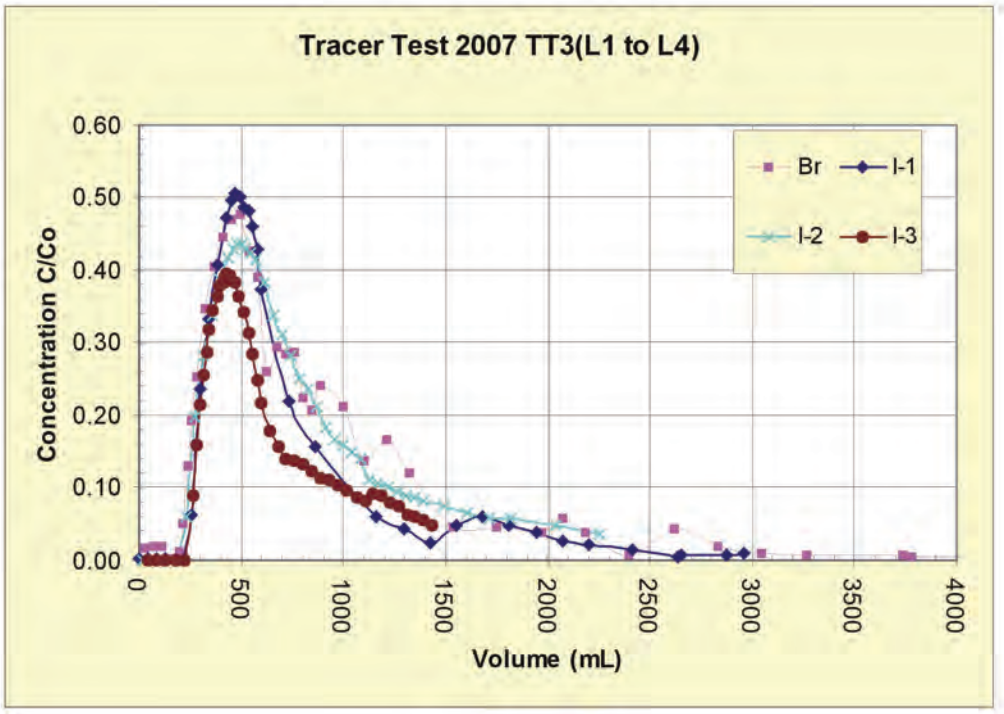

Figure 11: Breakthrough Curves of Solutes, Including Separately Injected Br and I Co-Injected with Colloids. I-1 with 20 nm, I-2 with 100 nm, and I-3 with 1 micron.

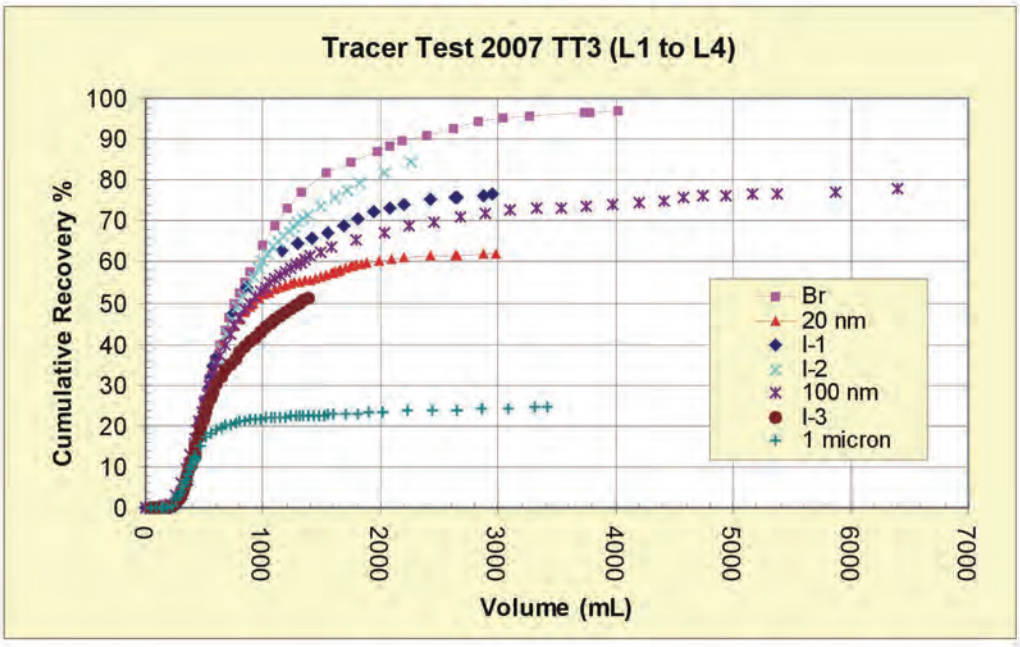

Figure 12: Recovery Curves of Solute and Colloidal Tracers from Mono-Disperse Injections (2007 TT3)

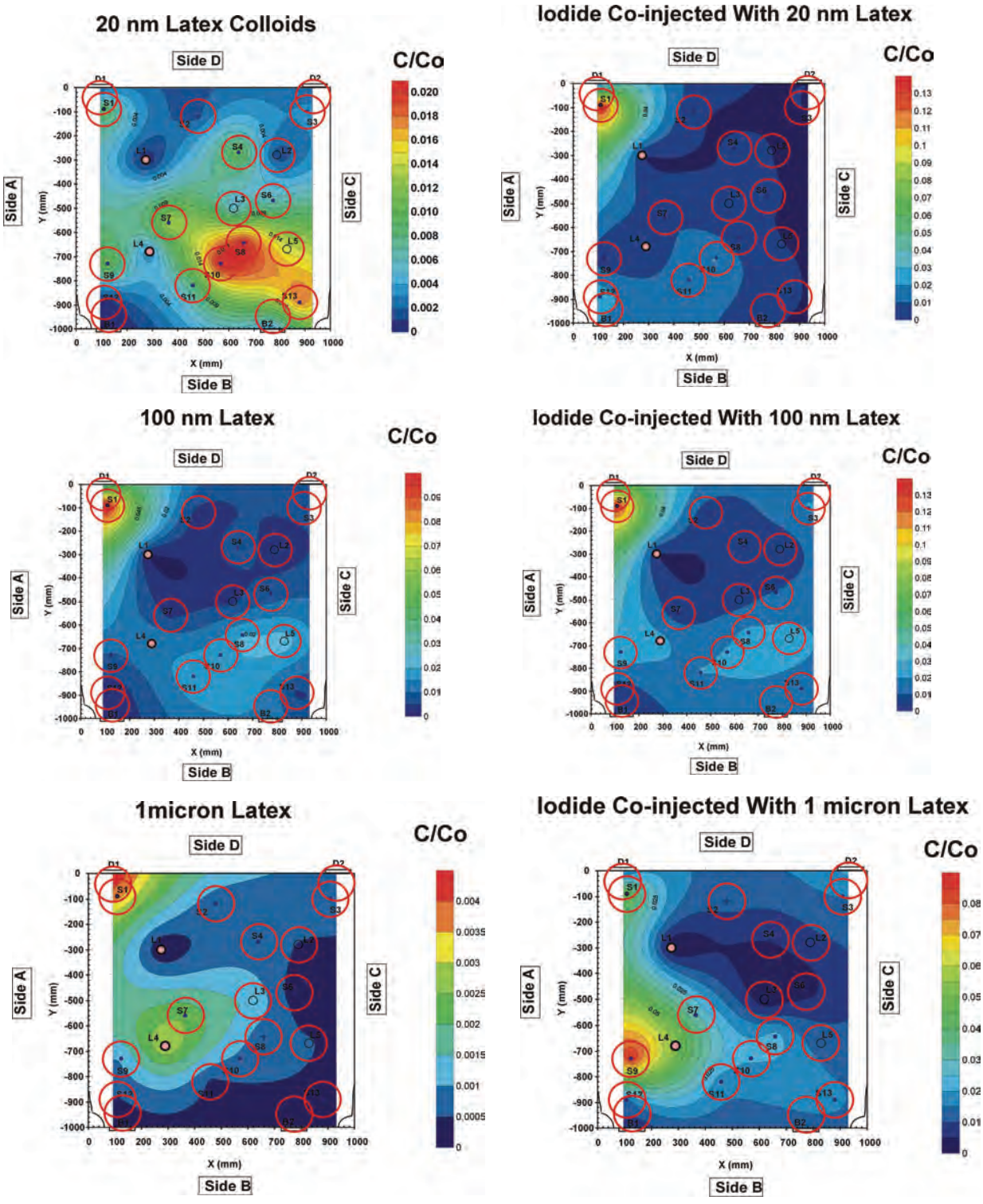

Figure 13: Post Test Survey For 2007 TT3

The colloid and solute breakthrough curves for 2007 TT4 tracers are illustrated in Figure 14, while the recovery curves are shown in Figure 15. The first arrivals of the different co-injected colloids were similar, although the main peak arrival of the 1 μm size was slightly ahead of the other colloids (Table 2). The main peak height was highest for the 100 nm colloids, followed by the 20 nm and 1 μm sizes. The tracer recoveries at 3600 mL were 66% (approximate) for bromide, 83% for co-injected iodide, 58% for 20 nm latex, 70% for 100 nm latex and 23% for 1 μm latex. Figure 16 compares the breakthrough curves for latex colloids injected as monodisperse suspensions with those of colloids with equivalent size injected as a single polydisperse suspension. Note that there is only one iodide breakthrough curve for iodide from 2007 TT4, while there are three separate iodide breakthrough curves for 2007 TT3. The colloid breakthrough curves for the polydisperse injection are similar to the curves obtained from monodisperse injections, although the peak heights and recoveries were slightly smaller for the polydisperse injection. The reductions in recovery for the polydisperse injection were 8% for the 20 nm colloids, 6% for the 100 nm colloids and 4% for the 1 μm colloids. These differences are within experimental error. The arrival times of the main colloid peaks from the mono-disperse and poly-disperse suspension were within 4%.

The post test fracture survey for 2007 TT4 is shown in Figure 17. For the 20 nm the pocket of high concentration around S8 and S10 during 2007 TT3, had shifted downward toward S11 and B2. Otherwise the distribution of 20 nm colloids was similar to the previous test, even though the elution volume at test time was longer. The concentration of 100 nm colloids at S1 was significantly reduced compared to the previous test, but the distribution patterns of 100 nm colloids were similar to the 2007 TT4 test in the other regions of the fracture. The 1 μm colloids still had a high concentration in the upper left hand corner, so their distribution was similar to the previous test. Therefore, the main difference between the monodisperse and polydisperse injections was the reduction of the high concentration pockets for the 20 and 100 nm colloids.

In summary, colloid transport from a poly-disperse injection does not appear to be significantly different from that observed from mono-disperse injections.

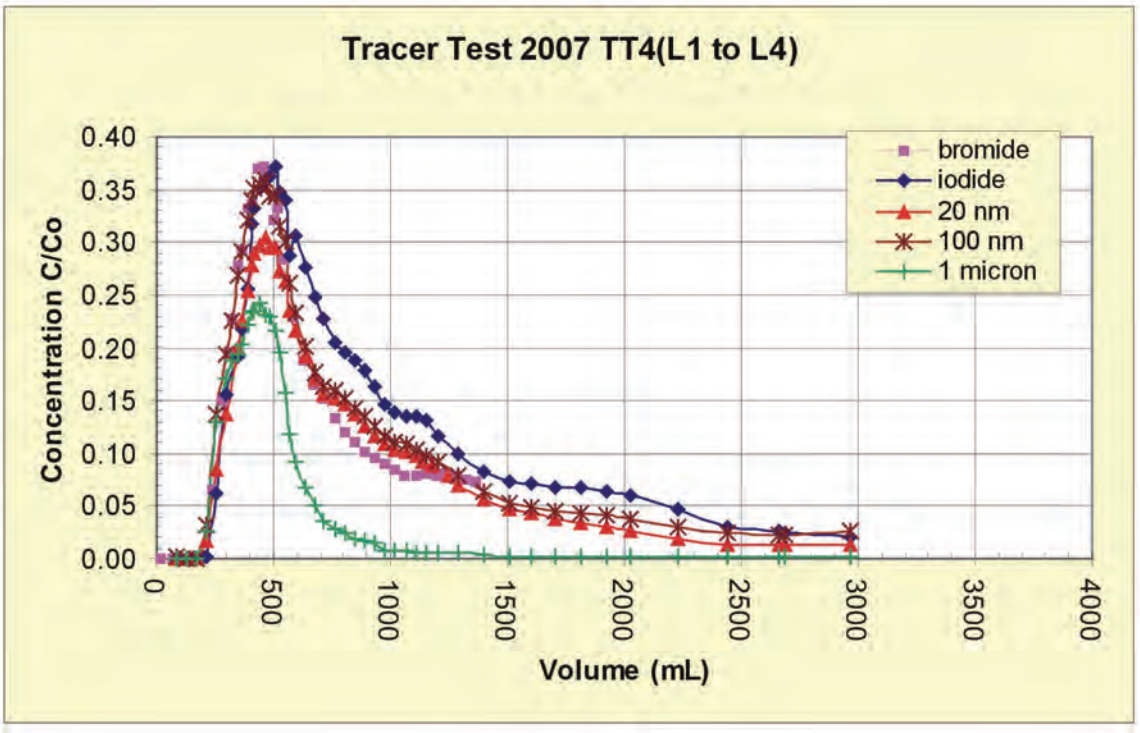

Figure 14 Breakthrough Curves of Solutes, Including Separately Injected Br and I Co-Injected With Colloids. I-1 with 20 nm, I-2 with 100 nm, and I-3 with 1 micron

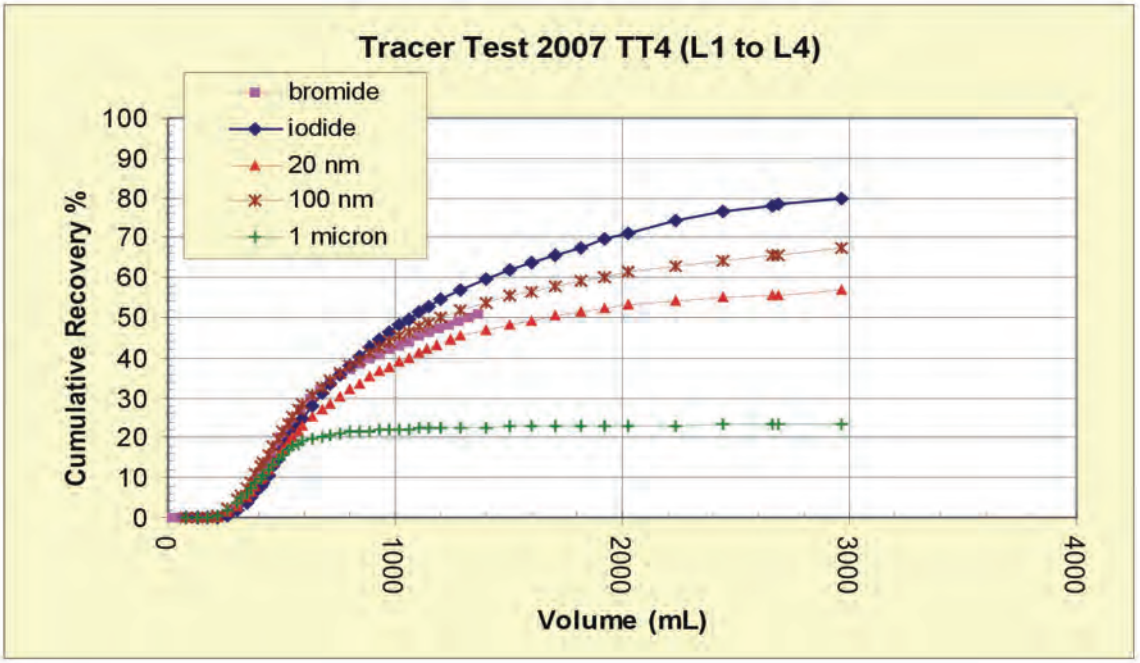

Figure 15: Tracer Recoveries from TT4

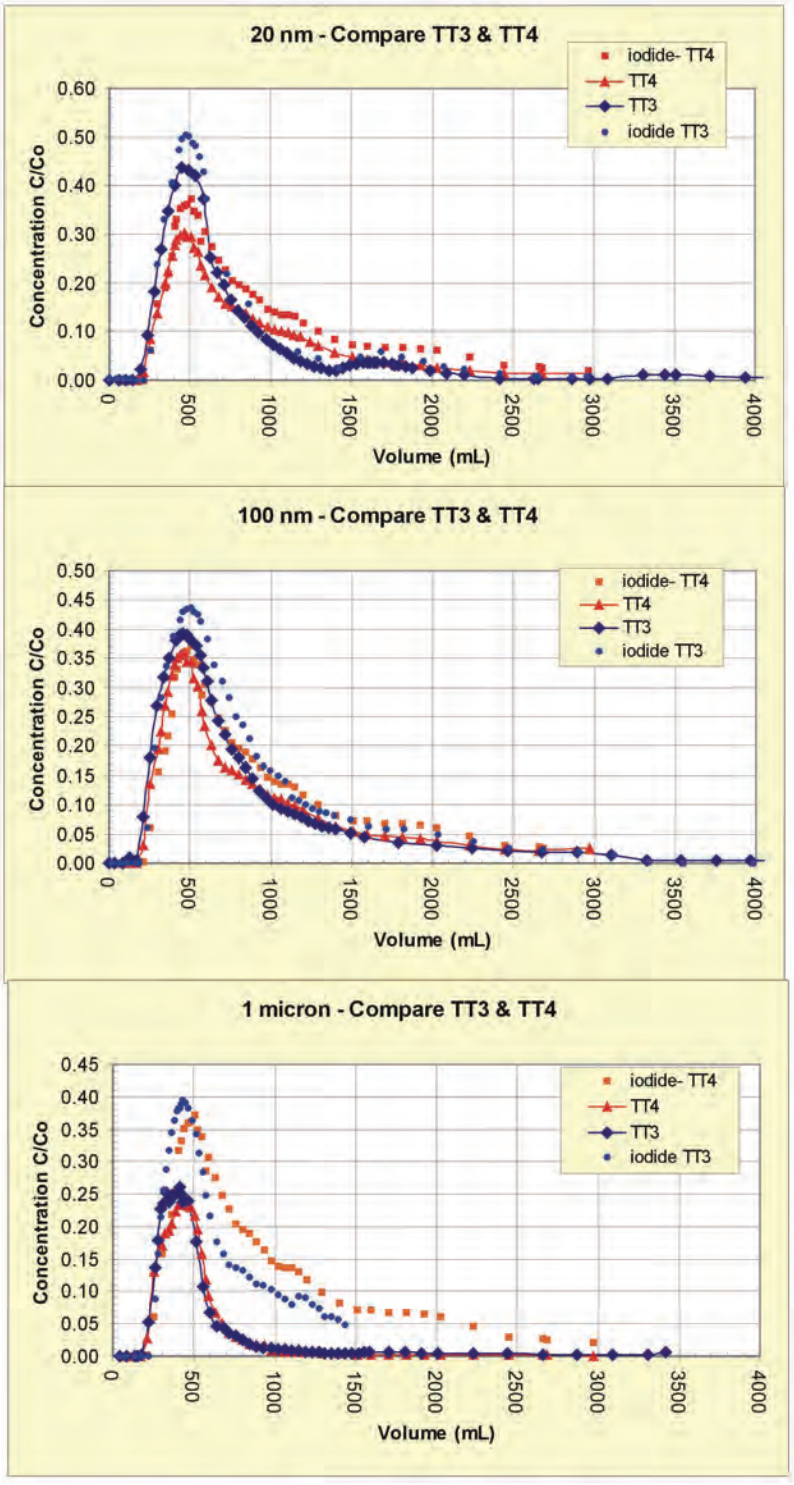

Figure 16: Compare 2007 TT3 and 2007 TT4

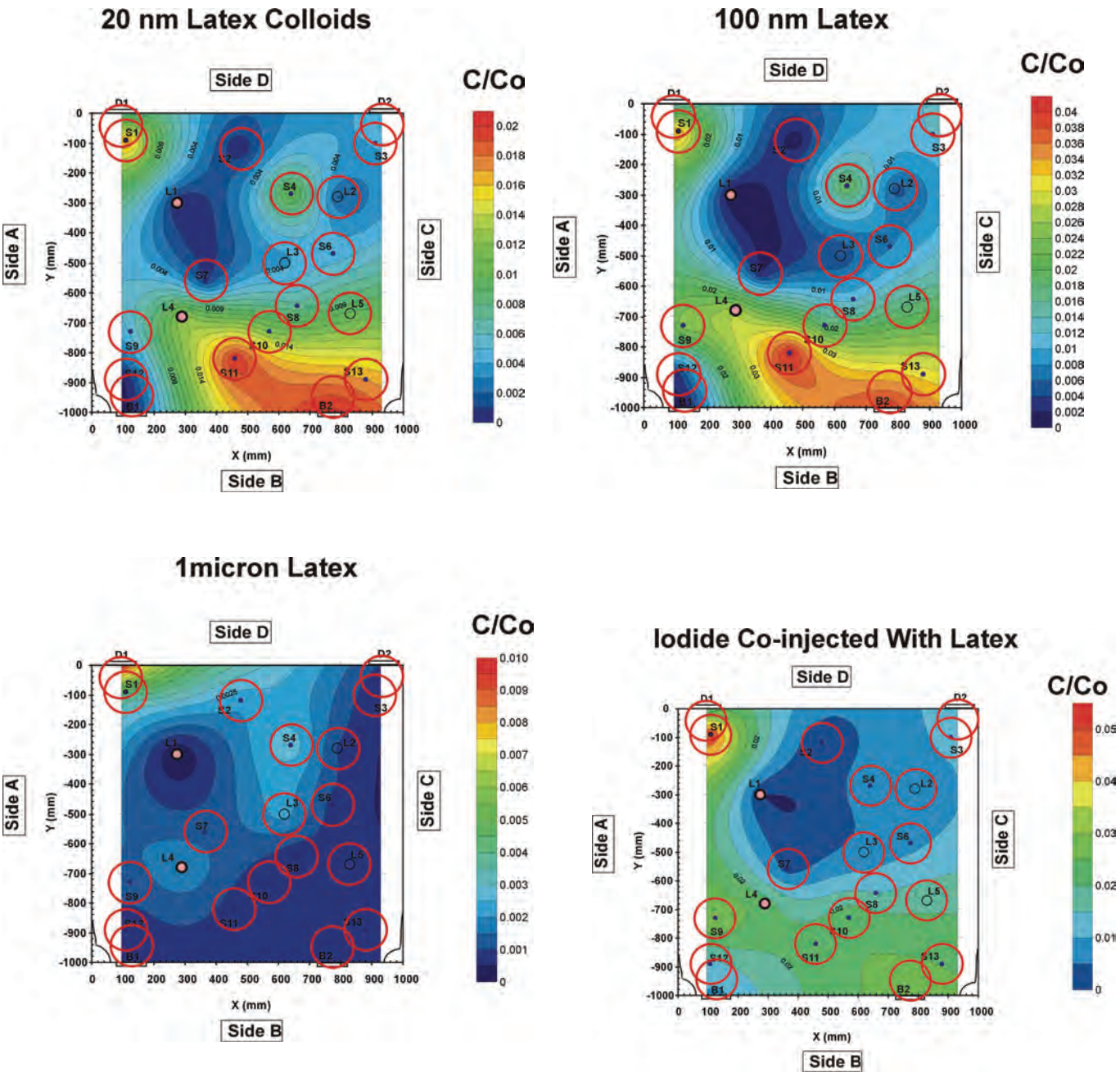

Figure 17: Post Test Survey for 2007 TT4

2.3.1.2 Effect of Size on Bentonite Colloid Transport

The intention of these experiments was to isolate bentonite colloids into 3 size fractions, corresponding to small colloids (4 to 15 nm), moderately large colloids (100 nm to 1 μm) and large colloids (>1 μm). These fractions were injected in separate tracer tests that included 2007 TT5, 2007 TT6, and 2007 TT7. The breakthrough curves from these experiments were compared to determine which size fractions are more mobile, and whether the transport of bentonite colloids with a more narrow size distribution is different from that of a more polydisperse mixture. The size distributions of eluted colloids were studied to determine whether the size distribution of a monodisperse bentonite tracer would change during transport as a result of flocculation and dispersion processes.

Methods: Tracer suspensions were derived from a suspension of MX-80 bentonite. A suspension of very small colloids (for 2007 TT5) was prepared by centrifuging the MX-80 suspension for 33 minutes at a speed of 10,000 rpm. The supernatant was recovered, characterized for size and injected shortly after. The centrifuged bentonite was resuspended and allowed to settle for 20 days. Using a 50 mL syringe, the bentonite suspension was separated into three fractions based on depth (top, middle, bottom). The average bentonite colloid sizes in these fractions were 0.15 to 0.44 μm for the top fraction, 0.18 to 0.50 μm for the middle fraction and 0.27 to 1.41 μm for the bottom fraction. The top fraction was used to prepare the tracer for 2007 TT6 (as well as 2007 TT8 and 2007 TT9), and the bottom fraction was used for 2007 TT7. The respective colloid concentrations for 2007 TT5, 2007 TT6 and 2007 TT7 tracers were 10.5, 14.7, and 108.6 mg/L. The actual particle size distributions for these tracer solution are given in Figure 18. The 2007 TT5 tracer was a monodisperse suspension of small colloids. The 2007 TT6 tracer was a polydisperse suspension, with 88.6% of the particles larger than 0.10 μm. This size distribution was more typical of the size distributions observed for bentonite colloid suspensions prepared from MX-80 bentonite and used in other tracer tests. Although the 2007 TT7 tracer was also polydisperse, 86.6% of the particles were larger than 0.7 μm.

In these tracer tests bromide was injected first, followed by the bentonite suspensions, which did not contain iodide. In all cases a flow rate of 50 mL/h was used between boreholes L1 and L4. In 2007 TT5 the first tracer (373 mL) contained 92.4 mg/L bromide. The bromide injection was followed by 777 mL of water before injecting the small bentonite tracer (442 mL). The fracture was surveyed 2960 mL after the start of the colloid injection. A total of 16.8 L was flowed without interruption through the fracture before the start of the next tracer test. Tracer test 2007 TT6 was started by injecting 76.2 mg/L of bromide (357 mL). This was followed by 683 mL of water before injecting 361 mL of the mid sized bentonite colloids. The fracture survey was performed 3220 mL after the start of the colloid injection. After this survey, 2.8 L of water were allowed to flow through the fracture before the start of the next tracer test. Tracer test 2007 TT7 was started by injecting 354 mL of 78.8 mg/L bromide. The bromide tracer was followed with 650 mL of water before injecting 357 mL of the large bentonite colloid tracer. A fracture survey was performed at 3190 mL since the beginning of the colloid injection. After the survey a total of 14.4 L of water was allowed to flow through the fracture before a second fracture survey was carried out. The experimental flow system was then altered so that S3 became the injection hole, while water was pumped from S12.

Results: Figure 19 compares the breakthrough curves in the three tracer tests, while Figure 20 illustrates the tracer recoveries. Table 4 summarizes the characteristics of the breakthrough curves. The locations of the major peak in the bromide breakthrough curves were similar, although the higher bromide concentration in the 2007 TT5 tracer (92 mg/L) may explain the higher peak height compared to the other two tests (Br values of 73 and 76 mg/L). The percent bentonite recovery was the highest for the injection of the small colloids (91 %), and progressively decreased to 82 % and 14 % as the portion of large colloids was increased. The breakthrough curves in the experiments with larger colloids had earlier first arrivals compared to the test with only small colloids. The arrival times of the major peak progressively became faster with increasing concentrations of the larger colloids. The bentonite colloids in 2007 TT5 and 2007 TT6 displayed a strong secondary peak at 1223 mL, which was absent in the test with the largest colloids.

The eluted colloids in 2007 TT5 and 2007 TT6 were all small. However, larger colloids did appear under the main elution peak of 2007 TT7, as illustrated by a typical size distribution in Figure 21. Figure 22 shows average sizes of bentonite colloids eluted during 2007 TT7. Although larger colloids were transported, their average sizes were about 40% lower than in the injected tracer.

The results of post test surveys are summarized in Figure 23. Although solute and colloid tracers were found to the left and right of the L1-L4 borehole pair, the pocket of high concentrations at S9 appears to be common in the tracer distributions. The bentonite distributions were similar in all three tests, although in 2007 TT7 the concentrations of bentonite colloids to the right of the borehole pair L1-L4 had diminished compared to the previous two tests. With the higher bromide tracer used in 2007 TT5, the bromide distribution appeared more uniform throughout the fracture. Size analyses of colloids recovered during post test surveys showed only the presence of small bentonite colloids. This suggests that the larger bentonite colloids (or flocs), which had not eluted from the fracture, had become fixed and were not readily mobilized by the higher local water flows induced during post test surveys.

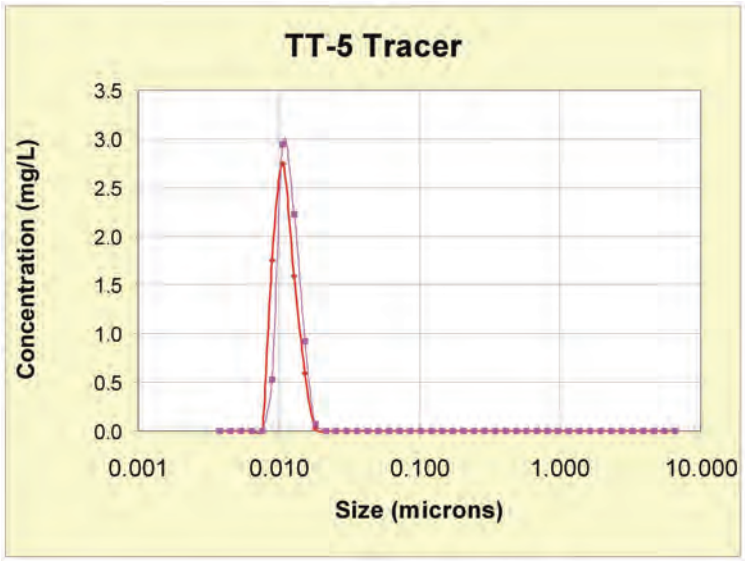

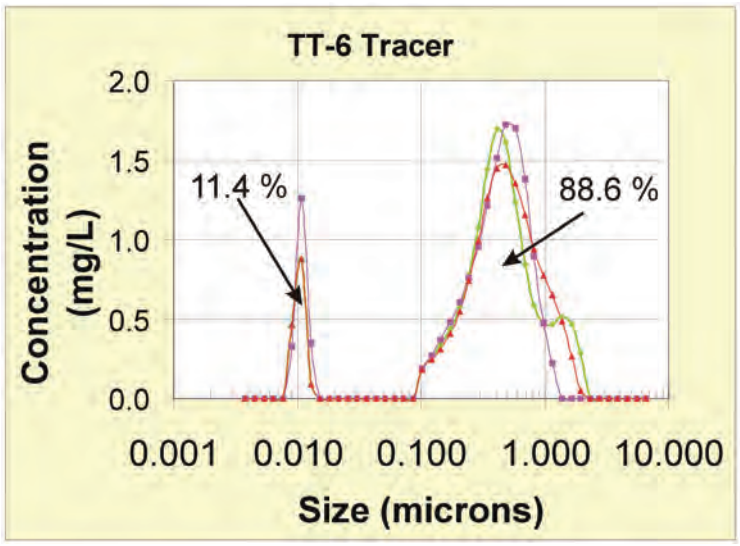

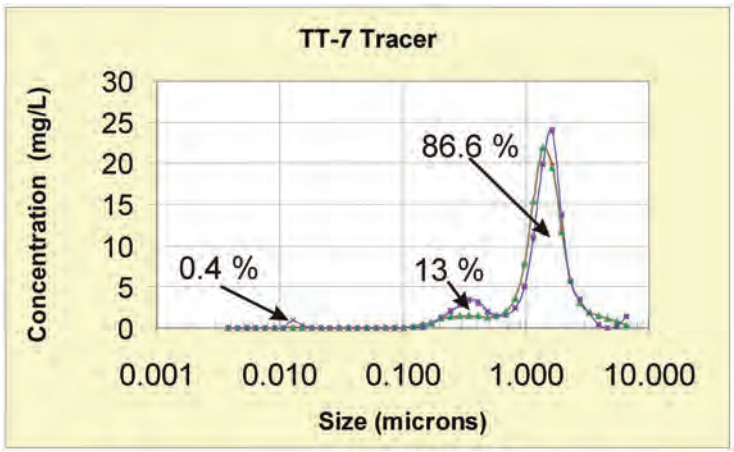

Figure 18: Bentonite Tracer Size Distributions used in Experiments to Evaluate the Effect of Particle Size on Bentonite Colloid Transport

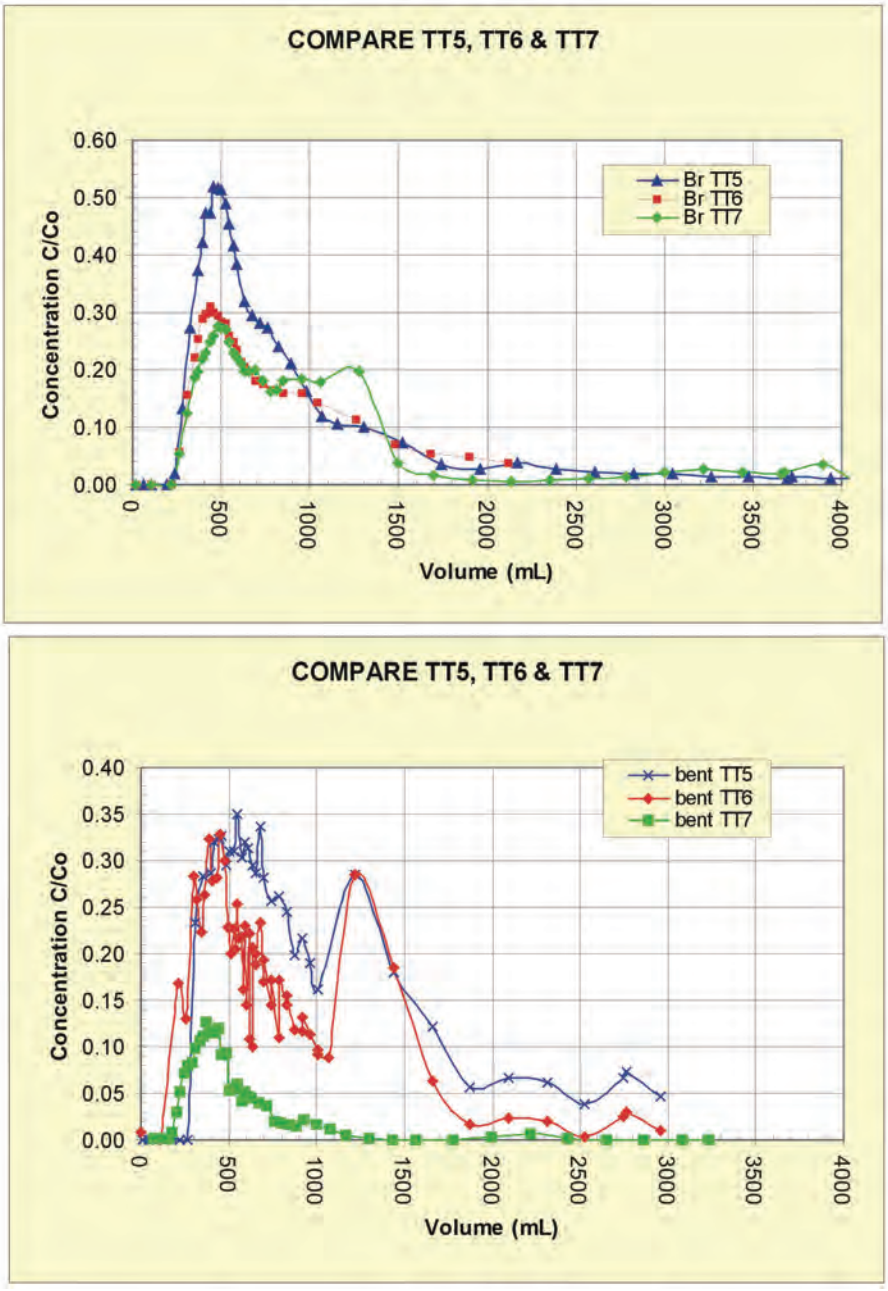

Figure 19: Breakthrough Curves for 2007 TT5, 2007 TT6 and 2007 TT7

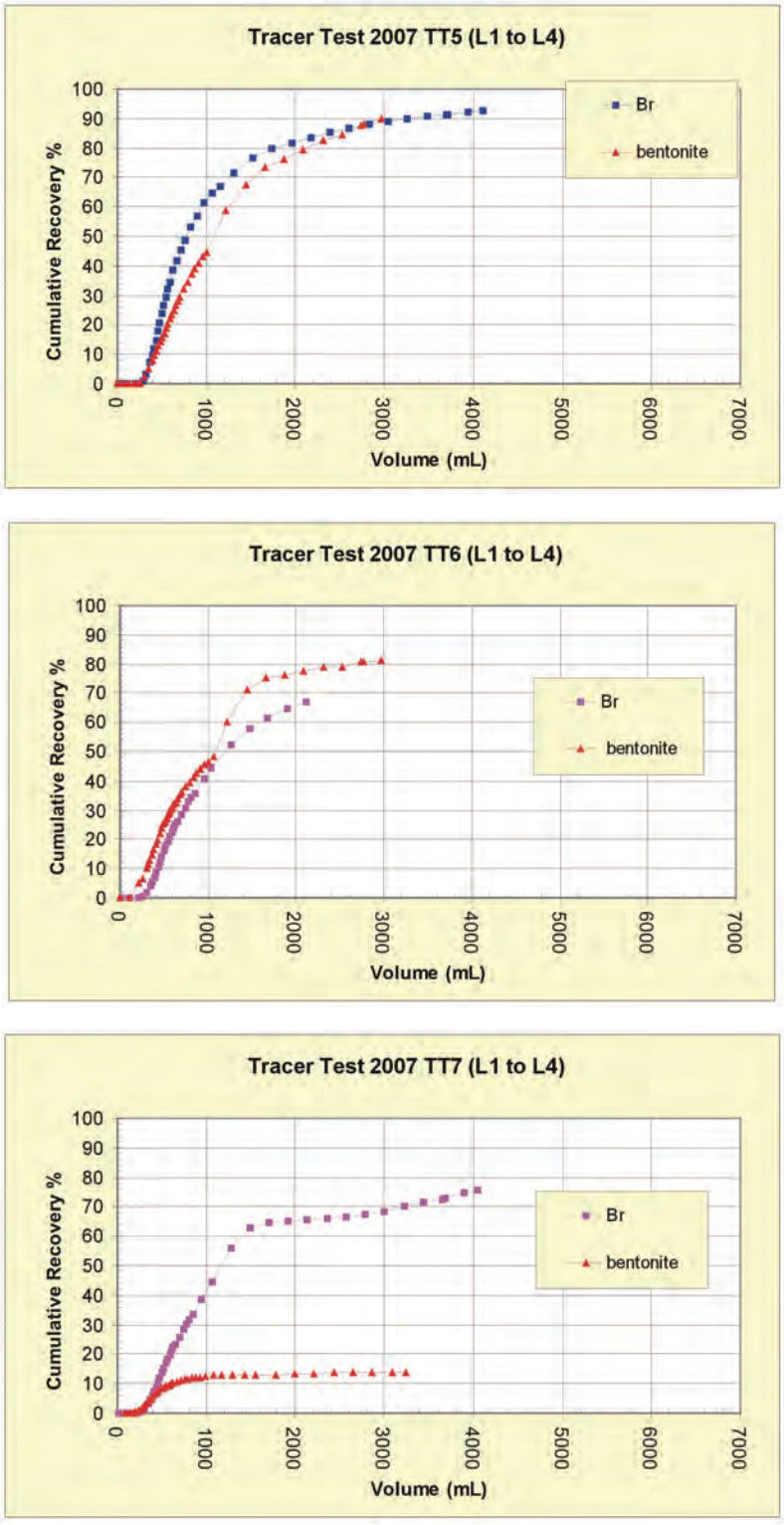

Figure 20: Bromide and Bentonite Recoveries for 2007 TT5, 2007 TT6 and 2007 TT7

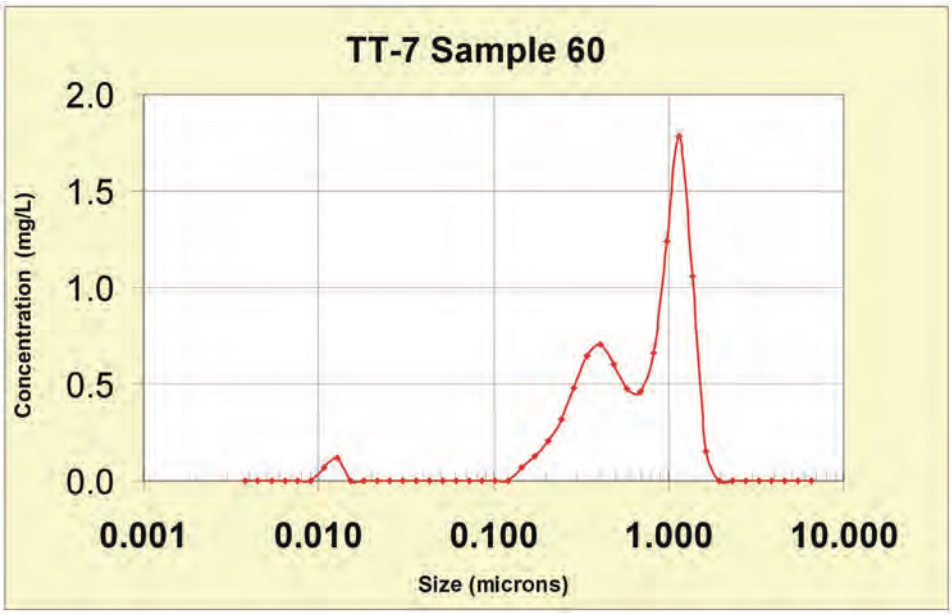

Figure 21: Example of Bentonite Size Distribution Appearing in Major Peak of 2007 TT7 Breakthrough Curve

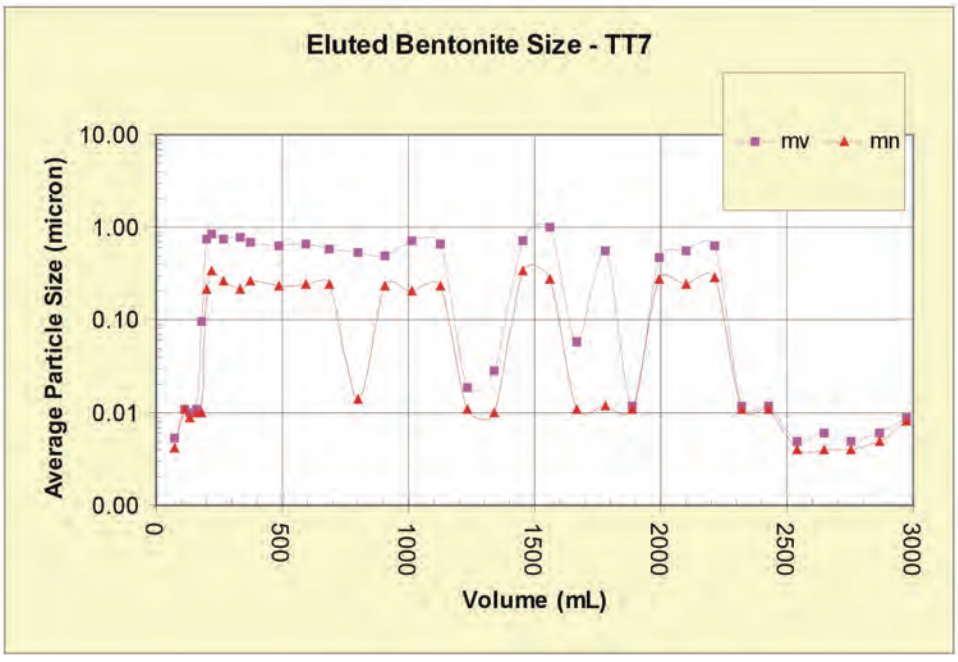

Figure 22: Average Bentonite Colloid Sizes Determined by the UPA. The average size based on particle volume is mv, while the average size based on particle number is given by mn.

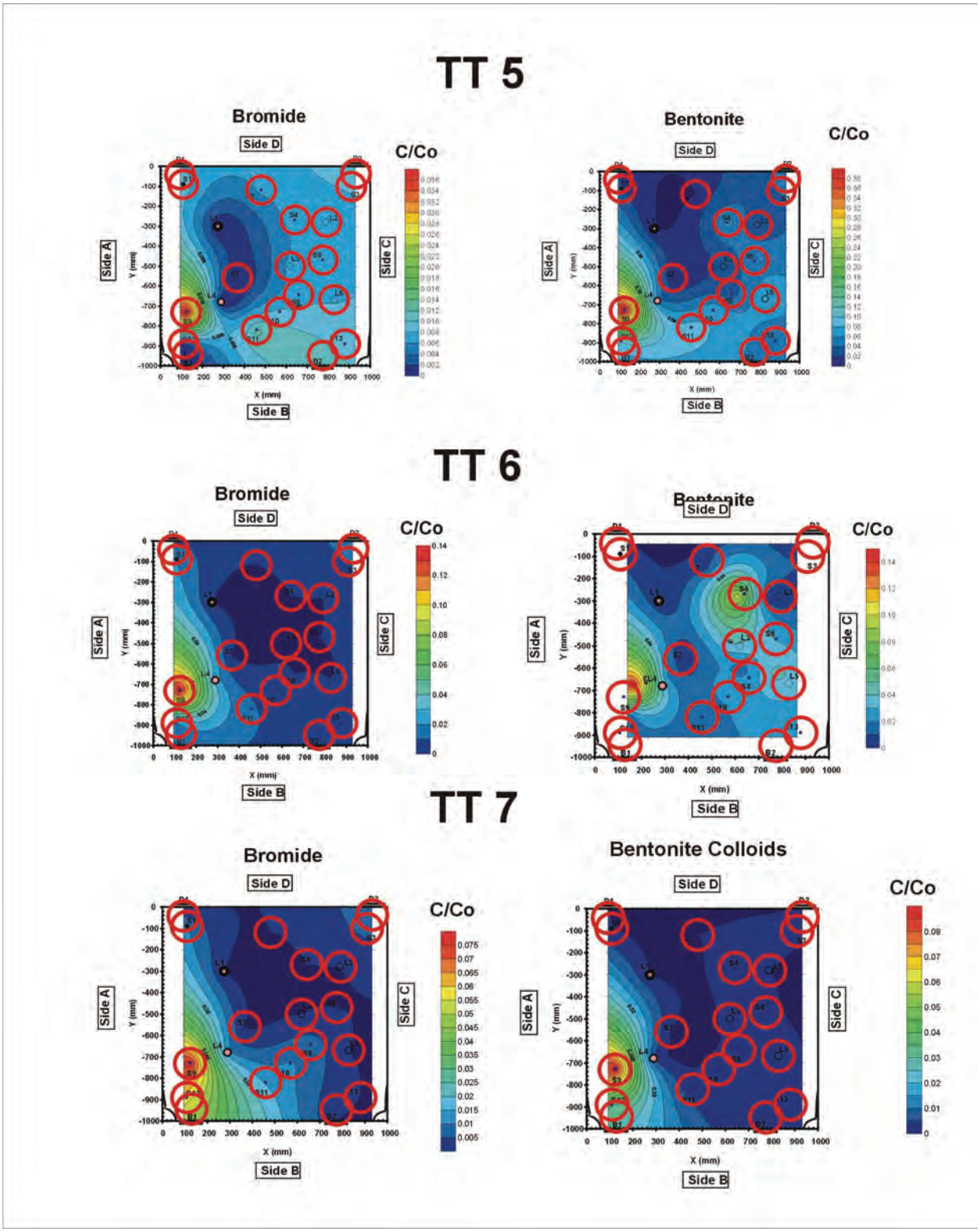

Figure 23: Post Test Surveys for 2007 TT5, 2007 TT6 and 2007 TT7

2.3.2 Phase 3: Long Borehole Separation for Colloid Transport

The objective of this experiment was to provide bentonite and latex colloid migration data for a longer transport distance using a close to natural flow velocity and dilute water. This experiment was intended to help address issues of experimental scale and the effect of flow path variability on filtration coefficients or retardation factors for colloids in natural fractures. The borehole pair S3 to S12 represents one of the longest possible separation distances (1100 mm) in the Quarried Block (Figure 2). This flow path from one corner of the block to the other, covers a wide fracture aperture distribution.

Before initiating testing at the low flow rate (6 mL/h), a tracer test (2007 TT8) with bentonite and 100 nm latex colloids was performed at a high flow rate (500 mL/h) to scope out colloid behaviour before proceeding with a longer duration experiment (2007 TT9 and 2007 TT10). This would also characterize the effects of flow velocity for this experimental configuration. Both the high flow and low flow rate tests began with an injection of colloid-free bromide. This was followed by an injection of bentonite, and finally latex colloids with iodide. Due to the long time period of the low flow experiment, the initial injection of bromide and bentonite colloids was assigned to 2007 TT9 and the injection of latex with iodide as performed during 2007 TT10.

2.3.2.1 High Flow Rate

Methods: During the high flow rate experiment the outflow from S12 was set to 500 mL/h using a needle valve. Tracer-free water was allowed to flow from S3 to S12 (8 L) overnight before starting 2007 TT8 with an injection of a bromide tracer (81.8 mg Br). The tracer volume of 441 mL was followed by 12 L of water before injecting the bentonite colloid tracer. The injected tracer had a volume of 480 mL and a colloid concentration of 38.2 mg/L. The bentonite tracer had a size distribution (Figure 24), which was similar to that used in 2007 TT6. The bentonite colloid was followed by 13 L of water before injecting the final colloid tracer, containing 54.6 mg/L of 100 nm latex and 102 mg/L iodide. The fracture was surveyed three times for tracer, corresponding to 2930 mL since the start of bromide tracer, 2830 mL since the start of bentonite tracer, and 2930 mL since the start of the latex colloids. A total of 12 L of tracer-free water was pumped through the fracture before the start of the next tracer test.

Results: The tracer breakthrough curves for 2007 TT8 are given in Figure 25 and the cumulative recoveries are shown in Figure 26. The first arrivals of tracers were from 850 to 910 mL, about a factor 4 longer than for the tests between L1 and L4. The breakthrough curves of bromide and the iodide co-injected with latex, were similar. The bentonite first arrival and peaks were significantly ahead of solute tracer and latex colloids. The latex main peak was also ahead of the solute tracers, but not to the same extent as bentonite. At the high flow rate all tracers had similar recoveries, with 84% for Br, 82 % for I, 84% for bentonite, and 72% for latex.

The eluted bentonite colloid sizes were all in the low range, except for two samples at 1800 and 1920 mL , which had average sizes of 200 to 300 nm (Figure 27). The only sample from the post test analyses to contain larger bentonite colloids (average 415 nm) was from S9. These observations illustrate that even at high flow rates the larger bentonite colloids tend to become immobilized. There is also a possibility that the larger particles that are trapped may continue to release smaller particles into suspension.

The results of post test analyses are shown in Figure 28. The tracer distribution patterns were somewhat similar, with high concentrations remaining at S9. In general, the higher solute and tracer concentrations were found toward the lower left hand corner, to the left of a line that could be drawn from S1 to S10 or S11. This is to be expected because the flow was from the upper right corner to the lower left corner. The solute tracers appeared to have moved further to the left compared with the colloid tracers.

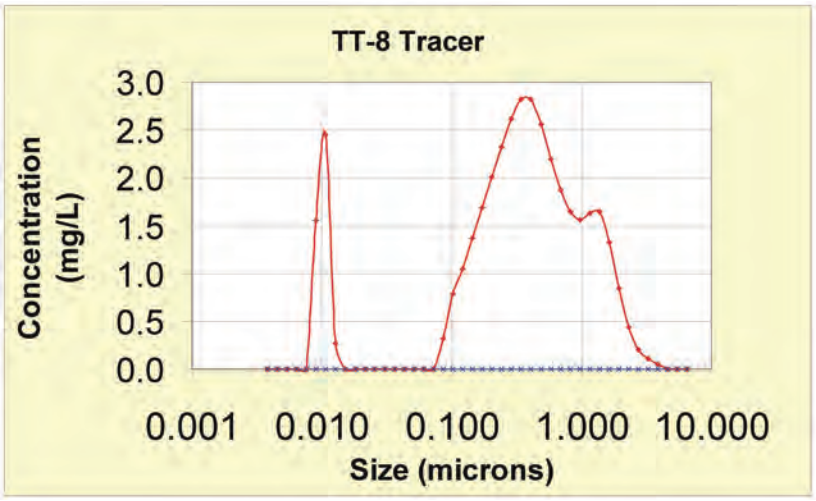

Figure 24: Size Distribution of 2007 TT8 Tracer

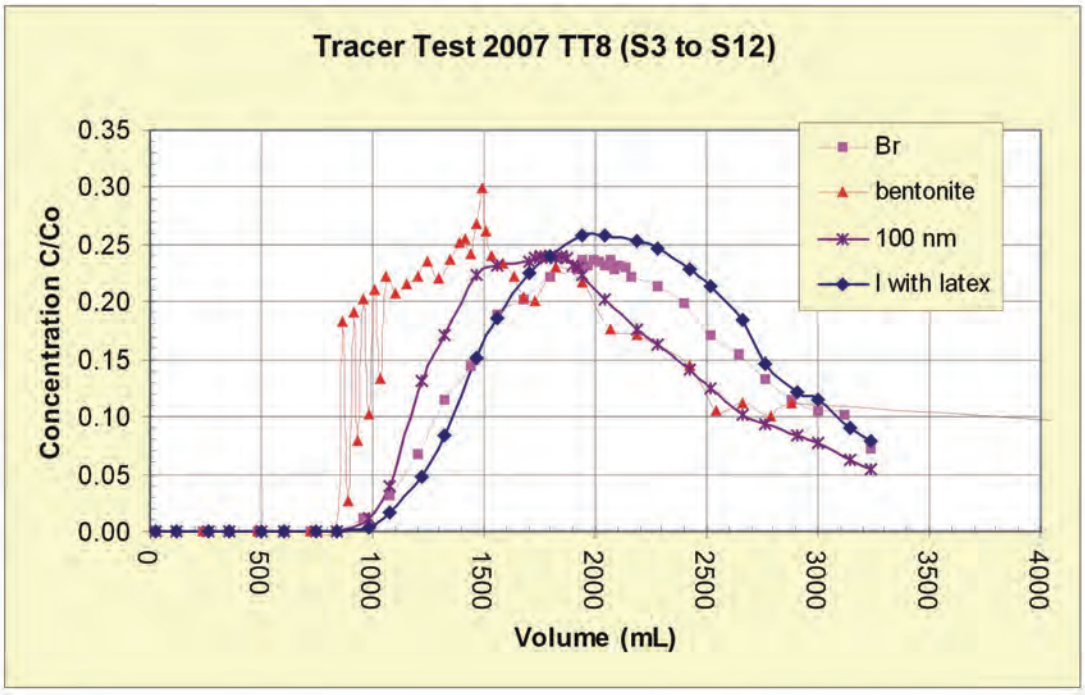

Figure 25: Breakthrough Curves for 2007 TT8

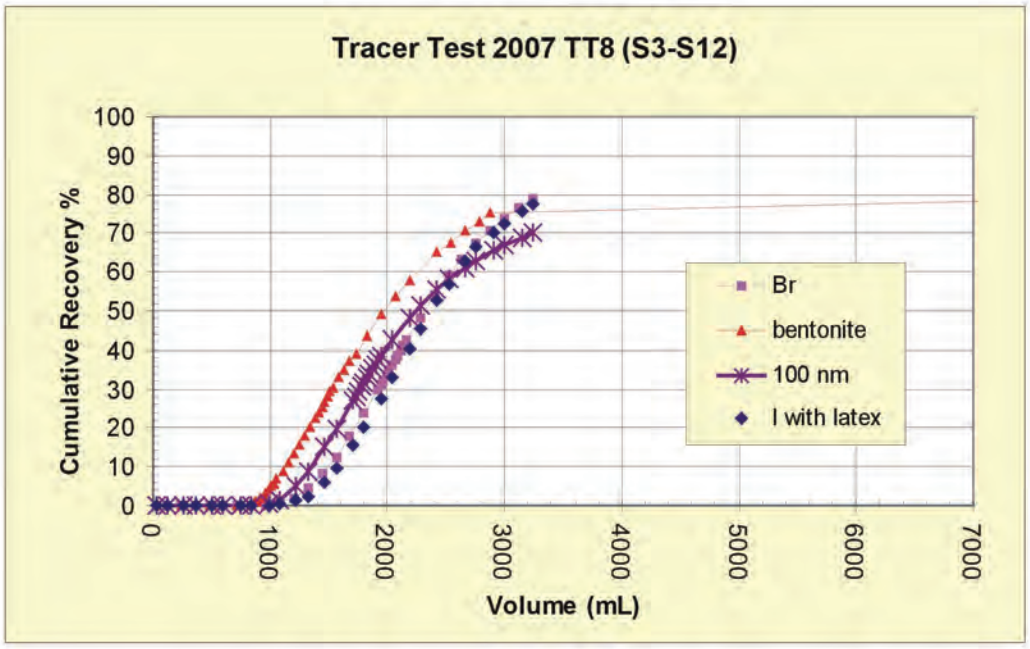

Figure 26: Tracer Recovery for 2007 TT8

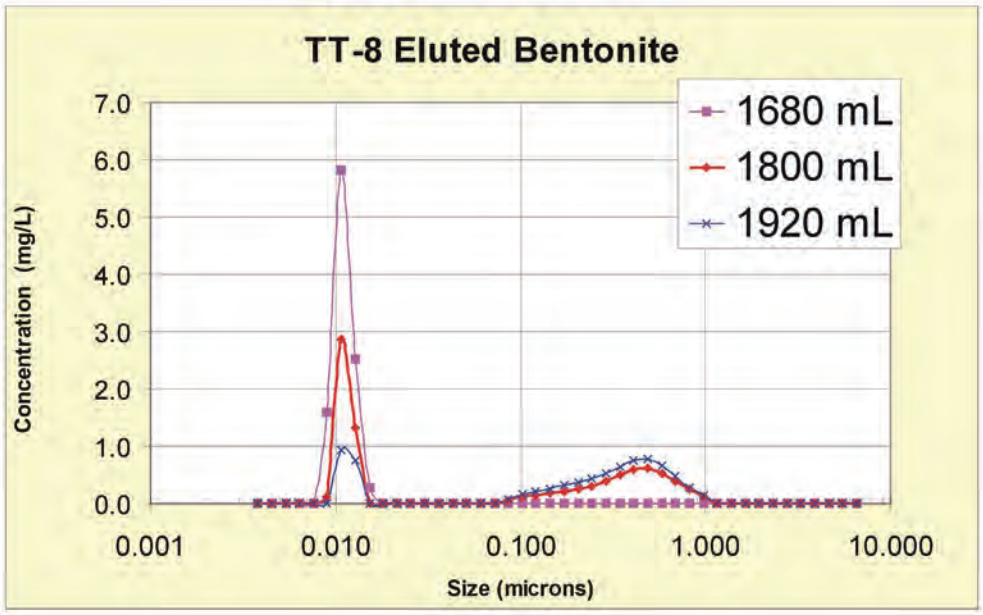

Figure 27: Size Distribution of Bentonite Colloids Eluted from 2007 TT8, showing the Typical Size as Illustrated by the 1680 mL Sample and the Two Samples at 1800 and 1920 mL with Larger Colloids

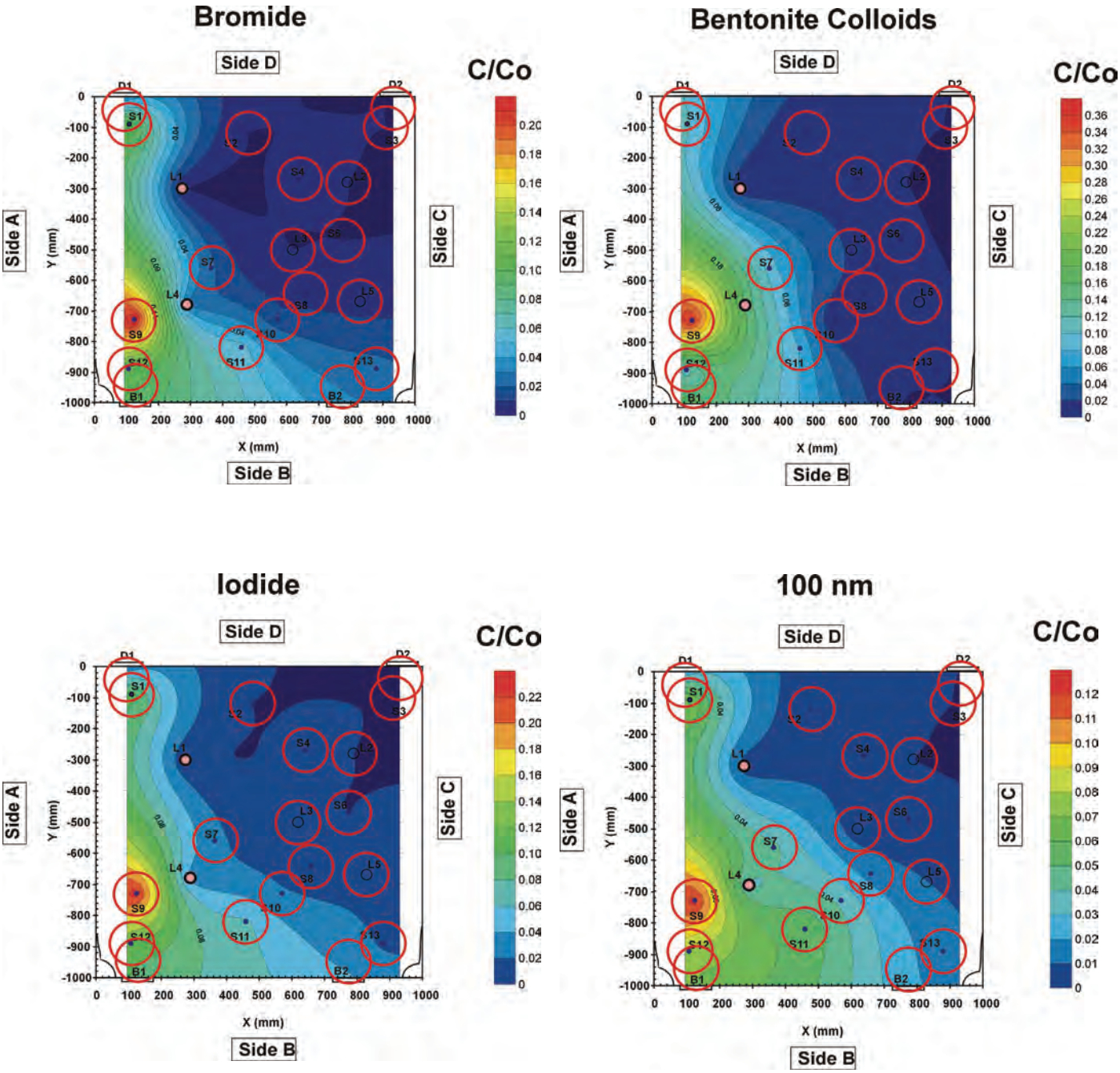

Figure 28: Post Test Survey for 2007 TT8

2.3.2.2 Low Flow Rate

Methods: The flow rate between S3 and S12 was reduced to 6 mL/h by using a peristaltic pump to control water flow from S12. Water was allowed to flow for 72 h before starting 2007 TT9 with an injection of 419 mL of colloid-free tracer with 57.3 mg/L bromide. This was followed with 2480 mL of water before injecting 424 mL of bentonite colloids with a concentration of 44.1 mg/L. These colloids were produced from the same source as those used in 2007 TT6 and 2007 TT8, and consequently had a similar size distribution (Figure 29). A fracture survey was performed 3450 mL after the start of the colloid injection. Tracer test 2007 TT10 was initiated at 3060 mL after the completion of the bentonite colloid injection. This test was started by injecting 421 mL of tracer containing 22.9 mg/L 20 nm colloids, 41.2 mg/L 100 nm colloids, 12.2 mg/L 1 μm colloids, and 82.8 mg/L iodide. A mixture of different latex colloid sizes was used to obtain additional information on the effects of particle size and because results from previous tests indicated that the interference between different particle sizes was not significant. A fracture survey was performed at 4000 mL since tracer injection. At this point flow between S3 and S12 was terminated.

Results: The bromide and bentonite breakthrough curves from 2007 TT9 are shown in Figure 30, and tracer recovery curves are illustrated in Figure 31. Compared to high flow rate test (2007 TT8), the bromide and bentonite breakthrough curves at the low flow rate had approximately half the peak heights and their first arrivals were significantly faster in terms of eluted volume. At the high flow rate the respective first arrivals of bromide and bentonite were at 900 mL (1.8 h) and 852 mL (1.7 h), while at low flow the corresponding first arrivals were at 204 mL (34 h) and 150 mL (25 h). Also, while at the high flow rate the bromide breakthrough curve consisted of one large peak, at low flow a number of smaller peaks have appeared, suggesting the presence of multiple flow paths. The bentonite breakthrough was characterized by one major peak, with several minor peaks before it. The concentration of eluted bentonite dropped rapidly at 1000 mL, before the start of the bromide peaks. Although the bentonite breakthrough curve after 1000 mL was characterized by low concentrations, some of the minor peaks in this section corresponded to peaks in the bromide breakthrough curve. At the low flow rate the bromide recovery was reduced to 53 % and the bentonite recovery had dropped to 24%. The results of post test fracture analyses for 2007 TT9 are shown in Figure 32. The maximum bromide and bentonite concentrations measured at the low flow rate were about an order of magnitude lower than at the high flow rate. However, the tracer distribution patterns were similar to those measured for the high flow rate experiment. Size analysis showed that only small bentonite colloids were eluted or recovered from the post test fracture survey.

The breakthrough curves for latex colloids and co-injected iodide for 2007 TT10 are illustrated in Figure 33, and Figure 34 shows the corresponding tracer recovery curves. The latex colloids and co-injected iodide had breakthrough curves with single broad peaks with similar shapes. Although the latex colloid first arrivals were ahead of the co-injected iodide, their peak arrivals were similar. Compared with the high flow rate conditions, the 100 nm colloids in 2007 TT10 had a lower peak concentration (reduced from 0.25 to 0.17). In terms of volume the first arrival of latex colloids was sooner at 514 mL (86 h), compared with 912 mL (1.8 h) at high flow. The tracer recoveries at 3600 mL in 2007 TT10 were 78% for iodide, 24% for 20 nm colloids, 51% for 100 nm colloids and 1% for 1 μm colloids. As with the L1-L4 borehole pair, the mid sized 100 nm colloids were more efficiently transported than the other colloids sizes. Figure 35 compares the breakthrough curves of bentonite and latex colloids, with all concentrations plotted on the same y-axis. As during the high flow rate experiment, the breakthrough of the bentonite colloids was ahead of the latex colloids. The bentonite breakthrough peaked at a

similar location as the latex colloids, but than dropped very sharply while the latex colloids displayed long gradually decreasing tails. In terms of recovery, the transport efficiency of bentonite colloids was close to that of the 20 nm latex colloids. However, based on the shapes of the breakthrough curves their transport paths appeared to be different.

Figure 36 illustrates the results of post test fracture surveys for 2007 TT10. The iodide tracer distribution was similar to the bromide distribution in 2007 TT9 in terms of concentration, except that the bromide concentrations were higher in the central part of the block (S7, L3). The 20 nm and 100 nm latex colloid distributions were similar to that of co-injected iodide, although the colloid concentrations tended to be a factor 4 to 10 lower than iodide. The 1 μm colloids were concentrated in the upper right hand corner near of the fracture, which is consistent with their low recovery from S12.

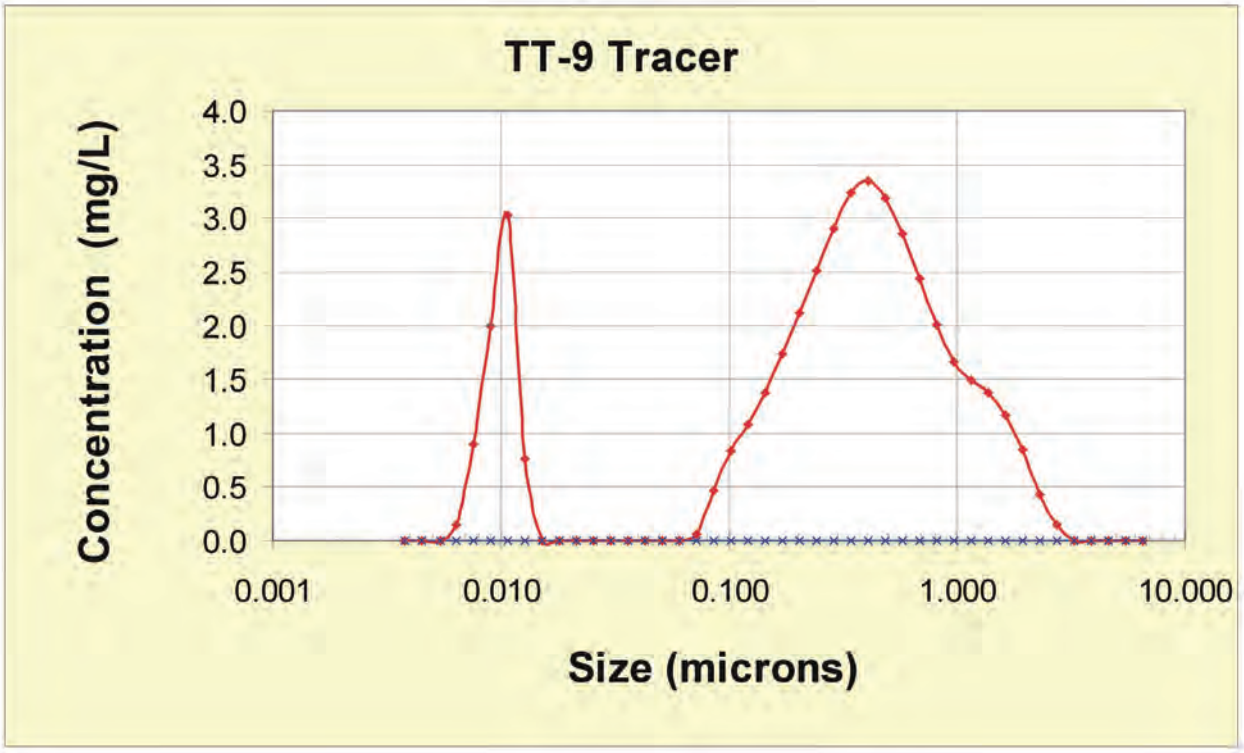

Figure 29: Size Distribution for 2007 TT9 Bentonite Tracer

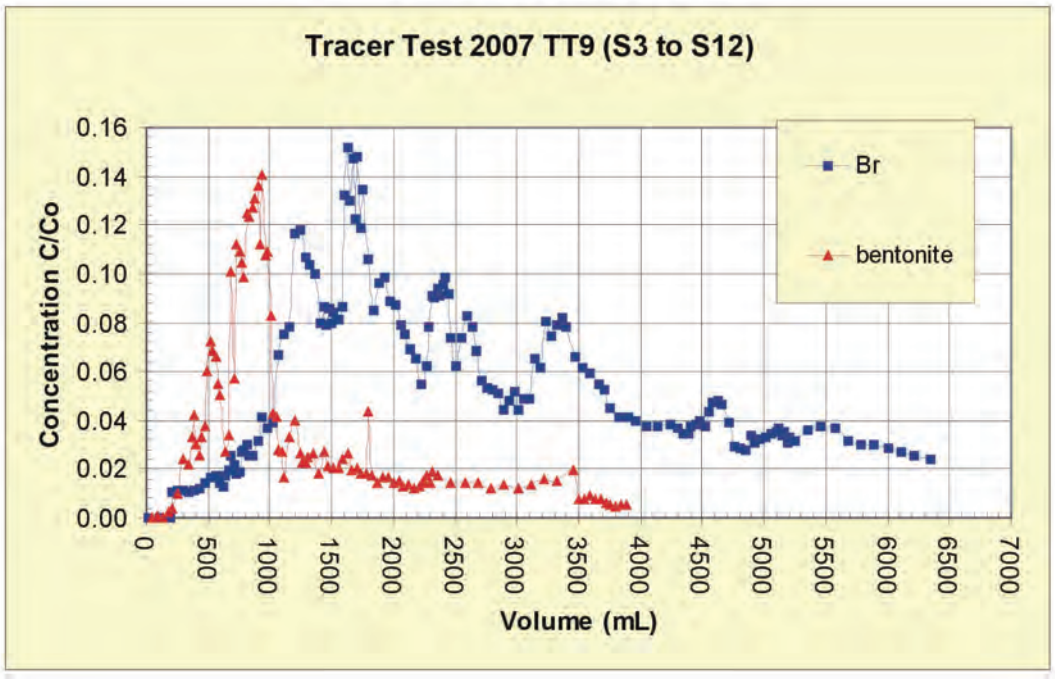

Figure 30: Breakthrough Curves for 2007 TT9

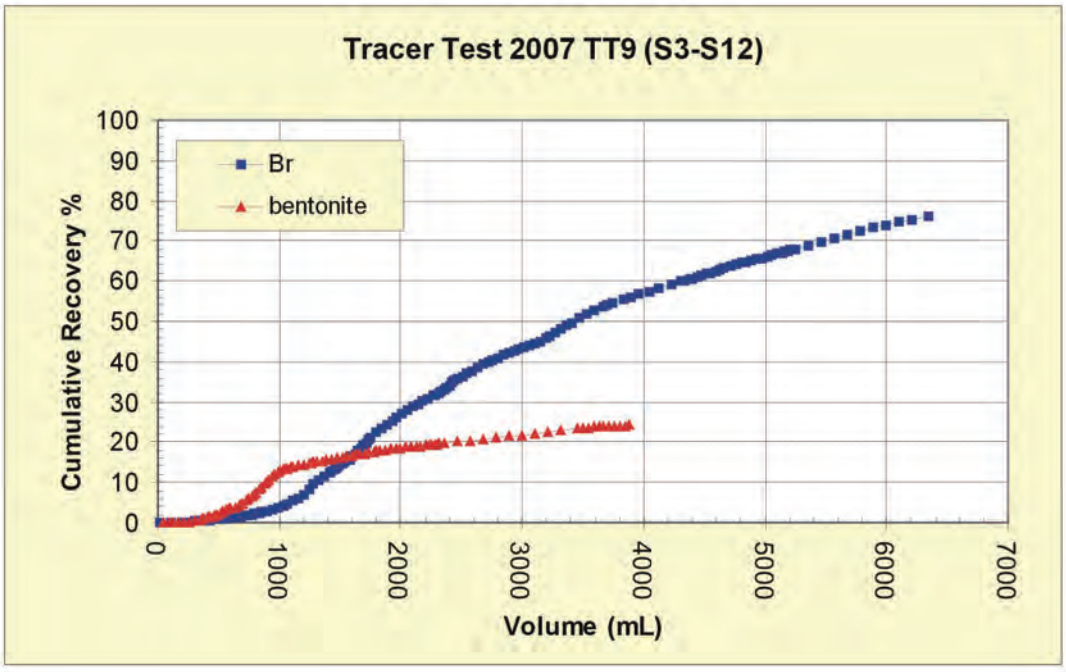

Figure 31: Recovery for 2007 TT9

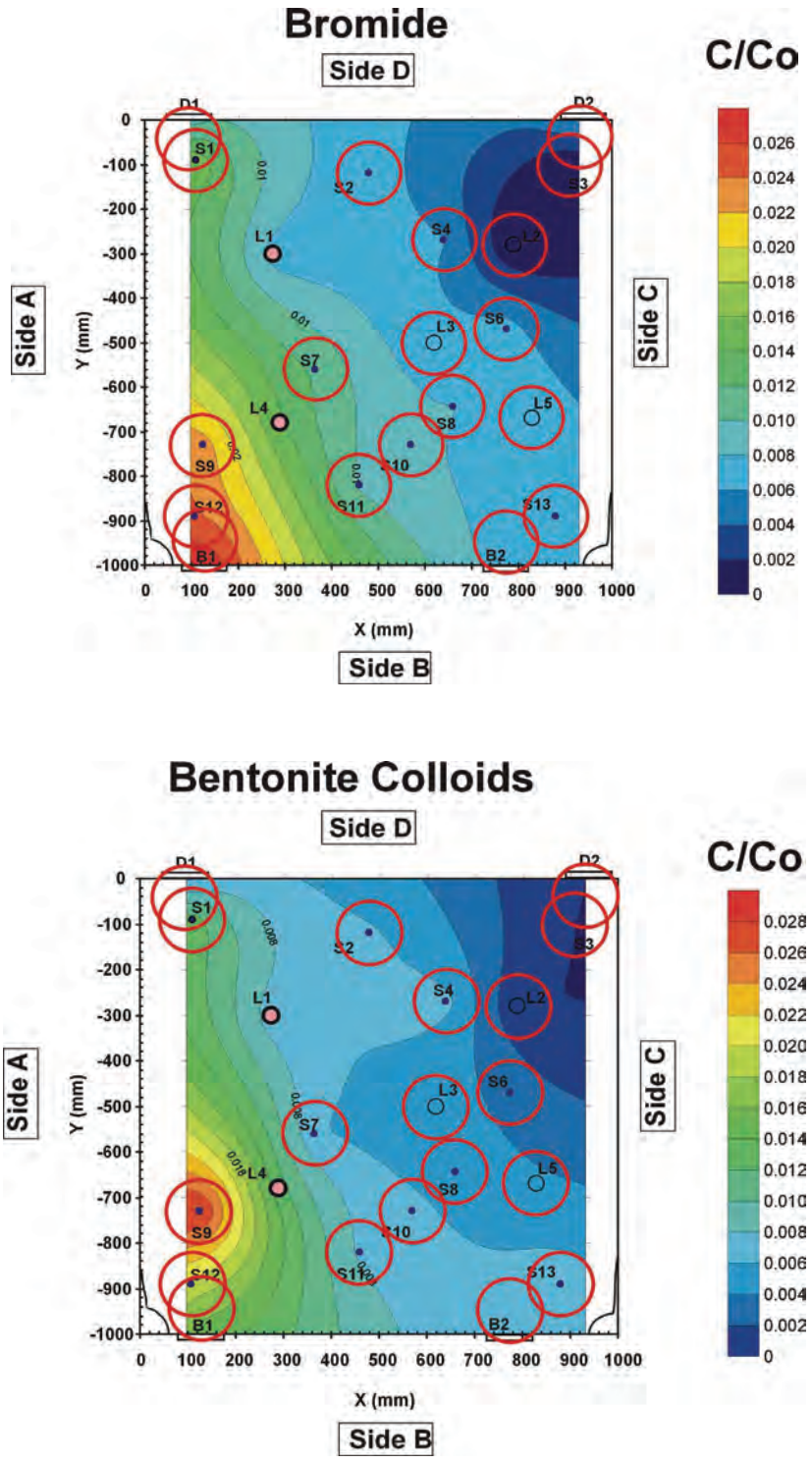

Figure 32: Post Test Analyses for 2007 TT9

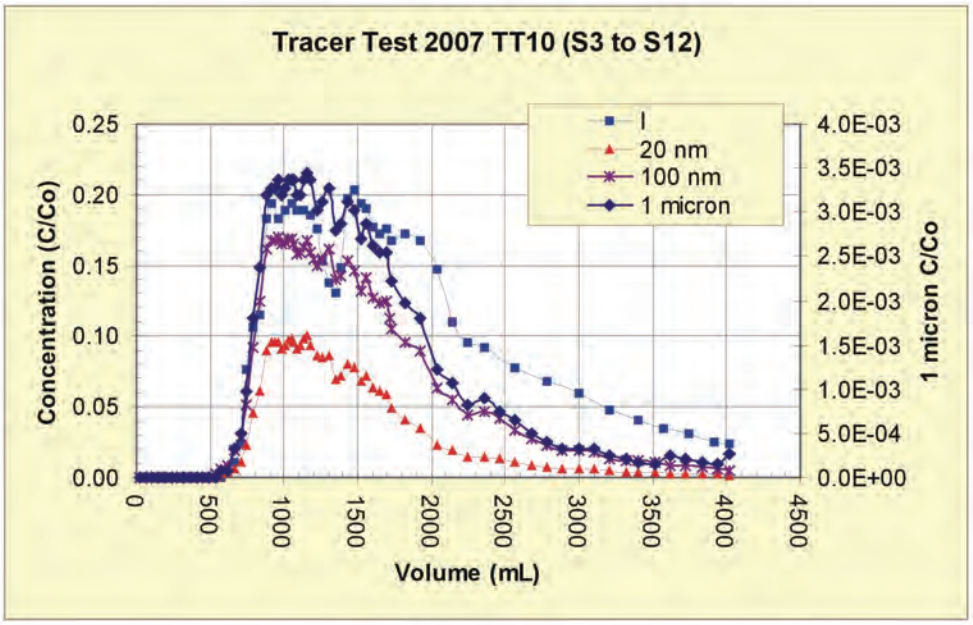

Figure 33: Breakthrough Curves for 2007 TT10

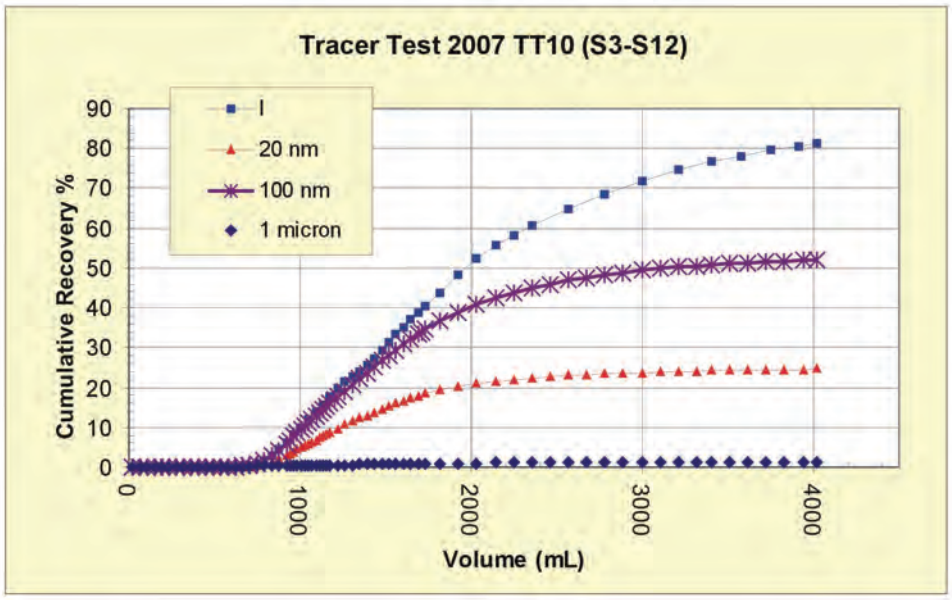

Figure 34: Tracer Recovery for 2007 TT10

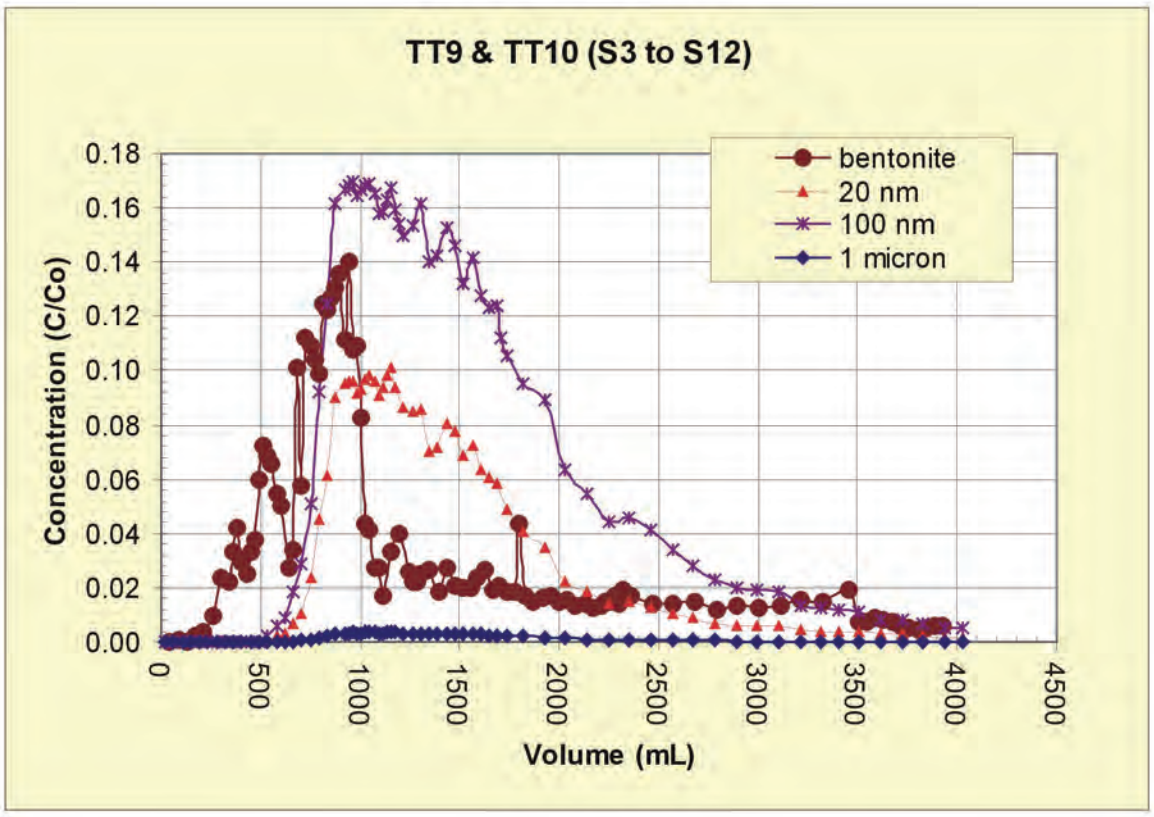

Figure 35: Compare Bentonite and Latex Colloids at Low Flow Rate

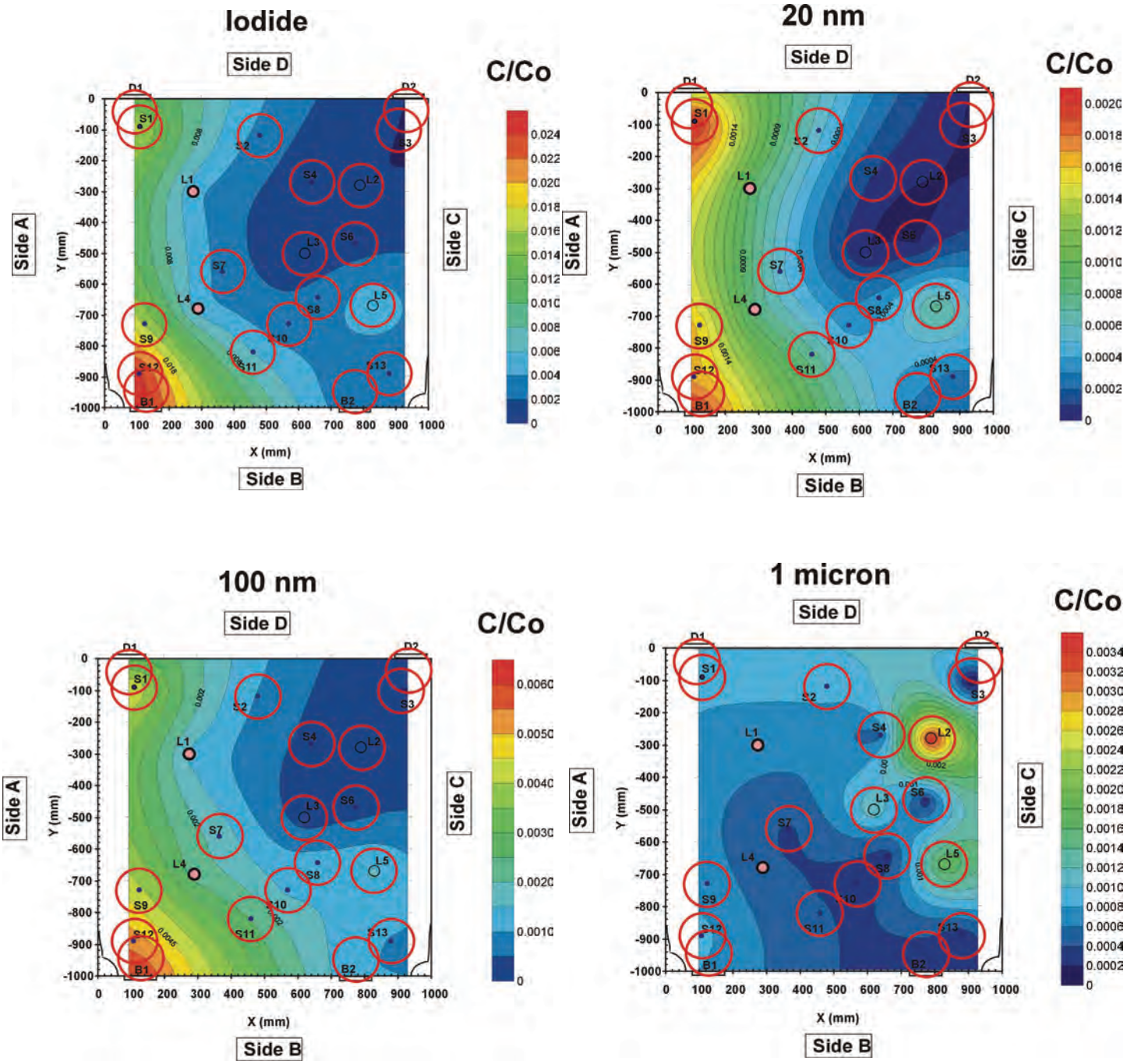

Figure 36: Post Test Analyses for 2007 TT10

3. POST TEST ANALYSIS

The objectives of the post test analysis (Phase 4) were to quantify the amount of latex and bentonite colloids left on the fracture surfaces followingthe Phase 3 testing, and to visualize the flow paths taken by latex colloids. From previous experience it is known that the amount of fluorescence left on the fracture surfaces after standard tracer tests may be too small for good visualization with fluorescence. Therefore, it was decided to inject additional fluorescing colloids in the L1 to L4 flow path, which had been the focus of many previous experiments. It was hoped that by using this flow path it would minimize the impact on the colloids deposited in the Phase 3 test (S3 to S12). The total amount of injected colloids was higher than normally used in tracer tests, and the injection was stopped as the peak began to arrive at L4. The Quarried Block was then drained slowly to minimize redistribution of latex colloids within the fracture. The Quarried Block was then opened and illuminated with UV light to reveal the presence of deposited latex colloids. Once this visualization phase was complete, selected sections of the fracture surfaces were swabbed in an attempt to recover and quantify deposited colloids.

3.1 METHODS

In order to mark a flow path for visual characterization by fluorescence it is necessary to use a fluorescent marker that will attach to fracture surfaces and remain fixed while water is drained from the fracture. The strategy used in this study was to use a tracer containing 103 mg/L fluorescent blue 1 μm latex and 58.4 mg/L fluorescent yellow-green 500 nm latex colloids. Tracer test 2007 TT11 consisted of establishing a high flow rate of 500 mL/h between L1 and L4, and injecting 1102 mL of tracer. Once the injection was completed the flow was stopped and the tracer was allowed to remain undisturbed for 5 days. It was anticipated that during this time the 1 μm latex colloids are likely to settle to the bottom fracture surface and possibly become loosely attached. The 500 nm latex colloids may not settle to the same extent. The next important step was to carefully drain the water from the block in such a way as to minimize colloid mobilization. This was achieved by first draining the water from the standpipes. Then the fracture was slowly drained by starting with the boreholes accessing the parts of the fracture with higher elevation to minimize extra flow in those parts of the fracture with lower elevation. The draining operation was progressively switched to boreholes accessing lower fracture elevations. While the fracture was being drained, the water in the upper sections of the L series holes was pumped out to prevent this water from draining into the main fracture via possible connecting fracture splays. The total volume removed from the L series holes was 1130 mL, while the total volume drained from the fracture was 2930 mL.

Once the fluid was drained from the fracture the silicon cement was cut away from the edge of the fracture, and the four mini-plena were removed. Four keys were attached to sides B and D. The main function of the keys was to help reposition the fracture surfaces after post-test analyses. Reference lines were inscribed on each key to help estimate changes in fracture aperture once the Quarried Block was reassembled. After the four retaining bars (used to ensure that the upper and lower halves remained firmly attached to each other) were removed, the upper steel frame was bolted to the Quarried Block using previously installed bolt holes. A lifting yoke was attached to the upper frame, and the Quarried Block was repositioned under the hoist in the Quarried Block Facility (Figure 37). Using the hoist, the upper half of the Quarried Block was gently separated from the lower half. The upper half was turned over and placed beside the lower half for post-test analyses (Figure 37).

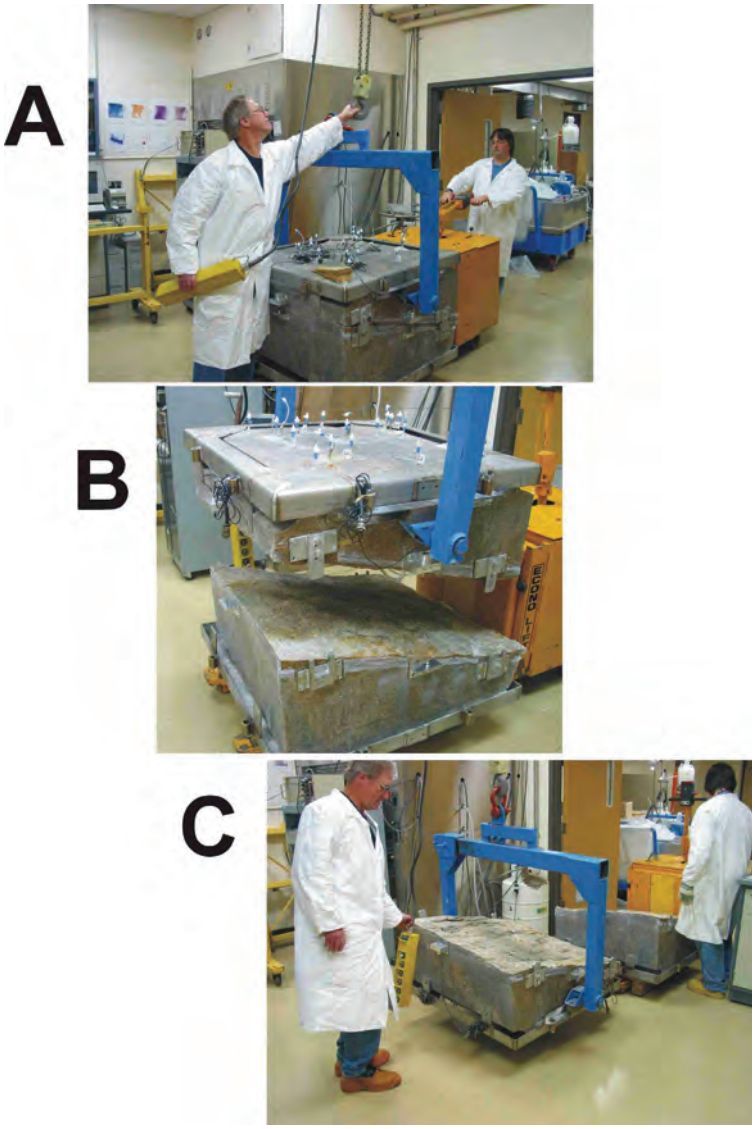

Figure 37: Opening of Quarried Block Showing (A) The Lifting Yoke Connecting the Upper Frame to the Hoist, (B) Initial Opening of the Fracture, and (C) Orientation of the Upper Fracture Once it has been Turned Over

The freshly opened upper and lower fracture surfaces are illustrated in Figure 38 and Figure 39. A UV lamp, with a spectral range of 310 to 400 nm, was used to induce fluorescence in latex colloids. Although the optimum excitation wavelengths of red, orange and yellow-green colloids are outside of the spectral range of the UV lamps, the UV radiation is able to make these colloids fluoresce. The optimal excitation wavelength of the blue colloids is very close to the peak height of the UV lamp's spectral range, inducing a very good fluorescence. However, the

emission wavelength of the blue colloids is very close to the spectral range of the UV lamp, and one must be careful to distinguish between lamplight and fluorescence due to the blue colloids. The fluorescence due to deposited colloids on fracture surfaces was photographed with a Canon 20D, using a 17-40 mm zoom lens, and exposure times ranging from 4 seconds to 2 minutes. Digital processing of images was performed with Adobe Photoshop Elements 2 software.

In an attempt to quantify the distribution of colloids deposited on fracture surfaces, specifically marked surface areas were sampled with cotton swabs. These sample areas were identified on fracture surfaces by drawing 47 mm diameter circles. Colloids were sampled by first saturating a cotton swab with deionized water. The sample area was swabbed until the swab appeared to be loaded with material from the surface. The tip of the swab was squeezed to release material into a sample vial. The swab was resaturated with fresh deionized water and the procedure was repeated until the sample area appeared to be free of surface particles under natural light. Once the swabbing was complete the cotton swab from each sample area was placed in the sample vial, and 20 mL of deionized water was added. The total amount of water used to saturate the swab was less than 1 mL. The swabs were soaked for several days and then each sample was subjected to an ultrasonic probe for 30 seconds to liberate attached colloids. The fluorescence of the resulting aqueous samples was measured to determine the concentrations of bentonite and latex colloids.

Once the study of colloid deposition on the fracture surfaces was complete, the remaining colloid deposits were removed by water and gentle scrubbing with a toothbrush. This was done under UV light to ensure complete removal of fluorescing colloids.

Figure 38: Bottom Fracture Surface

Figure 39: Top Fracture Surface

3.2 RESULTS

The UV light revealed apparent deposits of fluorescent blue, yellow and red colloids on the two fracture surfaces. The top fracture surface (Figure 40) appeared to have lower concentrations of 1 μm blue colloids compared to the bottom fracture surface (Figure 41). This was to be expected since the 1 μm colloids were subject to sedimentation. The pattern of deposited 1 μm colloids was likely determined to a large extent by the last tracer injection (2007 TT11), particularly in the L1-L4 region on the bottom half of Figure 41. Although 99 % of the 1 μm colloids injected during 2007 TT10 were left behind, this amount was only 5 mg. In contrast, the amount left by 2007 TT11 was 81 mg. Remnants of the 1 μm colloids injected during 2007 TT10 are likely to be found in the upper part of Figure 41. The 2007 TT10 post test fracture survey suggested that these colloids were located close to L2 and L5. The region of 1 μm colloid deposition ended abruptly below L4, along a line that corresponds to a fracture splay. A region of significant deposition of yellow colloids (upper and lower fracture surfaces) can be observed in the lower left corner, beyond the region of 1 μm colloid deposition.

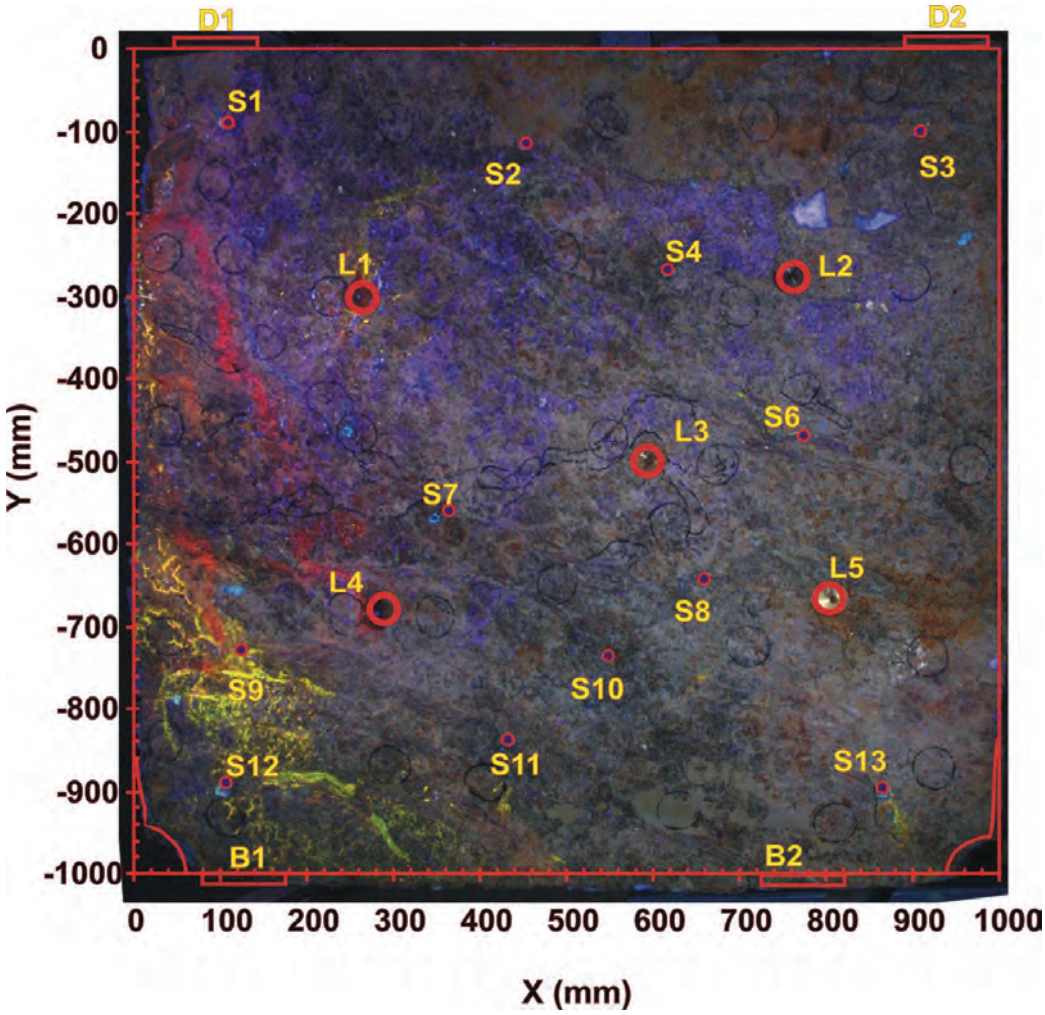

Figure 40: Top Fracture Surface Under UV Light, Showing Selected Boreholes. The image has been flipped over to correspond to the orientation of the bottom fracture.

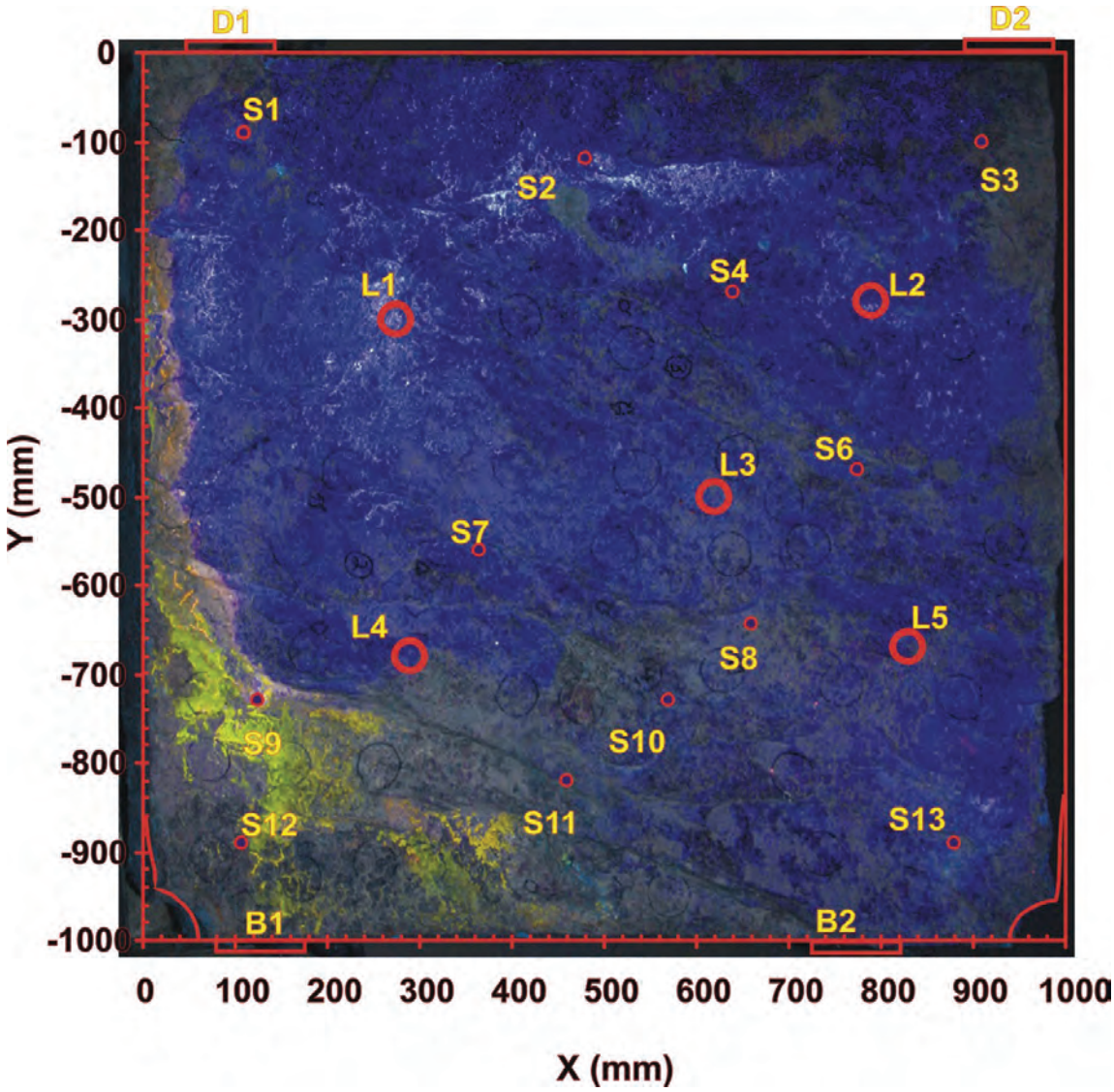

Figure 41: Bottom Fracture Surface Under UV Light, Showing Selected Boreholes

Swab analysis was performed in an attempt to quantify colloid deposition on the top and bottom fracture surfaces to assist in the interpretation of the observed fluorescence on fracture surfaces. Unfortunately, analyses of the swab samples revealed problems that created an unacceptable level of uncertainty. The major problem was a significant level of interference between some colloid types. The analysis of bentonite colloids was strongly affected by the presence of latex colloids, mainly because latex and bentonite colloids were present in similar concentrations, and bentonite analyses were based on total particle counts, regardless of their composition. Only the blue and red colloids were not significantly affected by the other colloids. The second problem was that in many cases the swab analyses did not recover all of the deposited colloids, as shown by close inspection of swabbed areas under UV light. This shows that a fraction of latex colloids deposited on fracture surfaces may stick strongly and require a more vigorous method for removal.

Although swab analyses had a high level of uncertainty that prevented quantification of colloid deposition, it did provide some information that was useful for interpreting the observed pattern of fluorescence under UV light. Swab analyses confirmed that the regions of more intense blue fluorescence could be attributed to higher concentrations blue 1 μm colloids. Yellow fluorescence in the lower left corner was from orange and possibly red colloids, not the yellow green injected during 2007 TT11. The red-orange fluorescence on the left side of the upper fracture appears to be mainly from the 100 nm orange colloids. Higher concentrations of red 20 nm and orange 100 nm colloids are present on the left side of the bottom fracture surface. Their presence is masked by the blue colloids in the images taken under UV light.

A more detailed view of fluorescence under UV, attributed to 1 μm latex colloids, is shown in Figure 42, which focuses on the pocket of high colloid deposition above S4 in the sample area of B10. The region around B10, as highlighted by higher fluorescence, corresponds to a pocket of higher fracture aperture created when several pieces of the lower fracture surface were dislodged before the start of colloid migration experiments. On a smaller scale, the highest colloid concentrations, as shown by the lighter more intense fluorescence, appear to be associated with local low spots. Figure 43 shows a region on the bottom fracture between sample points B47 and B48, which is close to the boundary between the areas of blue and yellow fluorescence. Again the locations of higher blue fluorescence appear to be associated with local depressions, which probably correspond to areas of greater fracture aperture when the block is closed. This photo was taken after the swab analysis. The remaining blue fluorescence in sample area B47 shows that a significant portion of the 1 μm colloids were not removed during swab sampling. Figure 44 shows another detailed view of the bottom fracture surface, beside sample location B46. Local areas of highest fluorescence correspond to local depressions and places where small fracture splays intersect the main fracture surface.

Figure 45 shows yellow fluorescence beside S12, and between sample areas B61 and B53. There is some correlation between fluorescence and the pink lines and brownish dusting visible under normal light. The fluorescence and the pink-brown colouration appears to cross over grain boundaries and be independent of underlying mineralogy. Figure 46 is a close up of an area between B49 and B53. Although in some cases the fluorescence is associated with what might be a local alteration zone, in many cases the deposition pattern appears to cut across mineral boundaries. This suggests that latex colloid deposition was determined by other factors than granite mineralogy.

Figure 47 shows a close up of sample area B55, located in a region of high fluorescence on the left side of the Quarried Block. B55 is situated beside a location where a fracture splay intersects the main fracture surface, and at the border of the main fluorescent blue region. Yellow-green fluorescence is located where small fractures intersect the main fracture surface. The yellow green fluorescence is still present in the sample area B55 after the swab sampling was complete. It should be noted that the yellow-green fluorescence disappeared after the fracture surface was washed with water and a brush.

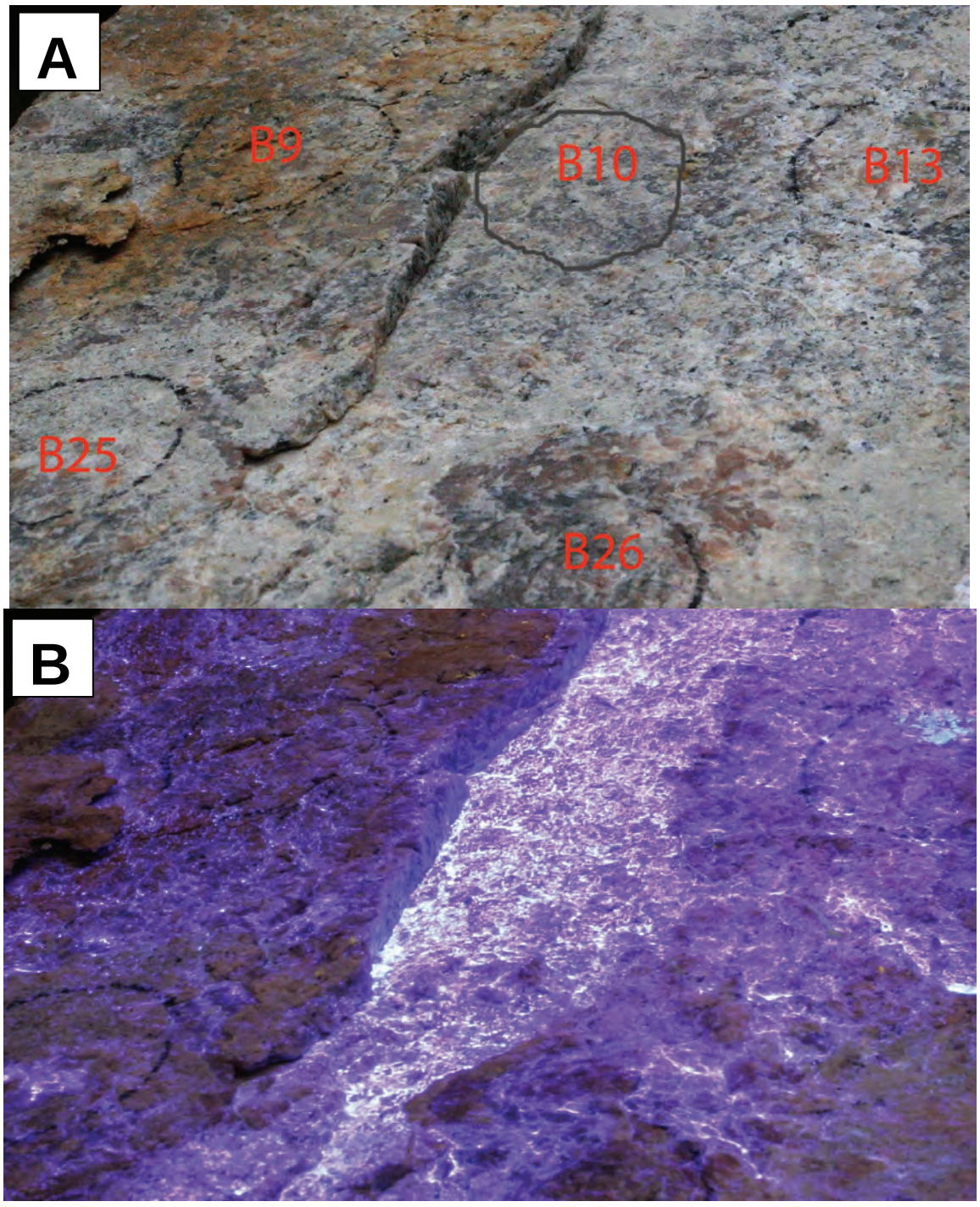

Figure 42: Detailed Views of Fluorescent Blue Colloids on Bottom Fracture Surface Focusing on the Region of High Colloid Deposition Above S4 and Sampled by B10, Under Normal Light (A) and Under UV Light (B). Photo was taken before swab sampling.

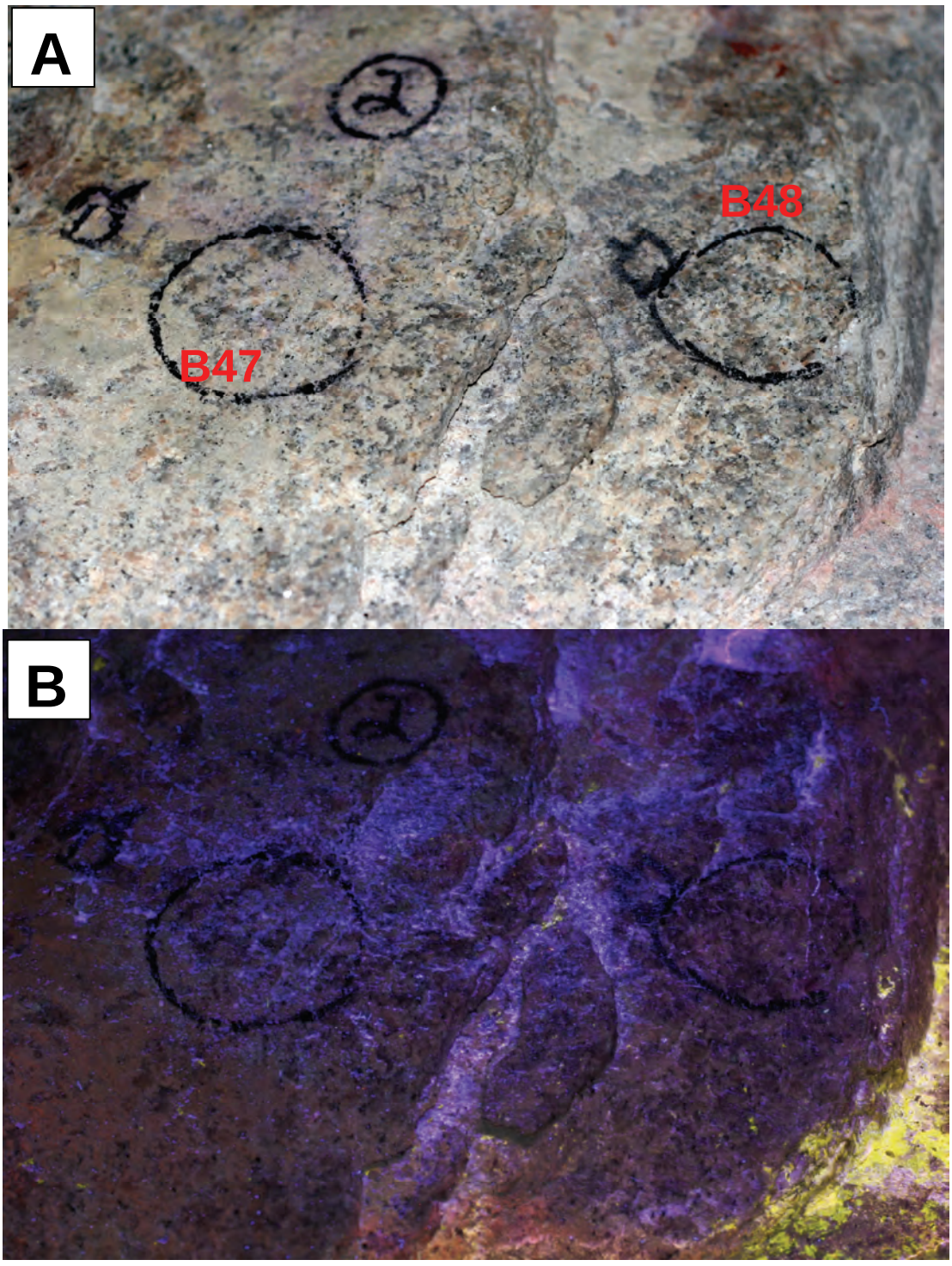

Figure 43: Detailed View of Bottom Fracture Surface Between Sample Locations B47 and B48 Under Normal Light (A) and Under UV Light (B). Photo was taken after swab sampling.

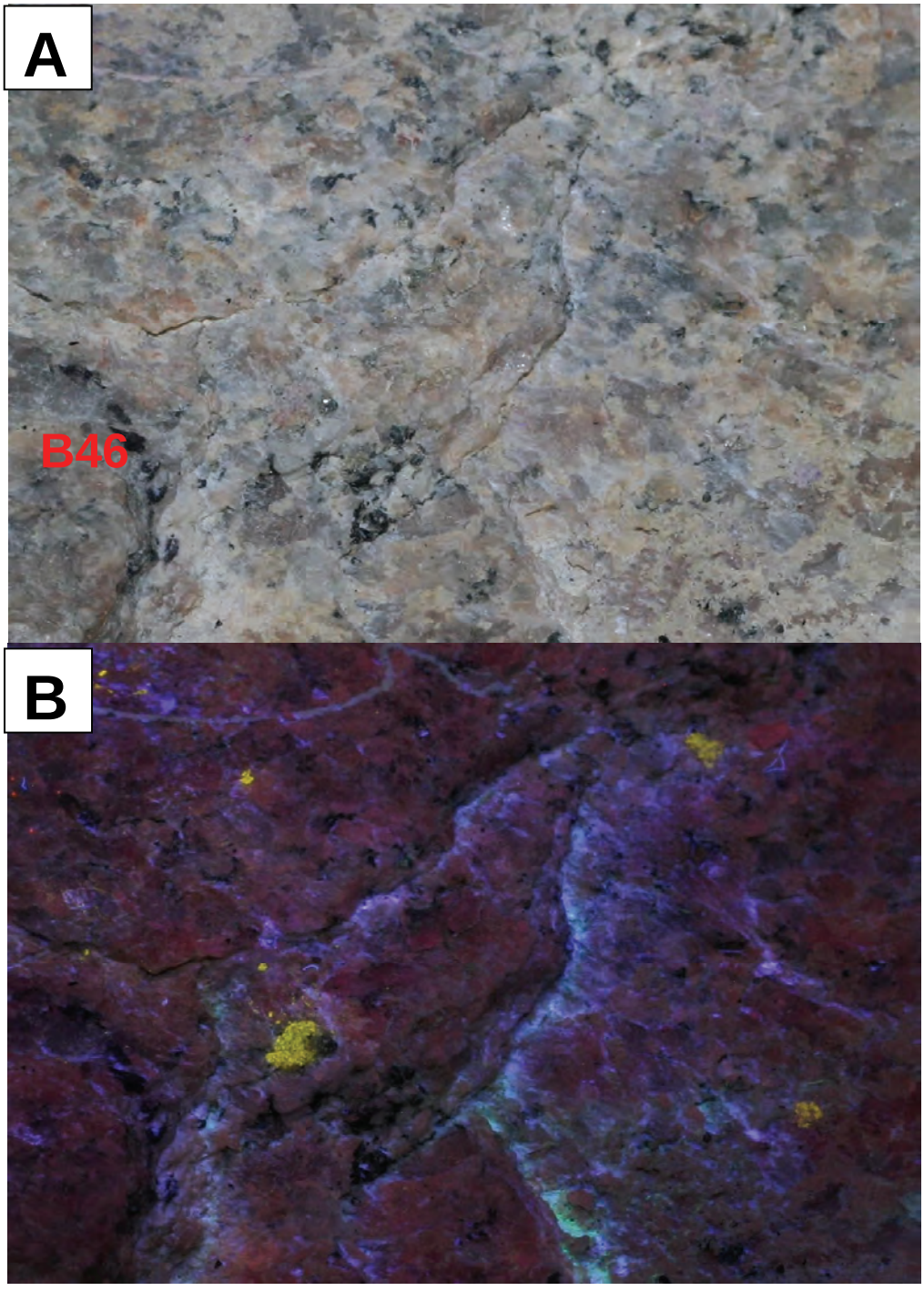

Figure 44: Detailed View of Bottom Fracture Surface Near Sample Location B46 Under Normal Light (A) and Under UV Light (B)

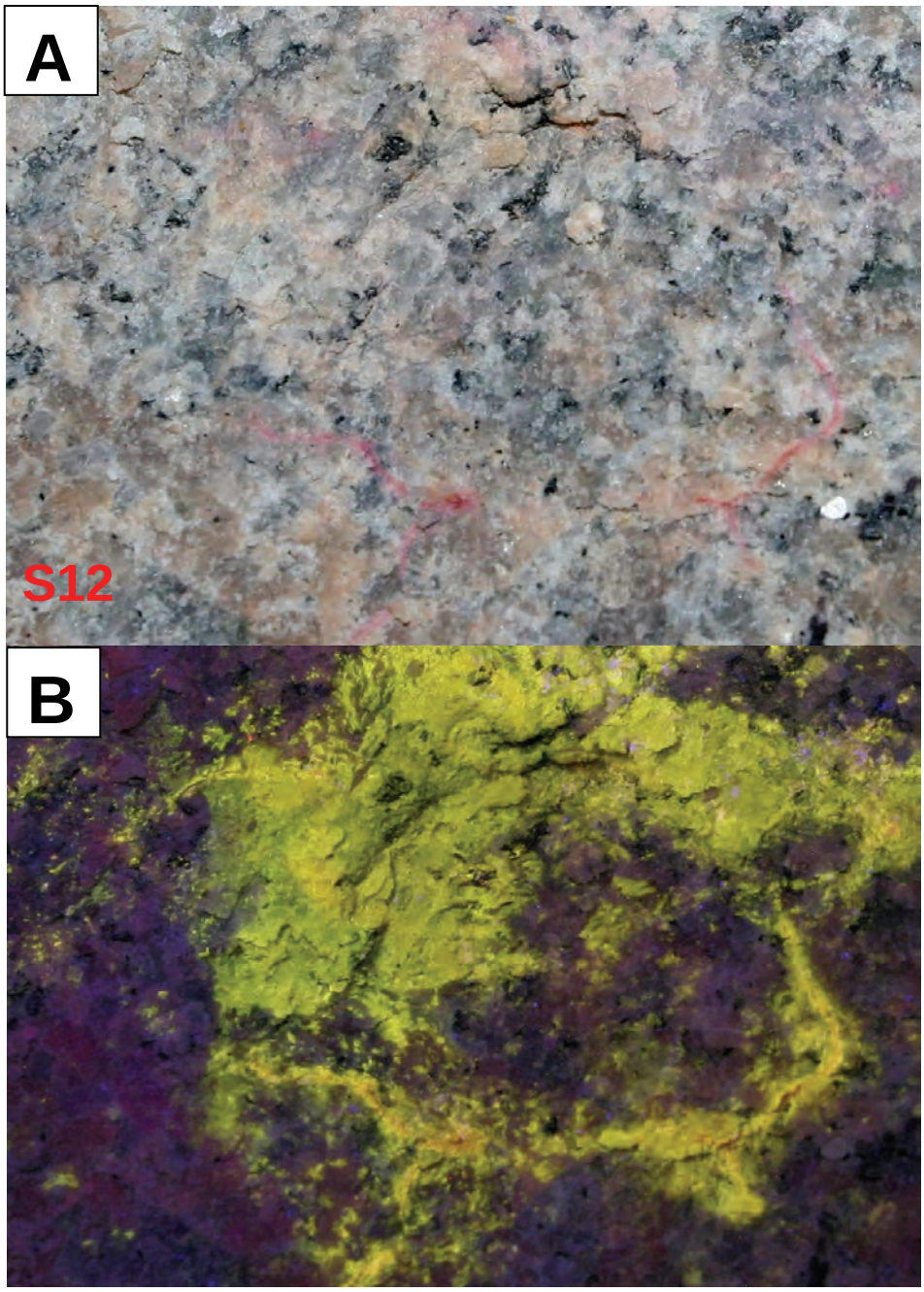

Figure 45: Detailed View of Bottom Fracture Surface Near S12 and Between Sample Location B61 and B53, Under Normal Light (A) and Under UV Light (B)

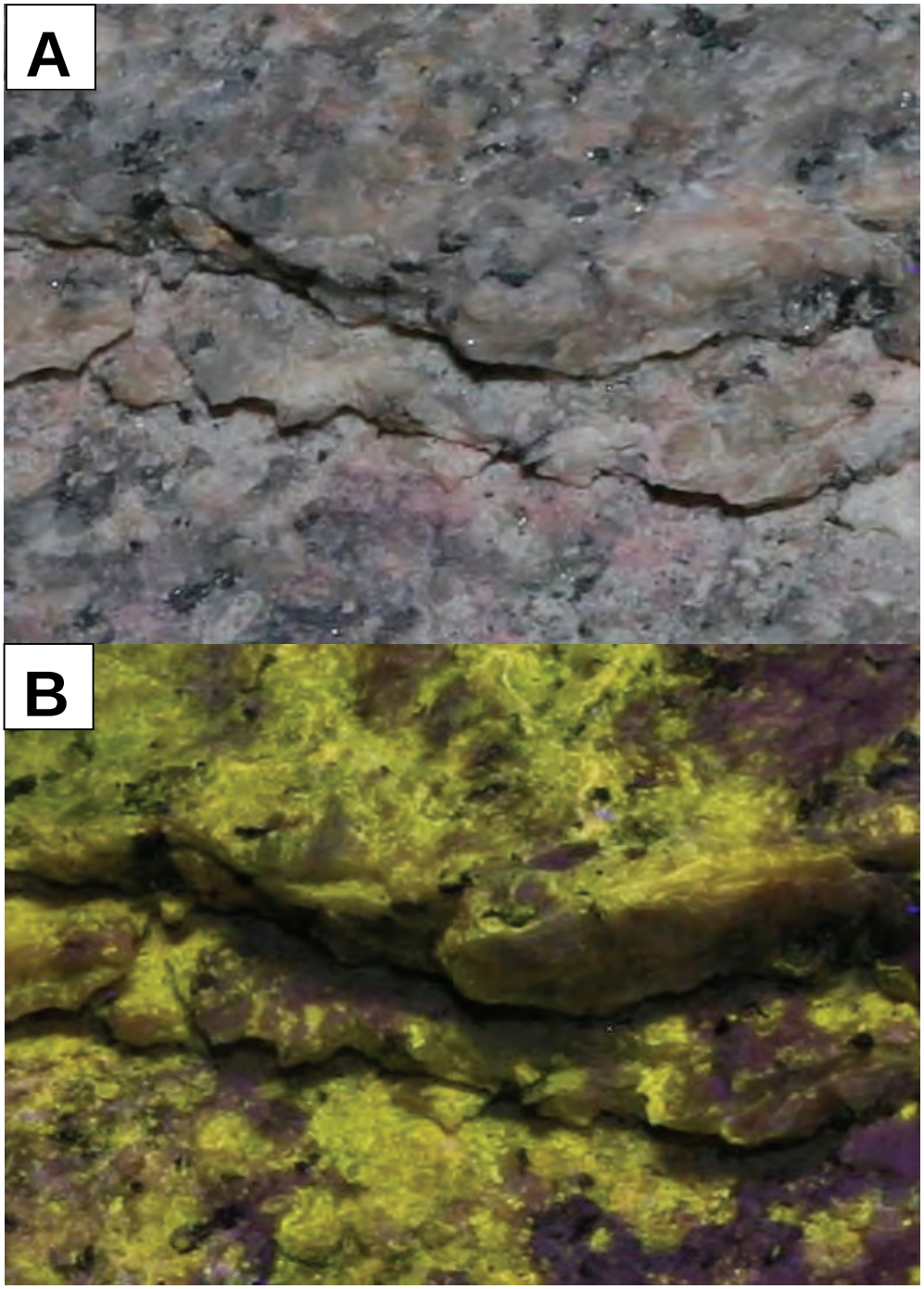

Figure 46: Detailed View of Bottom Fracture Surface Between S12 and Sample Locations B49 and B53, Under Normal Light (A) and Under UV Light (B)

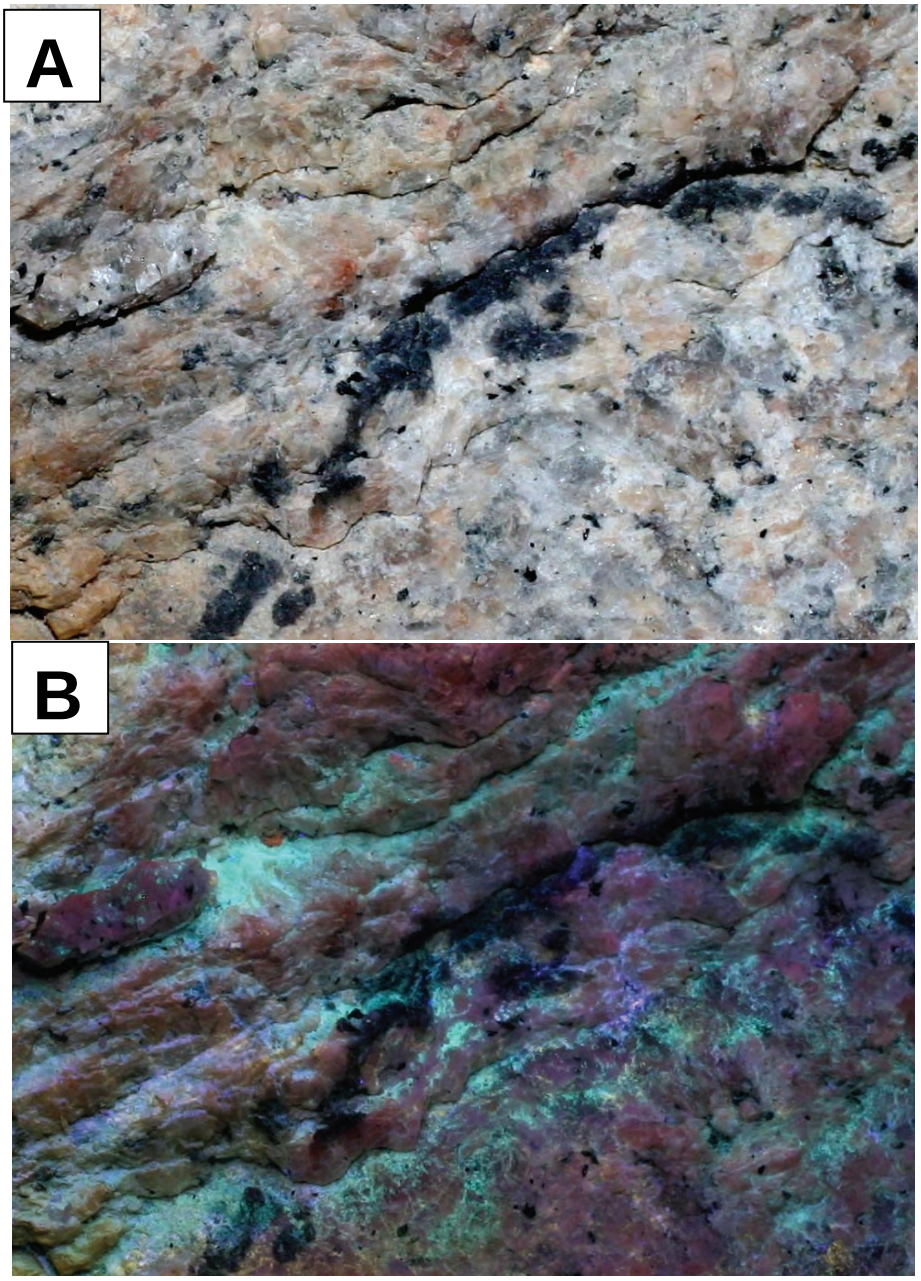

Figure 47: Detailed View of Sample Location B55 on the Bottom Fracture Surface Under Normal Light (A) and Under UV Light (B)

4. DISCUSSION

The characteristics of tracer breakthrough curves from tracer tests performed in this study (with the exception of 2007 TT11) are summarized in Table 2. Since most tests included several injections, the injection number is given for each tracer to clarify which tracers were co-injected. The table includes the elution volume of the first tracer arrival, and percent recovery for a reference elution volume of 3600 mL. The approximate location of peaks in the breakthrough curves are also given in terms of elution volume, and the peaks are arbitrarily designated as being major or minor. Table 2 provides a convenient reference for assessing the effects of experimental reproducibility, solution composition, particle size, particle composition and flow velocity on the transport behaviour of colloidal and solute tracers in the Quarried Block.

Transport in Higher Ionic Strength Water: Previous laboratory studies of bentonite colloid transport in the Quarried Block (Vilks and Miller 2007) included a test with synthetic Äspö groundwater to determine to what extent bentonite mobility is reduced by the high ionic strength and presence of divalent cations. In the previous L1-L4 transport experiment work the Quarried Block fracture was saturated with synthetic Äspö groundwater and bentonite colloids were injected as a suspension in deionized water to ensure that their concentrations in the suspension remained uniform during the time of injection. The colloid tracer was followed with tracer-free synthetic Äspö groundwater. The tracer solution would mix with the saline water once in the fracture. As calcium and sodium concentrations would reach critical levels, bentonite colloids would begin to flocculate and either drop out of suspension or be transported as flocs. At the same time, individual bentonite particles could begin to adhere to the fracture surfaces. The distance to which bentonite colloids are transported would depend upon the water mixing rate, the kinetics of flocculation and adherence to fracture surfaces, and the water flow rate. An intermediate flow rate was chosen for this experiment to allow sufficient opportunity for mixing, flocculation and sedimentation to take place.

As suspected, the process of injecting dilute solutions of tracer into saline water created buoyancy effects, which appeared to force tracer movement upslope and to the right side of the block. This conclusion was based on the distribution of electrical conductivity and iodide concentration values in the fracture during the tracer test. The denser synthetic Äspö water injected after the tracer probably had a tendency to bypass the less dense water with tracer on the right hand side of the fracture and move towards L4.

Since buoyancy had a significant impact on the transport paths taken by injected tracers, it was not possible to make a direct comparison with transport experiments performed in dilute water. However, a comparison of bentonite breakthrough curves and deposition patterns with those of co-injected iodide made it possible to establish the transport behaviour of bentonite in saline water (Vilks and Miller 2007). When bentonite colloids were injected followed by saline water, the recovery of iodide was 5 times higher than bentonite. In contrast, in the tracer tests performed under the same flow conditions with dilute water, the recovery of bentonite was only a few percent different from that of iodide. Therefore, even though buoyancy effects impacted the transport of both tracers in this test, the bentonite colloids were significantly retarded compared to solute. The fracture surveys supported this conclusion by showing that bentonite colloids had not been transported much further than 30 cm from L1.

Table 2: Summary of Breakthrough Curve Characteristics

Test	Test Param.	Inj.	Tracers	% Rec.	First Arrival (mL)	Peak Locations (mL) Major [Minor]
TT1	saline, 50 mL/h L1-L4	1	I	86 ± 5	150	603
		1	100 nm	22 ± 1	139	388
TT2	saline, 50 mL/h L1-L4	1	I	0	none	none
		1	100 nm	0.3	167	[786-2312]
TT3	dilute, 50 mL/h L1-L4	1	Br	95 ± 5	190	515, [886], [1210], [2075]
		2	I-1	76 ± 4	234	472, [1682]
		2	20 nm	62 ± 8	172	450, [1617]
		3	I-2	90 ± 5	211	502, [1086]
		3	100 nm	73 ± 4	193	479
		4	I-3	65 ± 5	239	446, [1147]
		4	1 micron	25 ± 1	197	421
TT4	dilute, 50 mL/h L1-L4	1	Br	66 ± 8	215	455, [1238]
		2	I	83 ± 5	235	505, [1108]
		2	20 nm	58 ± 3	191	462, [1246]
		2	100 nm	70 ± 4	191	462
		2	1 micron	23 ± 1	191	440
TT5	dilute, 50 mL/h L1-L4	1	Br	91 ± 5	209	478, [1304]
		2	Bentonite	92 ± 13	244	[462], 549, [679], 1223
TT6	dilute, 50 mL/h L1-L4	1	Br	76 ± 8	239	435, [953]
		2	Bentonite	82 ± 11	157	[212], [299], 451, [386], 1223, [2766]
TT7	dilute, 50 mL/h L1-L4	1	Br	73 ± 4	239	478, [696], [898], 1277
		2	Bentonite	14 ± 2	169	375, [440], [549], [929], [2211]
TT8	dilute, 500 mL/h S3-S12	1	Br	84 ± 4	900	1800-2136
		2	Bentonite	84 ± 11	852	[1272], 1704, [2040]
		3	I	82 ± 4	912	1944
		3	100 nm	72 ± 4	912	1560-1920
TT9	dilute, 6 mL/h S3-S12	1	Br	53 ± 2	204	1241, 1627, [1926], 2418, 2590, 3360
		2	Bentonite	24 ± 3	150	[385], [514], [728], 942, [1119], [1797], [3453]
TT10	dilute, 6 mL/h S3-S12	1	I	78 ± 4	600	920, 1049, 1477, [1691], [3453]
		1	20 nm	24 ± 1	535	942, 1049, 1156, 1306, 1434, 1562
		1	100 nm	51 ± 3	514	963, 1049, 1156, 1306, 1434, 1562
		1	1 micron	1.2 ± 0.1	557	963, 1049, 1156, 1306, 1434, 1562

% REC: Percent recovery after 3600 mL

In this study colloid migration experiments were performed in synthetic Äspö groundwater using 100 nm latex colloids and iodide to provide a comparison with bentonite colloids and to provide a link to field-scale tests performed at Äspö using latex colloids. When latex colloids were injected as a suspension in dilute water (2007 TT2) to recreate the 2006 experiments with bentonite colloids, buoyancy effects forced the tracer to migrate up the fracture slope to the right side of the Quarried Block. Virtually no tracers were recovered in the experimental time frame because the more buoyant tracer solutions remained in the upper part of the fracture while the denser Äspö-type water flowed from L1 to L4 in the lower part of the fracture. The post test fracture survey suggested that the latex colloids had migrated as far as the conservative tracer, although the recovered colloid concentrations, as C/Co values, were an order of magnitude lower than the solute tracer. This suggests that the latex colloids were becoming retained within the fracture. However, the presence of high latex colloid concentrations near L2 showed that latex is significantly more mobile than bentonite colloids, which did not move much further than S2 (Vilks and Miller 2007).

The experiment performed with an injection of latex colloids suspended in synthetic Äspö water (2007 TT1) was not subject to the same buoyancy effects since the density of tracer and fracture water were matched. The recovery of conservative tracer was similar to that observed in experiments using dilute water. The recovery of the 100 nm colloids was significantly lower than that of conservative tracer and that of 100 nm colloids in dilute water. The latex colloid recovery was similar to that of 1.0 μm in dilute water, which is not surprising since the 100 nm latex had formed flocs with an average diameter of 1.6 μm in the higher salinity water. This demonstrates the importance of particle diameter, whether as individual particles or as flocs, to colloid transport. Therefore, when using latex spheres as tracers the effects of flocculation need to be considered in field experiments where high ionic strength groundwater is present.

In summary, latex colloids are more mobile than bentonite colloids in higher salinity water. However, with the colloid concentrations used in this study latex colloids were flocculated, resulting in reduced transport because of the larger particle size. In tracer tests it is important to try to match the density of tracer solutions with that of groundwater as closely as possible, otherwise the experimental outcome could be affected by buoyancy and reduced mixing between groundwater and tracer solutions.

Colloid Size: The results of this study have provided further insight into the effect of particle size on colloid transport. A review of latex colloid recoveries in Table 2 indicates that the mid-sized 100 nm colloids were more mobile than other particle sizes, which is consistent with concepts of colloid filtration (McDowell-Boyer et al. 1986) that suggest that mid-sized colloids, such as the 100 nm latex, are more readily transported compared to smaller and larger colloids. Smaller colloids are more efficiently filtered because their higher diffusion rates increase their collisions with fracture surfaces, while larger colloids tend to be lost by gravitational settling. The recoveries of the 1.0 μm colloids were always the lowest. At moderate flow rates, the recoveries of 20 nm colloids were not much lower than those of the100 nm colloids. However, at the lowest flow rate and the longest flow path the difference in transport behaviour became more significant with the recovery of 20 nm colloids being about one half of the 100 nm colloids.

Since latex colloids of different size were shown to have different transport properties, one could expect that under certain conditions the larger colloids could affect the transport of smaller colloids in poly-disperse suspensions. However, results have shown that with the colloid concentrations used in this study, colloid transport from a poly-disperse injection does not appear to be significantly different from that observed from mono-disperse injections. This

implies that it is feasible to perform tracer tests using latex colloids with a mixture of sizes. Although it is tempting to extrapolate this conclusion to bentonite colloids, this might not be valid since bentonite colloids have more complex surface chemistry with a mixture of positive and negative surface charges. Also it is not possible to simulate a bentonite colloid breakthrough curve by using a poly-disperse mixture of latex colloids.

Typical bentonite colloid tracers used in migration experiments were suspensions of polydisperse particles with sizes ranging from a few nm to approximately 2 microns. Previous experiments (Vilks and Miller 2007) indicated that the small size fraction (4 to 15 nm) was most likely to be transported. These experiments also suggested that a portion of the larger particles in bentonite suspensions were flocs, which could disperse into smaller particles during transit. In this study the transport properties of small bentonite colloids were compared with those of larger bentonite colloids by performing a set of experiments with colloid tracers containing a variable fraction of small colloids ranging from 0.4 % to 100 %. Test 2007 TT5, using only small bentonite colloids, had the highest recovery (90 ± 12 %), which was also higher than previously determined bentonite recoveries at intermediate flow rates. Conversely, the bentonite recovery from 2007 TT7, with only 0.4 % small colloids, had dropped to 14 ± 2 %, implying that a majority of larger colloids had not migrated very far. This tracer test did show that when sufficiently high quantities of larger colloids are injected the breakthrough of larger colloids may be observed. However, the size distribution of these eluted larger colloids was reduced compared to that of injected tracer. Even though the transport of larger bentonite colloids is possible, the results of post test fracture surveys indicate that the larger colloids become immobilized within the fracture system.

It is difficult to relate the transport behaviourof bentonite colloids to latex colloids of a particular size. For example, at low flow the bentonite colloid recovery during flow from S3 to S12 was similar that of the 20 nm colloids, yet their breakthrough curves were different. In the test between L1 and L4 at medium flow and using only small bentonite colloids, the bentonite colloids had a higher recovery than both the 20 nm and 100 nm latex.

Effect of Flow Rate on Tracer Breakthrough: In previous experiments (Vilks and Miller 2007) it was shown that at high transport velocities the migration behaviour of bentonite colloids and latex spheres were similar. The breakthrough curves of all colloid and solute tracers exhibited a single major peak. However, with decreasing flow velocities bentonite and latex colloids began to exhibit different transport behaviour. While the latex colloids tended to retain their single breakthrough peak at intermediate flow, the bentonite colloids displayed an increasing number of peaks with decreasing flow. As flow velocity decreased the recovery of bentonite colloids decreased more rapidly than that of latex colloids.

In this study flow velocity was varied only in tests performed with the longer flow path between S3 and S12. When the flow rate was reduced from 500 mL/h to 6 mL/h the recovery of bromide was reduced by 42 percent. Bentonite recovery decreased by 73 percent, which was not significantly different from the previous test results from the L1 to L4 borehole pair. The 100 nm latex recovery decreased by 24 percent, which was somewhat higher than in L1 to L4 experiment. As in previous experiments between L1 and L4 (Vilks and Miller 2007), at the high flow rate the breakthrough curves of solute, and latex and bentonite colloids were similar. Bentonite breakthrough curves were ahead of bromide and latex at both high (500 mL/h) and low (6 mL/h) flow rates. Differences in transport behaviour became more evident at low flow rates. In comparison to the high flow rate, the following was noted at the low flow rate. (1) the peak heights of bromide, bentonite and 100 nm latex were reduced. (2) Tracer first arrivals

were significantly faster in terms of volume. (3) The single broad bromide and bentonite peaks observed at high flow had been replaced by a series of smaller peaks. (4) The separation between bentonite and bromide had increased, with bromide peaks arriving after the main bentonite peaks had eluted. More separation was also evident between bentonite and latex. (5) The breakthrough curve of the latex colloid did not break up into a number of smaller peaks, as did the bromide.

These observations indicate that at low flow, tracer transport tends to occur in preferential pathways, as evidenced by an increased number of peaks in the breakthrough curve. At low flow, differences in diffusion properties become more important, causing changes to breakthrough curves and creating more separation between solutes and colloids. At low flow the first arrivals of bromide and the smaller bentonite colloids were ahead of the 100 nm latex. This illustrates the increased dispersion associated with tracers of smaller sizes and higher diffusion coefficients. In addition, the tracers with the higher diffusion coefficients displayed multiple peaks at the low flow rate, while the 100 nm latex did not.

Effect of Colloids on Co-injected Solute: The results of previous experiments (Vilks and Miller 2007) showed that the solute tracer co-injected with 100 nm latex displayed a breakthrough that was typical of 100 nm latex, while the solutes co-injected with bentonite displayed the variability shown by bentonite colloids. Solutes injected in the absence of colloids displayed breakthrough curves that were unlike those when co-injected with colloids. The consistent variation in solute tracer breakthrough curves with the type of co-injected colloid, suggested that solute transport was being influenced by the presence of colloids. The proposed explanation for the effect of colloids on solute tracer was based on differences in diffusion coefficients associated with solute and colloids, particularly at low flow velocities (Vilks and Miller 2007). Due to their larger size, colloids have diffusion coefficients that are significantly smaller than those of solutes. For example, the diffusion coefficients of 20 nm and 100 nm colloids would be two and three orders of magnitude, respectively, smaller than that of solute. Therefore, the 100 nm colloids are more likely to stay in the main flow path, producing well-defined breakthrough curves. In comparison, solutes and very small colloids are more likely to diffuse out of the main flow path, producing more tailing or a larger number of peaks that represent multiple flow paths. At the time of tracer injection, the concentration of colloidal particles could have been high enough to interfere with solute diffusion. To diffuse out of the tracer solution into more stagnant parts of the fracture the solute molecules had to diffuse around the colloidal particles, effectively reducing solute diffusivity by a tortuosity factor. When injecting into a fracture via a single borehole, the direction initially taken by the tracer may have an important influence over the ultimate migration behaviour of tracer. Therefore, the transport behaviour of solute tracers could be determined at the point of injection when they are swept along by a relatively concentrated colloid suspension.

In this study an injection of colloid-free bromide was used to define the transport properties for a given experimental set of parameters. Iodide was co-injected with latex colloids to obtain additional data on the effect of colloids on solute transport. Solute tracers were not co-injected with bentonite colloids to minimize any risk of inducing additional flocculation. The results from this study provide additional evidence that latex colloids affect solute transport. Figure 11 compares the breakthrough curves of iodide co-injected with colloids of different size with the breakthrough curve of bromide injected without colloid. The iodide breakthrough curves were influenced by co-injected colloid in terms of shape and recovery (Table 2). In the test between S3 and S12 at high flow rate (2007 TT8) the bromide and iodide had similar breakthrough curves and recoveries, suggesting no interference from colloids at high flow rate. However,

when the flow was reduced to 6 mL/h, (2007 TT9 and 2007 TT10) the breakthrough curve of bromide is significantly different from the iodide co-injected with latex colloids. The bromide breakthrough curve had multiple peaks, suggesting multiple flow paths that could have been caused by diffusion related dispersion. The iodide had a significantly higher recovery and a breakthrough curve with a single broad peak similar to the colloid breakthrough curves. This would be consistent with reduced dispersion caused by colloids interfering with solute diffusion.

Effect of Fracture Aperture on colloid deposition: The fracture aperture distribution has a direct influence on local flow velocity and on the path(s) taken by colloids and solute in a given tracer test. The Reynolds equation or the local cubic law can be used to provide a good approximation of local small scale hydraulic head and fluid velocity (Brush, 2003, and Brush and Thompson, 2003). These equations show that fluid velocity is proportional to the square of the fracture aperture. Since natural fractures have a variable aperture distribution it follows that the fracture plane will have a heterogeneous flow field. Fluid flow simulations (Brush, 2003) have shown that in the Quarried Block the higher flow fields are found in regions of larger aperture. Based on the larger aperture distribution on the upper and left sides (Figure 53) (as well as flow simulations by Brush, 2003), if a flow field is established by injecting into S3 and withdrawing from S12 (Figure 48), the major flow path will probably be along A, while a lesser flow path will be along B. The aperture anisotropy tends to be oriented along flow path A, but tends to be transverse to flow path B. Simulations by Chrysikopoulos and James (2003) indicate that if aperture anisotropy is oriented in the flow direction, there is an increase in colloid spreading. However, if the aperture anisotropy is transverse to flow direction, colloid transport is retarded.

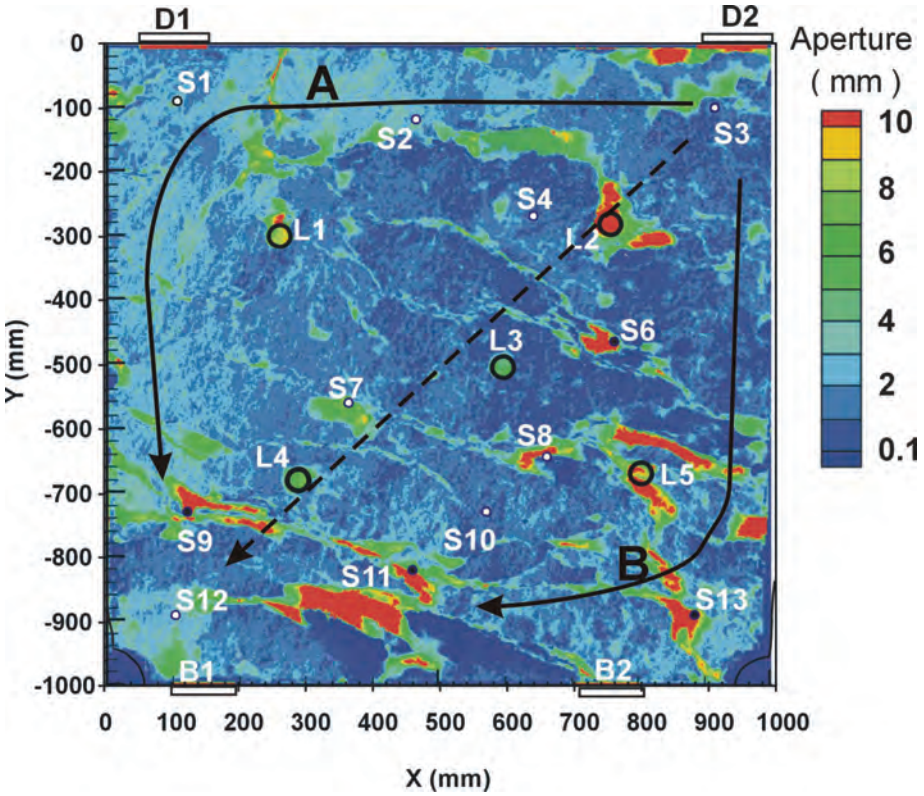

Figure 48: Predicted Main (A) and Secondary (B) Flow Paths with S3 as the Injection Hole and S12 as the Withdrawal Hole.

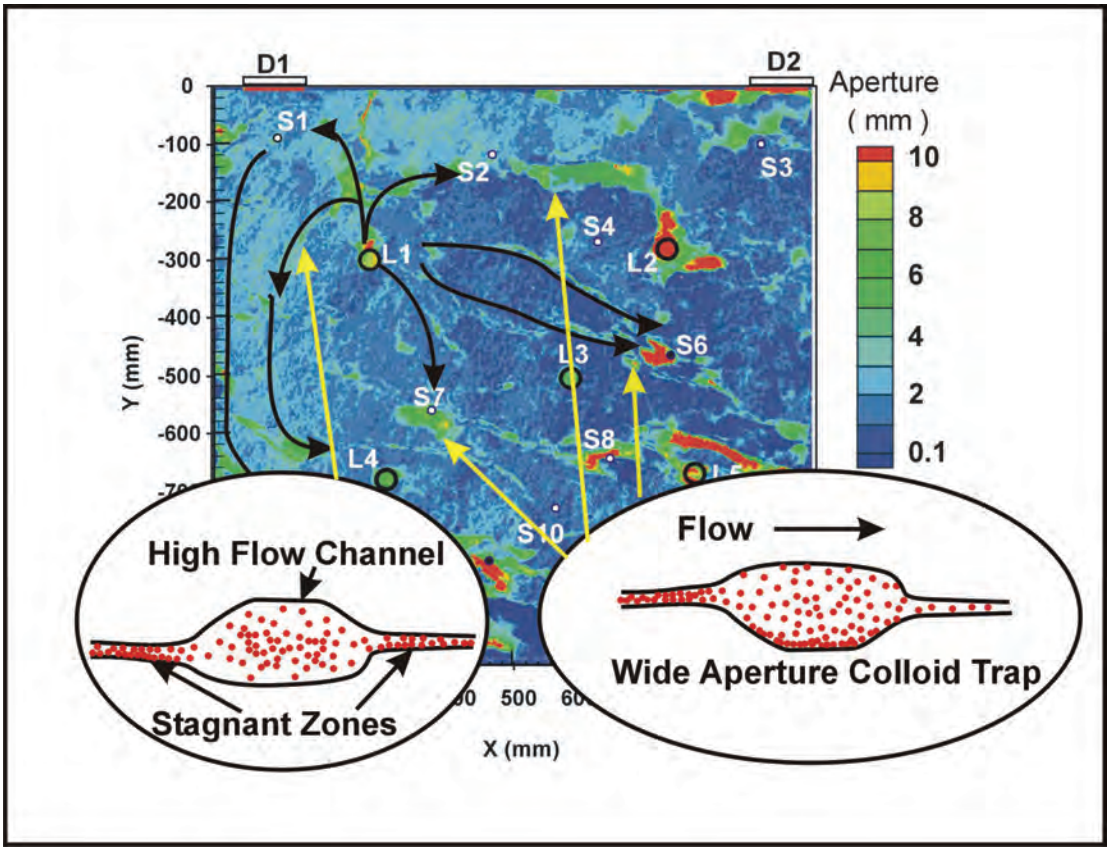

Figure 49: Main Flow Paths for the Last Tracer Injection before the Quarried Block was Opened for Post-test Analyses.

Blue (1 μm) and yellow-green (500 nm) latex were injected into L1 and withdrawn from L4, just prior to opening the Quarried Block for post-test analyses. Based on aperture distribution, post-test fracture sampling and flow simulation (Brush, 2003) the probable flow paths are shown in Figure 49.

The fluorescence observed under UV light during post-test analyses provides an indication of where fluorescing colloids were deposited. Measurable colloid deposition can occur at a given location only if sufficient amounts of colloid are transported to that location and if local conditions are favourable for deposition. In order to study the influence of aperture distribution on colloid deposition, the fluorescence under UV light from the bottom fracture (Figure 41) was superimposed on the fracture aperture model and presented in Figure 50. Figure 50A shows the fracture aperture model in grey scale as a reference, and Figure 50B shows the fluorescence superimposed over the aperture model. From Figure 50 one can see that some regions of larger aperture, such as the region starting above L1 and extending through S2 and above S4, and reaching L2, have high colloid concentrations. Not only do connected regions of larger aperture provide an accessible flow path for colloid tracers, but the larger local fracture volume may result in a reduced flow velocity, a longer residence time and an increased likelihood of sedimentation. In general, regions of lower aperture appear to have lower colloid

concentrations. However, this general pattern is complicated in the proximity of the injection borehole (L1) used in TT11.

Figure 51 shows a close up view of Figure 50, in the region around L1. The scale for the aperture model is the same as in Figure 50. This detailed view shows that the distribution pattern of the fluorescence appears to have slightly finer detail than the aperture distribution. However, there appears to be a correlation between the distribution of fluorescence and aperture. In many cases, regions of wider aperture appear to trap colloids. However, in some cases the higher aperture regions have low colloid concentrations, either because they received only small colloid concentrations or else flow conditions did not favour deposition. For example, the region, labelled as 1, has a slightly higher aperture and is connected to the large aperture area above L1. Although the larger aperture area above L1 contains high colloid concentration, area 1 does not. Possible explanations could be that the large aperture area trapped colloids and supplied region 1 with low colloid concentrations, or the flow was too high through region 1 to allow colloid deposition. The smaller aperture areas to the left and right of region 1 contain higher concentrations. If region 1 supplied colloids to these surrounding areas, it could be that the smaller and more variable aperture distributions in these areas reduced flow and acted as stagnant zones to promote colloid deposition. The left boundary of the blue region in Figure 51 does not appear to correlate with aperture distribution, and was probably an edge effect imposed by the side of the Quarried Block.

Figure 52 is a detail from the lower left corner of the Quarried Block, illustrating the transition between blue and yellow fluorescence. The boundary of the blue region appears to be partially defined by a lineament of higher aperture extending from S9 to B2. This lineament marks the exposure of a fracture splay that may have induced a boundary effect on the flow field between L1 and L4. Had 2007 TT11 been run for a longer time frame, the blue colloids would have moved beyond this boundary, as indicated by post-test analyses in previous experiments. Region 1 in Figure 52 provides another example of a higher aperture lineament that contains less colloids than surrounding areas. The yellow fluorescence is mainly from orange 100 nm colloids that were used during tracer test 2007 TT10, during which S12 was the withdrawal well. Although high levels of yellow fluorescence are found in pockets of larger aperture, often this fluorescence occupies only a portion of the large aperture pocket. The deposition mechanism of the yellow fluorescence within the large aperture pocket is not known, and may reflect differences between the digital aperture distribution and the current aperture distribution. The bottom fracture surface appears to have higher colloid concentrations than the top surface. If this was not an artefact of dewatering the fracture, it may indicate that the bottom surface had features that favoured colloid deposition over the top surface. Such a feature might be a higher concentration of sand or silt sized material on the fracture surface that acted as a filter or trap for colloids.

A

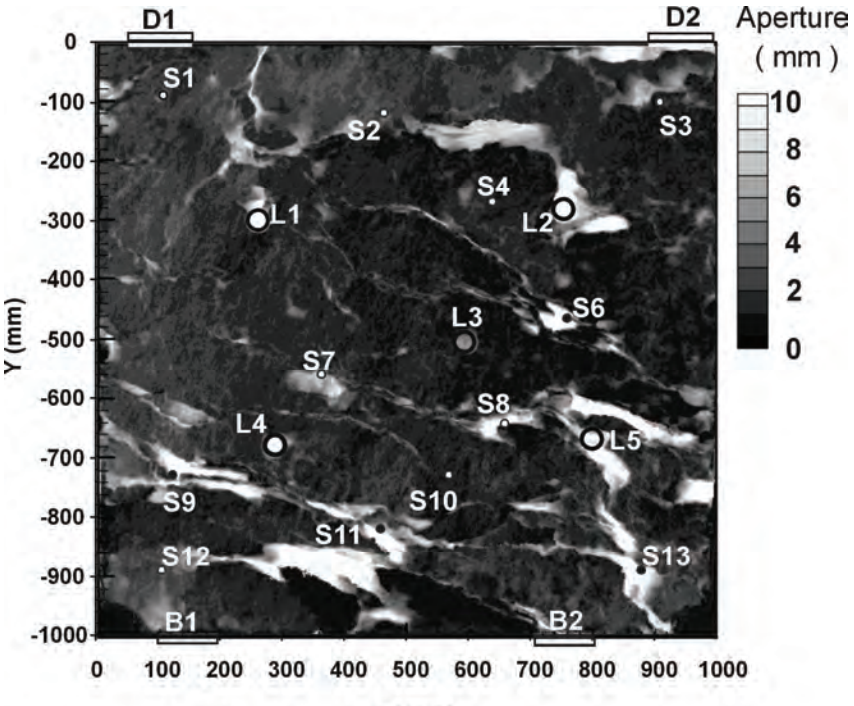

B

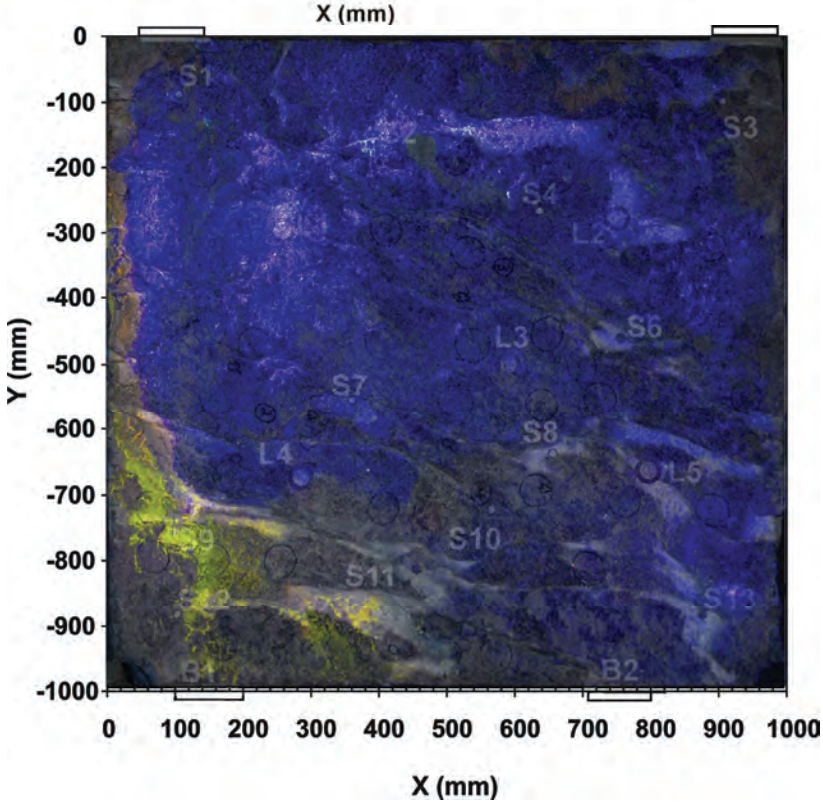

Figure 50: Fracture Aperture Distribution (A) Overlain By Fluorescence from Bottom Fracture (B)

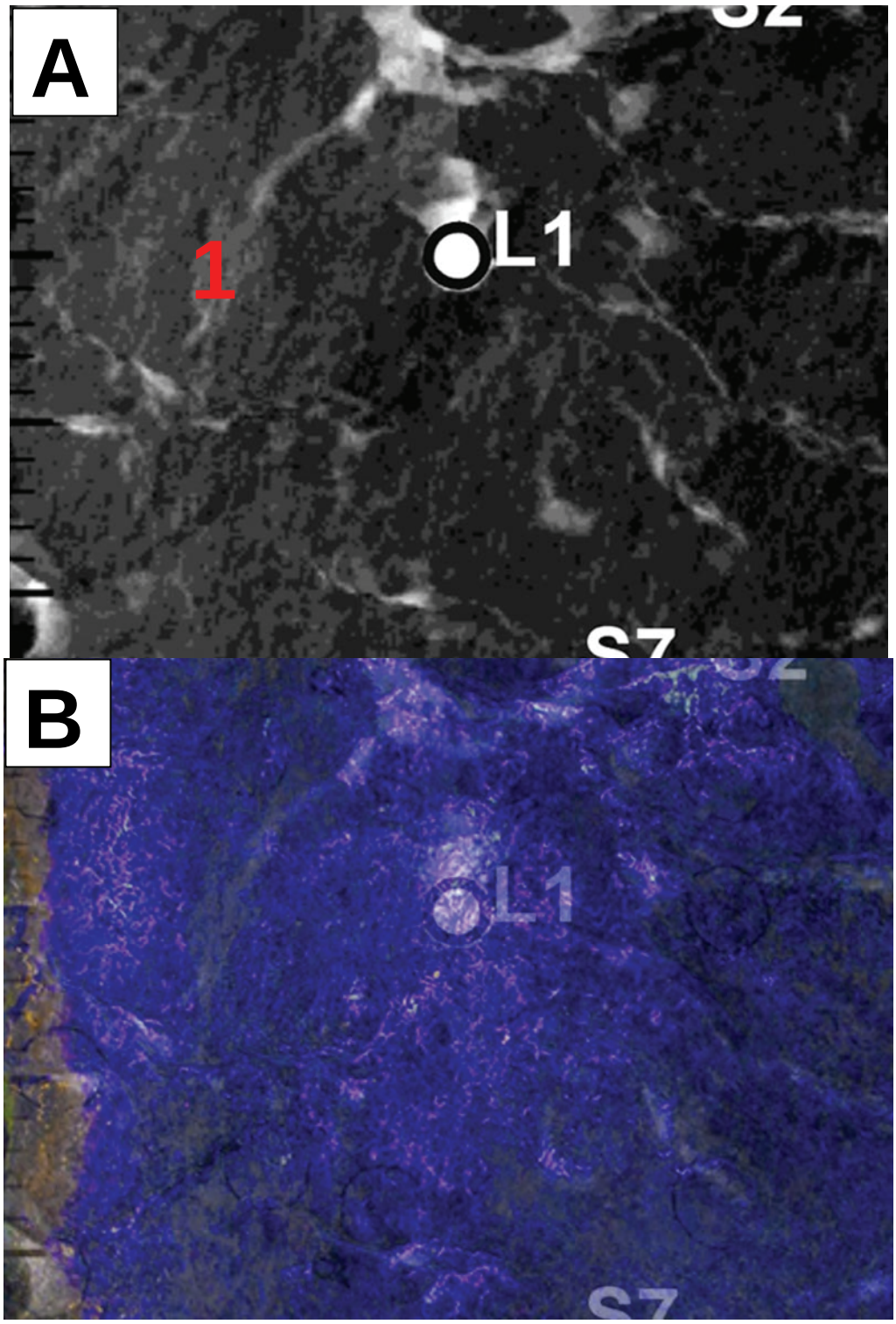

Figure 51: Detail from Region Around L1, from Figure 54, with (A) Fracture Aperture and (B) UV Fluorescence

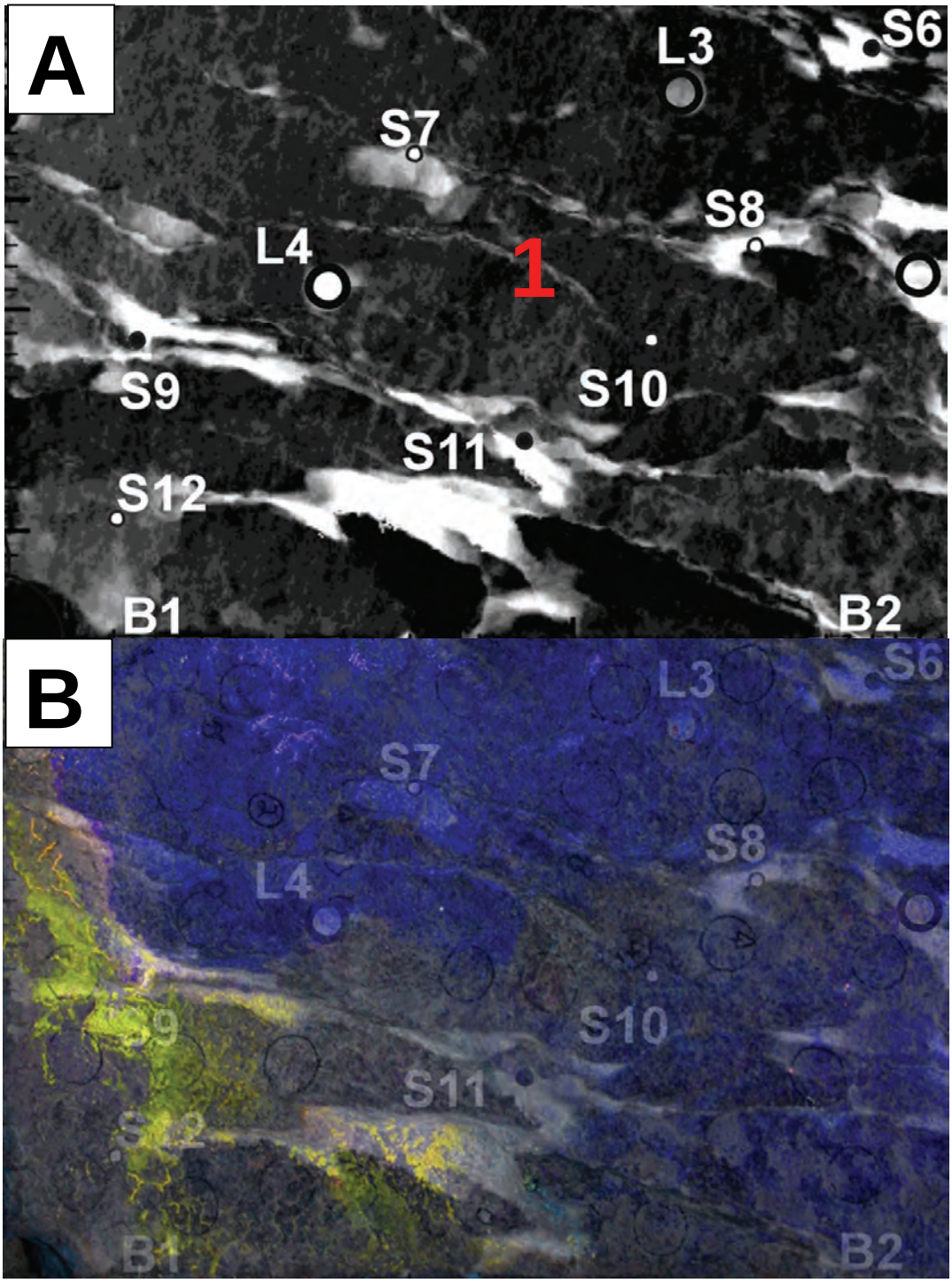

Figure 52: Detail from Lower Left Corner of Figure 54, with (A) Fracture Aperture and (B) UV Fluorescence

Tracer Mass Balance During Post-Test Fracture Surveys: In addition to giving a snapshot of tracer distribution within the fracture at a given point in time, the fracture survey data provide an indication as to whether a given tracer is present in the fracture in a form that is easily mobilized and recovered by sampling from boreholes. The total tracer mass in the fracture can be estimated by calculating an average tracer concentration from the concentrations determined from all boreholes. Assuming that the total fracture volume is 2.5 L, the average tracer concentration is used to derive the total tracer mass accessible to sampling. Table 3 reports tracer masses recovered from fracture surveys as percentages of the total injected mass. Table 3 also gives the tracer residence time in the fracture before the survey, and the percentage recovery determined from the breakthrough curve at the time of the fracture survey. The final column in Table 3 sums tracer masses recovered from fracture surveys with those calculated from breakthrough curves. If a tracer is not lost from the volume of fracture water as a result of diffusion into dead end spaces or attachment to fracture surfaces, the total tracer mass should approach 100 %. Since the solute tracers used in this study are not likely to sorb to fracture walls, total tracer masses of less than 100 % are most likely due to diffusion into dead end spaces not accessible to sampling during fracture surveys. Since colloids have significantly smaller diffusion coefficients than solute, total recovered colloid masses that are less than 100 % are more likely due to colloids sticking to fracture surfaces or being immobilized in regions not accessible to sampling from boreholes.

The total masses of recovered solute tracers were between 70 % and 100 %, decreasing slightly with longer residence times of around 600 h. The lower recovery for the longer residence time could be attributed to losses due to diffusion. Smaller mass recoveries from breakthrough curves were compensated by larger recoveries from fracture surveys. In most cases the fraction of solute tracer that was lost from the fracture water was less than 20 %. Total solute recovery in higher salinity water was not significantly different from that in dilute water.

The recovery of latex colloids during fracture surveys and from breakthrough curves depended upon colloid size and residence time within the fracture. At residence times of 60 to 70 h, the mid-sized 100 nm colloids displayed the highest recovery (10 %) during fracture surveys, followed by 20 nm colloids (5%) and 1 μm colloids (1%). Smaller recoveries of the 20 nm and 1 μm colloids from breakthrough curves were not compensated by larger recoveries from fracture surveys. The recovery during fracture surveys and the total recovery of 100 nm latex was similar to those of solute, suggesting that the 100 nm latex colloids could be mobilized by sampling and were not strongly fixed to fracture surfaces. However, the lower recoveries of 20 nm and 1 μm colloids indicate that they were becoming more easily fixed within the fracture system, compared to 100 nm colloids. When the residence time was increased to 600 h the recoveries of all latex colloids decreased, implying that with increased time it becomes more difficult to mobilize latex colloids that remain in the fracture system.

Table 3: Tracer Mass Balance During Post Test Fracture Surveys

Test	Tracers	Residence Time Before Survey (h)	Estimated % In Fracture From Post Test Survey	Estimated % Recovered From Breakthrough	Estimated % Total Recovered Tracer
TT1	I	55	7 ± 4	86 ± 5	93 ± 9
	100 nm	55	1.3 ± 0.4	22 ± 1	23 ± 1
TT2	I	72	69 ± 16	0	69 ± 16
	100 nm	72	4 ± 1	0.3	4 ± 1
TT3	I-1	48	10 ± 2	75 ± 4	85 ± 6
	20 nm	48	5 ± 1	61 ± 8	68 ± 9
	I-2	72	14 ± 4	90 ± 5	104 ± 9
	100 nm	72	9 ± 3	73 ± 4	82 ± 7
	I-3	67	13 ± 3	60 ± 5	73 ± 8
	1 micron	67	0.8 ± 0.2	24 ± 1	25 ± 1
TT4	I	59	11 ± 2	80 ± 5	91 ± 6
	20 nm	59	5 ± 1	57 ± 3	62 ± 4
	100 nm	59	11 ± 2	68 ± 4	79 ± 6
	1 micron	59	1.1 ± 0.3	23 ± 1	24 ± 1
TT5	Br	59	5 ± 1	89 ± 5	94 ± 6
	Bentonite	59	35 ± 12	90 ± 13	125 ± 25
TT6	Br	64	9 ± 5	73 ± 4	82 ± 9
	Bentonite	64	18 ± 5	81 ± 11	99 ± 16
TT7	Br	64	9 ± 3	69 ± 4	78 ± 7
	Bentonite	64	8 ± 4	14 ± 2	22 ± 6
TT8	Br	6	31 ± 9	70 ± 4	101 ± 13
	Bentonite	6	39 ± 12	76 ± 11	115 ± 23
	I	6	25 ± 8	70 ± 4	95 ± 12
	100 nm	6	17 ± 4	66 ± 4	83 ± 8
TT9	Br	575	6 ± 1	50 ± 2	56 ± 3
	Bentonite	575	5 ± 1	23 ± 3	28 ± 4
TT10	I	667	4 ± 1	81 ± 4	85 ± 5
	20 nm	667	0.5 ± 0.1	25 ± 1	26 ± 1
	100 nm	667	1.1 ± 0.2	52 ± 3	52 ± 3
	1 micron	667	0.5 ± 0.1	1.2 ± 0.1	1.7 ± 0.2

The recoveries of bentonite colloids depended upon the size distribution of the injected tracer and on the residence time within the fracture. When the bentonite tracer had a high concentration of large particles, the bentonite recovery during the fracture survey at a residence time of 60 h was 8%. With a decrease in the concentration of large particles the bentonite recoveries during fracture surveys increased to 18% and 35%. These latter recoveries were significantly higher than observed for solute and latex tracers. The cause of these high

recoveries has not been established, but could be due to the release of colloids in the 4 to 15 nm size range from bentonite flocs attached to fracture surfaces.

The recovery of bentonite colloids from fracture surfaces significantly decreases with residence times of about 600 h. This indicates that bentonite colloids will eventually become strongly attached, and is consistent with the results of pre-test fracture surveys showing relatively low colloid concentrations.

5. CONCLUSIONS

Observations From This Study: A series of laboratory colloid migration experiments were performed in a clean granite fracture to compare latex and bentonite colloid transport in dilute and higher salinity water and to explore the effects of water composition, flow velocity, colloid structure and surface charge density, particle size distribution, and fracture aperture distribution on colloid transport. The results showed that, unlike bentonite colloids, latex colloids are mobile in higher salinity, Äspö type water. However, due to the presence of Na and Ca concentrations in this water the latex colloids became less stable, forming flocs with larger diameters. The resulting transport properties of the latex colloids were determined by the size of their flocs (1.6 μm), as opposed to their individual particle size (100 nm). The density difference between a tracer solution/suspension and the water it is being injected into were shown to have a significant effect on the experimental outcome. If possible, these density differences should be minimized in future tracer tests.

The bulk of the experiments performed in dilute water were used to compare the transport properties of latex colloids with those of bentonite colloids. The carboxylate-modified latex spheres used in this study are almost perfectly spherical, resistant to biodegradation and are relatively stable in water through a combination of hydrophilic and negatively charged (at pH>5) surfaces (Becker et al., 1999). The transport of various latex colloid sizes was investigated. The 100 nm colloid size was transported most efficiently because its diffusion coefficient was too small to allow significant diffusion out of the main flow field, yet the size was still too small to be affected by sedimentation. The transport of 20 nm colloids was less efficient because their diffusion coefficient (about an order of magnitude higher than for the 100 nm colloids) was high enough to permit some diffusion out of the main flow field, thereby increasing the probability of contacting fracture surfaces or entering dead end zones. The 1 μm colloids were large enough to be affected by sedimentation, even though their density was only 1.055 g/cm^3. In principle all latex spheres are composed of the same material and have very similar surface properties. Therefore, their probabilities of sticking to the fracture surface after contact is made should be similar for all latex colloid sizes. The observed differences in latex colloid immobilization for different sizes (as defined by reduced recovery from breakthrough curves and post-test sampling) are likely determined by their probability of hitting a fracture surface or entering a dead end zone. With extended residence times all latex sizes appeared to become immobilized.

The transport of a poly-disperse, latex colloid suspension (a range of sizes) was compared to that of mono-disperse suspensions (single sizes). There were no significantly differences observed in the transport of single colloid sizes, whether injected in poly-disperse or mono-disperse suspensions. This implies that in dilute waters different sized latex colloids in a poly-disperse suspension behave independently of each other. Although latex colloids of different

size did not appear to interfere with each other, this study did provide further examples of latex colloids affecting the breakthrough curves of co-injected solute tracers, particularly at low flow rate.

Bentonite colloids have positive edge sites and negative basal surface sites, and a particle density that is as high as 2.5 g/cm^3, although the density of bentonite flocs could be less due to the presence of water between bentonite particles. The bentonite tracers used in this study had a broad size range from 10 nm to several µm. Some of the larger particles could have been flocs. Results indicated that the large bentonite particles (and/or flocs) intersected fracture surfaces relatively quickly (sedimentation favoured by high density and large particle size), leaving the smaller 4 to 15 nm colloids in suspension to be transported. The dominance of small colloids in eluted water samples and the high bentonite recoveries during fracture surveys indicate that bentonite flocs deposited on fracture surfaces probably release the small 4 to 15 nm bentonite colloids during tracer tests and post-test fracture surveys. As with latex colloids, with prolonged residence times there was a tendency for bentonite colloids to become fixed within the fracture system. It is not possible to simulate the transport behaviour of bentonite colloids with a poly-disperse mixture of latex colloids with different sizes. It is the difference in particle density, structure and surface properties that makes the transport properties of bentonite different from latex spheres.

Under conditions of low flow and longer residence time within the fracture, the differences in transport properties between colloid and solute tracers become enhanced. The increasing influence of diffusion processes at low flow rate may be an important factor. At low flow those solute and colloidal tracers with higher diffusion coefficients tend to display more dispersion (as evidenced by earlier first arrivals) and show several flow paths (multiple peak breakthrough curves).

The fluorescence induced by UV light can be used to define the distribution pattern of fluorescing latex colloids deposited on fracture surfaces. The surface fluorescence illustrated a correlation between latex colloid deposition and fracture aperture. In some cases pockets of large aperture acted as traps for colloids. In other instances linear regions of slightly larger aperture were not favourable to colloid deposition, and may have functioned as pathways of higher flow, supplying surrounding lower aperture regions (lower flow) with colloids. Although correlations between fracture aperture and colloid deposition were noted, detailed photos of mineral surfaces did not show a correlation between granite mineralogy and latex deposition.

Implications for Performance Assessment: The conditions that favour colloid transport are low ionic strength and neutral pH water to promote colloid stability, high flow rates to counter the effects of diffusion and sedimentation, and channelled transport paths that lack tortuosity, aperture variation and surface roughness. Conditions that minimize colloid transport include high ionic strength water in which colloid stability is reduced. In the synthetic Äspö type groundwater, bentonite colloid transport did not occur over distances greater than about 30 cm . It should be noted that while the Äspö groundwater is considered as brackish (TDS between 1 and 10 g/L), typical deep groundwater in other locations (McMurry, 2004; Vilks, 2009) may be saline (TDS between 10 and 100 g/L) or even brines (TDS > 100 g/L). Colloid transport is also significantly reduced when groundwater flow velocities are low, typical of natural conditions in deep geologic formations. Fracture aperture heterogeneity and surface roughness promote colloid entrapment even for negatively charged colloids that should be stable under conditions of low ionic strength.

The conditions that favour colloid transport are more likely to occur in shallow systems, consisting of unconsolidated porous media or highly fractured rock, where groundwater is more dilute and flow rates are higher due to hydraulic gradients induced by local topography. Conditions that reduce colloid transport tend to occur at greater depths in the type of setting proposed for deep geologic repositories. An important limitation to colloid mobility is the presence of higher ionic strength groundwaters. There is a possibility that these higher salinity waters could be displaced by more dilute glacial melt water during a limited time frame of a retreating glacier. However, this possibility is still the subject of considerable debate. Even under dilute conditions, colloid transport would be limited by the features of deep geologic formations such as lower porosity, reduced number of fractures, and lower groundwater velocities.

The issue of colloid facilitated contaminant transport will likely remain, mainly because of observations of colloid-facilitated transport made in shallow systems being considered for landfills or containing radioactive contamination from historic disposal practices. Although conditions in deep geologic systems are significantly different, the proponents of deep geologic disposal will have to be prepared with reasoned arguments as to why the colloid issue is not applicable to their system.

Implications for Transport Experiments: Laboratory and field-scale tracer tests with colloids and solute are performed to improve the understanding of colloid transport properties or to help characterize the subsurface transport system. In either case it is important to understand the physical nature of a colloid tracer. Brackish water, such as found at Äspö, is able to flocculate latex colloids of all sizes. For example, 100 nm latex spheres were flocculated, altering their migration behaviour to resemble that of 1 μm latex particles. Therefore, when planning field-scale tracer tests where groundwater is brackish or saline, one must check for and characterize flocculation that is likely to take place. Even in the presence of high experimentally induced flow rates, latex colloid transport was not detected in field-scale tests within a body of moderately fractured rock at AECL's Underground Research Laboratory in which flow was governed by an intersecting network of fractures (Vandergraaf et al., 2001).

Since flow rate has a significant effect on colloid migration, one should try to use flow velocities that are relevant to natural groundwater flow conditions. Alternatively the effects of flow rate must be explored to provide enough understanding to extrapolate the experimental results to natural flow conditions. Often high flow rates are required for field tests due to the longer travel distances, time limitations and the need to establish a flow regime that is distinct from natural flow conditions. Therefore, field tests may be more useful for characterizing the properties of natural systems, as opposed to studying colloid migration properties. On the lab-scale the migration properties of solute and various colloids at high flow rates appear to be similar. On the field-scale the longer travel distances might create more separation between solute and colloids of various sizes, even at high flow rates. This could be tested further.

The ideal size for fluorescent latex colloid tracers used in field experiments could be around 200 nm. This is in the mid-sized range that is the most efficiently transported, increasing the probability of being able to detect colloid tracers in eluted water. Also, 200 nm colloids can be detected by epifluorescent microscopy. The identification of individual colloidal particles by this method improves the detection limit of colloidal tracers by many orders of magnitude.

To better understand colloid transport in relation to the migration properties of water molecules, it is useful to compare colloid breakthrough curves with those of conservative solute tracers.

For convenience and to avoid issues of changing flow conditions, there is often a desire to inject colloid tracers together with solute tracers. However, the tests in this study have consistently demonstrated that the breakthrough curves of solute tracers can be affected by the presence of co-injected colloids. Therefore, it is better to inject solute tracers separately from colloids, despite uncertainties that may be caused by time dependent changes in experimental flow conditions. This study has also illustrated that a density difference between tracer and groundwater can have a significant effect on tracer transport, particularly if the flow system contains sloped fractures. Therefore, one should attempt to match the density of a tracer solution with that of the water in the experimental system.

ACKNOWLEDGEMENTS

The work described in this report was carried out by AECL with funding from NWMO Technical Program, under Contract GS04, and from SKB as part of the Colloid Dipole Project F91P1.

REFERENCES

Becker, M.W., Reimus, P.W. and Vilks, P., 1999. Transport and attenuation of carboxylate-modified latex microspheres in fractured rock laboratory and field tracer tests. Ground Water, 37, 387-395.

Bonano, E.J. and W.E. Beyeler. 1984. Transport and capture of colloidal particles in single fractures. Sandia National Laboratories Report, SAND-84-0810C.

Brush, D.J. 2003. Quarried Block Experiment: Numerical simulations of flow and transport experiments in a natural fracture. Prepared by University of Waterloo for Ontario Power Generation. Ontario Power Generation, Nuclear Waste Management Division Report 06819-REP-01300-10075-R00, Toronto, Ontario.

Brush, D.J. and N.R. Thomson. 2003. Fluid flow in synthetic rough-walled fractures. Navier-Stokes, Stokes, and local cubic law simulations. Water Resour. Research 39(4), 1099.

Chrysikopoulos, C.V. and S.C James. 2003. Transport of neutrally buoyant and dense variably sized colloids in a two-dimensional fracture with anisotropic aperture. Transport in Porous Media, 191-210.

Chrysikopoulos, C.V., and A. Abdel-Salam. 1997. Modelling colloid transport and dispersion in saturated fractures. Colloids Surf. A. 121, 189-202.

De Marsily, G. 1986. Quantitative Hydrogeology. Academic Press, Inc., Harcourt Brace Jovanovich, Inc., San Diego, CA.

Guzy, C.J., B.J. Bonano and B.J. Davis. 1983. The analysis of flow and colloidal particle retention in fibrous porous media. Journal of Colloid and Interface Science 95, 523-543.

Iwasaki, T. 1937. Some notes on sand filtration. Journal of American Water Works Association 29, 1591-1602.

Kersting, A., D. Efurd, D. Finnegan, D. Rokop, D. Smith, and J. Thompson. 1999. Migration of plutonium in the groundwater at the Nevada Test Site. Nature 397, 56-59.

McDowell-Boyer, L.M., Hunt, J.R. and Sitar, N., 1986. Particle transport through porous media. Water Resources Research 22, 1901-21.

McMurry, J. 2004. Reference water compositions for a deep geologic repository in the Canadian Shield. OPG Report No: 06819-REP-01200-10135-R01.

Mori, A., W.R. Alexander, H. Geckeis, W. Hauser, T. Schäfer, J. Eikenberg, T.H. Fierz, C. Degueldre, and T. Missana. 2003. The colloid and radionuclide retardation experiment at the Grimsel Test Site: Influence of bentonite colloids on radionuclide migration in a fractured rock. Colloids and Surfaces A: Physicochemical and Engineering Aspects Vol. 217, No. 1-3, p. 33-47.

SKB. 2004. Äspö Hard Rock Laboratory Annual Report 2002. SKB TR-04-10, 197 pp.

Vandergraaf. T.T., E.T. Kozak, N.W. Scheier, F.W. Stanchell, J.D. Ross and P. Vilks. 2001. Moderately Fractured Rock Experiment Stage 2 report: Large and medium-scale migration experiments. Prepared by Atomic Energy of Canada Ltd. for Ontario Power Generation, Report No: 06819-REP-01300-10028-R00.

Vilks, P. 2009. Sorption in highly saline solutions – State of the science review. NWMO Technical Report, NWMO-TR-2009-18.

Vilks, P. and N.H. Miller. 2006. Laboratory bentonite colloid migration experiments to support the Äspö Colloid Project. Ontario Power Generation, Nuclear Waste Management Division Report 06819-REP-01300-10123-R00, Toronto, Ontario.

Vilks, P. and D.B. Bachinski. 1994. Colloid and Suspended Particle Migration Experiments in a granite fracture. In Proceedings of th e Fourth International Conference on the Chemistry and Migration Behaviour of Actinides and Fission Products in the Geosphere, Charleston, SC, (December 12-17, 1993), Special Issue of Radiochimica Acta 66/67, 229-234.

Winberg, A., P Andersson, J. Hermanson, J. Byegård, V. Cvetkovic and L. Birgersson. 2000. Äspö Hard Rock Laboratory. Final report of the first stage of the tracer retention understanding experiments. SKB Technical Report TR-00-07.

Yao, K., M.T. Habibian and C.R. O'Melia. 1971. Water and wastewater filtration: Concepts and applications. Environment Sciences Technology 5, 1105-1112.